

Ezh2 and Runx1 Mutations Collaborate to Initiate Lympho-Myeloid Leukemia in Early Thymic Progenitors

Authors

Christopher A. G. Booth^{1,2}, Nikolaos Barkas^{1,2+}, Wen Hao Neo^{1,2+}, Hanane Boukarabila^{1,2}, Elizabeth J. Soilleux³, George Giotopoulos^{4,5,6}, Noushin Farnoud⁷, Alice Giustacchini^{1,2,8}, Neil Ashley^{1,2}, Joana Carrelha^{1,2}, Lauren Jamieson^{1,2}, Deborah Atkinson^{1,2}, Tiphaine Bouriez-Jones^{1,2}, Rab K. Prinjha⁹, Thomas A. Milne², David T. Teachey¹⁰, Elli Papaemmanuil⁷, Brian J. P. Huntly^{4,5,6}, Sten Eirik W. Jacobsen^{1,2,11*†}, Adam J. Mead^{1,2,12*†‡}

⁺Equal contribution

^{*}Equal senior contribution

[†]Correspondence: adam.mead@imm.ox.ac.uk and sten.jacobsen@imm.ox.ac.uk

[‡]Lead contact

Affiliations

¹Haematopoietic Stem Cell Biology Laboratory, ²MRC Molecular Haematology Unit, MRC Weatherall Institute of Molecular Medicine, Radcliffe Department of Medicine, University of Oxford, Oxford OX3 9DS, United Kingdom

³Division of Cellular and Molecular Pathology, Department of Pathology, University of Cambridge, Cambridge, United Kingdom

⁴Wellcome Trust-MRC Cambridge Stem Cell Institute, Cambridge, United Kingdom

⁵Department of Haematology, University of Cambridge, Cambridge, United Kingdom

⁶Cambridge Institute for Medical Research, Cambridge Biomedical Campus, Hills Road, Cambridge CB2 0XY, United Kingdom

⁷Center for Hematologic Malignancies, Memorial Sloan Kettering Cancer Center, New York, NY 10065, USA

⁸Department of Cell and Developmental Biology, University College London, London WC1E 6BT, United Kingdom

⁹Epigenetics DPU, Oncology and Immuno-Inflammation Therapy Area Unit, GlaxoSmithKline, Stevenage, United Kingdom

¹⁰Division of Oncology, Children's Hospital of Philadelphia and Department of Pediatrics, University of Pennsylvania Perelman School of Medicine, Philadelphia, PA, USA

¹¹Department of Cell and Molecular Biology and Department of Medicine Huddinge, Karolinska Institutet, and Center for Hematology and Regenerative Medicine, Karolinska University Hospital Huddinge Stockholm, Sweden

¹²NIHR Biomedical Research Centre, Churchill Hospital, Oxford OX3 7LE, United Kingdom

Summary

Lympho-myeloid restricted early thymic progenitors (ETPs) are postulated to be the cell of origin for ETP leukemias, a therapy-resistant leukemia associated with frequent co-occurrence of *EZH2* and *RUNX1* inactivating mutations, and constitutively activating signaling pathway mutations. In a mouse model, we demonstrate that *Ezh2* and *Runx1* inactivation targeted to early lymphoid progenitors causes a marked expansion of pre-leukemic ETPs, showing transcriptional signatures characteristic of ETP leukemia. Addition of a RAS-signaling pathway mutation (*Flt3-ITD*) results in an aggressive leukemia co-expressing myeloid and lymphoid genes, which can be established and propagated *in vivo* by the expanded ETPs. Both mouse and human ETP leukemias show sensitivity to BET inhibition *in vitro* and *in vivo*, which reverses aberrant gene expression induced by *Ezh2* inactivation.

Significance

How the identity of the normal stem and progenitor cells targeted by oncogenic mutations impacts on cancer stem cell biology and the clinical picture of the resulting cancer remains to be established. Therapy-resistant ETP leukemias were first identified by their transcriptional profile, which resembled that of mouse ETPs. However, direct experimental evidence that ETPs could be the primary target cell for mutations associated with ETP leukemia and can propagate the disease *in vivo* remains lacking. We targeted relevant mutations to early lymphoid progenitors in mice, generating an aggressive lympho-myeloid leukemia propagated by an expanded ETP population, which showed transcriptional signatures characteristic of ETP leukemia. Using this model we identified BET inhibition as a promising therapeutic approach for PRC2-inactivated ETP leukemias.

Introduction

Extensive efforts have shed light on the identity and biology of cancer stem cells (CSCs), required and sufficient for propagation of hematological malignancies and solid tumors (Magee et al., 2012).

Much less is understood about the identity and properties of normal stem and progenitor cells targeted by oncogenic lesions, and how the nature of the targeted cell impacts on the biology and clinical picture of the resulting cancer. While in hematological malignancies CSCs frequently originate in normal hematopoietic stem cells (HSCs) with intrinsic self-renewal (Shlush et al., 2014; Woll et al., 2014), it remains to be established to what degree progenitor cells that normally lack self-renewal potential can be transformed into leukemic stem cells (LSCs) (Magee et al., 2012), and propagate leukemias independently of HSCs.

Whilst most acute leukemias show restricted expression of either myeloid (acute myeloid leukemia; AML) or lymphoid (acute lymphoblastic leukemia; ALL) antigens, subgroups show aberrant co-expression of lymphoid and myeloid antigens. These are defined as the clinical entity of biphenotypic leukemia (Matutes et al., 2011). Acute leukemias can also undergo a lineage-switch from an ALL to AML phenotype (Dorantes-Acosta and Pelayo, 2012). These biphenotypic leukemias almost invariably share markers of one of the (B or T) lymphoid lineages with markers of the granulocyte-monocyte (GM) lineages, and rarely between B and T or lymphoid and megakaryocyte-erythroid lineages (Matutes et al., 2011). A common lympho-myeloid pathway has been established in normal mouse and human hematopoiesis, with lymphoid-primed multipotent progenitors (LMPPs) (Adolfsson et al., 2005; Goardon et al., 2011). The presence of LMPP-like LSCs in AML patients (Goardon et al., 2011) is compatible with targeting of leukemia-initiating lesions to LMPPs. A combined lympho-myeloid program is sustained even in the earliest T cell progenitors (early thymic progenitors; ETPs), closely related to LMPPs (Luc et al., 2012). ETPs sustain residual myeloid lineage potential of unknown significance (Bell and Bhandoola, 2008; Schlenner and Rodewald, 2010). Overexpression of a myeloid transcription factor is sufficient to switch ETPs from a T cell to myeloid

lineage fate (Laiosa et al., 2006), and introduction of the Mll-Enl translocation or enhanced Myc expression into T-lymphoid progenitors may give rise to AML (Drynan et al., 2005; Riemke et al., 2016). These findings suggest that targeting of relevant mutations to ETPs might underlie a clinically distinct subgroup of T cell ALL, characterised by aberrant co-expression of myeloid, stem/progenitor and T cell genes: so-called ETP acute lymphoblastic leukemia (ETP-ALL) (Coustan-Smith et al., 2009), distinct from other biphenotypic leukemias.

ETP-ALL is therapy-resistant, with a transcriptional profile resembling normal ETPs (Coustan-Smith et al., 2009), and a mutational landscape distinct from other cases of T-ALL (Zhang et al., 2012a), with increased frequency of inactivating mutations of the transcription factor *RUNX1* and components of the polycomb repressive complex-2 (PRC2) including *EZH2*. Hemizygous mutations (mutation combined with deletion of the other allele), causing complete loss of function, have been shown to occur at quite high frequencies for both of these genes in ETP-ALL (3 of 10 *EZH2*-mutant patients and 2 of 10 *RUNX1*-mutant patients) (Zhang et al., 2012a). Furthermore, *EZH2* and *RUNX1* mutations co-occur more frequently than expected by chance in ETP-ALL (Zhang et al., 2012a). Cases of ETP-ALL are also associated with a high frequency of activating mutations of cytokine receptors and components of RAS signaling in comparison with other T-ALL cases. Whereas *FLT3* activating mutations, including internal tandem duplication (*FLT3-ITD*) mutations, are common in AML and rare in other subgroups of T-ALL, they are frequently seen in ETP-ALL (Zhang et al., 2012a).

Although established as a clinically and molecularly distinct disease entity (Zhang et al., 2012a), the implication that ETP-ALLs derive from targeting of relevant mutations to ETPs remains to be established, as only correlative gene expression and immunophenotypic findings support this (Coustan-Smith et al., 2009). Also, direct evidence that ETPs, which normally lack self-renewal, can propagate acute leukemia upon introduction of ETP leukemia relevant genetic lesions remains to be demonstrated. The proposed origin in lympho-myeloid restricted progenitors of leukemias that

aberrantly co-express lymphoid and myeloid antigens remains an attractive hypothesis, yet to be experimentally validated. While some ALL mouse models have recapitulated certain aspects of ETP-ALL (Danis et al., 2016; Goossens et al., 2015; Treanor et al., 2014; Yu et al., 2012), relevant genetic lesions have not been specifically targeted to early lympho-myeloid progenitors, including ETPs.

Results

Inactivation of Ezh2 and Runx1 Targeted to Early Lymphoid Progenitors Collaborate to Cause a Marked Expansion of ETPs

Mutations of *EZH2* and *RUNX1*, found in ETP leukemias, confer loss-of-function (Della Gatta et al., 2012; Zhang et al., 2012a). Pan-hematopoietic deletion, including in HSCs, of *Ezh2* and *Runx1* using *Mx1Cre* resulted in a highly penetrant and fatal myelodysplastic syndrome (MDS) phenotype, with severe pancytopenia (Figure S1A), as reported for *Ezh2* deletion combined with retroviral overexpression of a dominant-negative *Runx1*-mutant (Sashida et al., 2014). To target the early lymphoid/lympho-myeloid progenitor compartment (Boiers et al., 2013), we generated *Ezh2^{fl/fl};Runx1^{fl/fl};Rag1Cre⁺* double knockout (DKO) mice as well as *Ezh2^{fl/fl};Runx1^{+/-};Rag1Cre⁺* (*Ezh2* KO) and *Ezh2^{+/-};Runx1^{fl/fl};Rag1Cre⁺* (*Runx1* KO) single knockout, and *Rag1Cre⁻* wild-type (WT) controls (Figure 1A). This induced close to 100% recombination in Lin⁻CD4⁻CD8⁻CD44⁺CD25⁻Kit⁺Flt3⁺ ETPs, with no detectable deletion in the bone marrow (BM) Lin⁻Kit⁺Sca1⁺CD150⁺CD48⁻ HSC compartment (Kiel et al., 2005) (Figure S1B). At 6 weeks of age, DKO mice developed significant leucopenia (Figure 1B; $x0.52$; $p<0.001$) caused by loss of CD4⁺ and/or CD8⁺ T cells and CD19⁺ B cells (Figure 1C). A similar leucopenia was present in both *Ezh2* KO and *Runx1* KO mice, in keeping with a block in B and T cell differentiation in both *Runx1* and *Ezh2* knockout (Ichikawa et al., 2004; Su et al., 2003; Su et al., 2005). DKO as well as *Ezh2* KO and *Runx1* KO mice developed mild anemia (Figure 1B). Although loss of *Runx1* is associated with megakaryocyte maturation defects (Ichikawa et al., 2004), no significant impact on platelet counts were seen upon *Runx1* or *Ezh2* deletion (Figure 1B), in keeping with absence of *Rag1Cre*-induced deletion during megakaryocytic differentiation (Boiers et al., 2013).

Thymus cellularity was markedly reduced in DKO ($\times 0.062$; $p < 0.001$), Ezh2 KO and Runx1 KO mice (Figure 1D). Staging of thymocytes (Figures 1E and S1C) revealed a striking increase in absolute numbers of ETPs ($\times 12.3$; $p < 0.001$; Figure 1F) and Lin⁻CD4⁻CD8⁻CD44⁺CD25⁺ DN2 cells ($\times 8.3$; $p < 0.001$; Figure S1D); stages of thymocyte progenitors which sustain myeloid and T lineage potential (Bell and Bhandoola, 2008). This was not observed in Ezh2 KO or Runx1 KO mice. DN3 (Lin⁻CD4⁻CD8⁻CD44⁻CD25⁺), DN4 (Lin⁻CD4⁻CD8⁻CD44⁻CD25⁻) and DP (Lin⁻CD4⁺CD8⁺) thymocyte progenitors, which lack myeloid potential, were unaffected or reduced in DKO mice (Figure S1D; Figure 1G). These data are consistent with a selective expansion of ETPs in DKO mice and a block at the DN2 to DN3 transition. Analysis at 6 months of age revealed an even greater expansion of ETPs ($\times 17.9$; $P = 0.021$), despite reduced overall thymus cellularity ($\times 0.098$; $P < 0.001$; Figure S1E). However, DKO mice did not show any evidence of MDS or leukemia development over follow-up for 1 year (Figure 1H).

Disrupted Gene Expression Signatures in DKO ETPs Recapitulate Features of ETP Leukemia

Disrupted gene expression was assessed by RNA-sequencing of WT (n=4) and DKO (n=4) ETPs (GEO: GSE75185), revealing 306 significantly differentially expressed genes (Table S1). Most showed upregulation in DKO ETPs (n=238), as expected following inactivation of a component of PRC2, which plays a key role in repression of gene expression (Margueron and Reinberg, 2011). A smaller number of genes were downregulated in DKO ETPs (n=68). WT and DKO ETPs clustered separately (Figures 2A and S2A), and gene set enrichment analysis (GSEA) revealed upregulation of PRC2 target genes in DKO ETPs (Figure 2B). The expanded ETPs showed upregulation of HSC (Figures 2C and S2B) and myeloid (pre-GM; Figures 2D and S2C) gene expression, characteristic of ETP leukemias (Zhang et al., 2012a). Lymphoid gene expression showed a mixed picture with many genes showing minimal change or upregulation (Hey1, Rag2, Il2ra), and some downregulation (Blk, Tcf7) (Figure 2E). *Blk* and *Tcf7* are tumor suppressor genes in leukemia, with loss of *Tcf7* implicated in ETP leukemia (Yu et al.,

2012; Zhang et al., 2012a). Megakaryocyte/erythroid-associated gene expression is low in WT ETPs (Luc et al., 2012), and was not affected in DKO ETPs (pre-MegE; Figure S2D).

We confirmed differential expression of a number of genes by quantitative real-time PCR (qPCR) (Figures S2E-G). Gene ontology analysis revealed a striking enrichment of differentially expressed genes in signal transduction pathways (Figure S2H). Unbiased GSEA (Table S2) revealed upregulation of cytokine signaling pathways; IL2/STAT5 (Figure 2F), IL6/JAK/STAT3 (Figure 2G), KRAS (also reciprocal downregulation of negative transcriptional targets; Figure 2H) and interferon signaling (Figure S2I). JAK/STAT pathway-associated transcription is upregulated in ETP leukemia relative to mature T cell leukemias (Zhang et al., 2012a). Characteristic of ETP leukemia (Zhang et al., 2012a), there was no significant enrichment of Notch1 signaling-associated gene expression (Figure S2J).

Some differentially expressed genes e.g. *Arpp21*, *Cpa3* and *Mpl* only showed strongly dysregulated expression in the presence of both mutations (Figure 2I). In contrast, downregulation of some genes was largely mediated by *Runx1* inactivation, e.g. *Ly6d* and *Tcf7* (Figure 2J), known direct *Runx1* target genes (Niebuhr et al., 2013; Wu et al., 2012). Conversely, upregulation of JAK/STAT signaling pathway target gene *Cish* was primarily mediated by *Ezh2* (Figure 2K).

Analysis at the cell population level cannot determine whether aberrant gene expression occurs in cells co-expressing lymphoid and myeloid genes, characteristic of ETPs (Luc et al., 2012). Single cell gene expression analysis of ETPs (Figure 3A) revealed that the frequency and level of expression of lymphoid genes in DKO ETPs was equivalent to (*Notch1*, *Ikzf1*, *Il2ra*, *Il7r*, *Nrarp*) or greater than (*Rag1*, *Rag2*, *Gata3*) that seen in WT ETPs. Moreover, HSC and myeloid genes were more frequently expressed in DKO than WT ETPs (Figure 3A) and, crucially, increased expression of HSC (Figure 3B) and myeloid (Figure 3C) genes occurred in the same cells that retained expression of multiple lymphoid genes. HSC and myeloid genes were also co-expressed in the same cells in DKO mice

(Figure S3). Importantly, these aberrant combinatorial gene expression signatures, in particular expression of HSC-associated genes, were not present in WT ETPs. This supports that the observed abnormal gene expression occurs in *bona fide* ETPs, and is not a result of expansion of a pre-existing subpopulation present in thymuses of WT mice, or infiltration of the thymus by BM HSC/multipotent progenitor or myeloid progenitor populations.

Activating Flt3 Mutation Collaborates with Inactivating Ezh2 and Runx1 Mutations to Cause Acute Leukemia Propagated by ETPs

ETP leukemia has a high incidence of signaling pathway mutations such as *FLT3-ITDs* in comparison with more mature subtypes of T-ALL (Zhang et al., 2012a). Expanded ETPs in DKO mice, showing aberrant signaling pathway gene expression programmes, might therefore be susceptible to transformation by an additional, signaling pathway activating mutation.

Ezh2^{fl/fl};Runx1^{fl/fl};Rag1Cre⁺;Flt3^{ITD/+} (DKOITD) mice showed a similar expansion of ETPs as in DKO mice (x17.3; p<0.001) (Figure 4A), whereas in *Rag1Cre⁻;Flt3^{ITD/+}* (ITD) mice ETPs were non-significantly reduced (x0.051; p>0.05) (Mead et al., 2013). DKOITD mice developed a highly penetrant and aggressive acute leukemia associated with leucocytosis, anemia, thrombocytopenia and splenomegaly (Figures 4B-D and S4A-B).

Since latency of leukemia development was relatively short (median 65 days) and penetrance very high in DKOITD mice (Figure 4B), we reasoned that the combination of DKO with *Flt3-ITD* was likely to be sufficient to cause leukemia without the requirement for additional mutations. We performed whole exome sequencing on BM cells from eight DKOITD leukemias and two WT control mice. In order to identify somatic variants, we also performed sequencing on eight WT mice from another (unrelated) C57BL/6 mouse colony (Figure S4C). Identifying mutated genes with human orthologs and comparing those with the list of cancer-implicated genes in the Cancer Gene Census (<http://cancer.sanger.ac.uk/census>), we did not identify any somatically acquired leukemia-

associated mutations, or copy number alterations in any cancer-implicated genes (Table S3), supporting that the combination of *Ezh2* and *Runx1* inactivation with *Flt3-ITD* is sufficient for generating ETP leukemia.

Circulating leukemic cells expressed the myeloid marker Mac1 but not lymphoid surface markers (Figure 4E). BM cellularity was unchanged, but Kit⁺Mac1^{low} myeloid precursor cells were increased (x4.02; p<0.001; Figure S4D). DKOITD leukemias displayed a number of lymphoid phenotypic features. Surface expression of CD3 was lacking on Mac1⁺ leukemia cells in DKOITD BM (Figure S4E), but immunohistochemistry revealed intracellular CD3 and TdT expression in leukemic cells (Figure 4F). Cytoplasmic but not surface CD3 expression is characteristic of immature T cell progenitors and leukemias with immature T cell phenotype (Van Dongen et al., 1988). RNA-sequencing of Mac1⁺ BM cells from leukemic DKOITD mice (GEO: GSE75187) revealed a relative downregulation of myeloid programs (Figure 4G) and upregulation of early T cell associated gene expression (Figure 4H). Upregulated lymphoid genes included *Ccr7*, *CD7*, *Il7r*, *Id3*, *Il2ra* and *CD48* (Figure 4I). Stem/progenitor associated genes including *Flt3*, *CD34* and *Ly6a* were also upregulated (Figure 4J). Leukemia oncogenes were markedly overexpressed in Mac1⁺ leukemic cells (*Tspan3*, *Rasgrp1*, *Pvt1*, *Ccnd2*, *Hmgn1*; Figure S4F). To determine whether gene expression in these cells recapitulated human ETP leukemia, we used published datasets comparing ETP-ALL with non-ETP T-ALL (Zhang et al., 2012a). As an equivalent comparison for our model, we used published RNA-seq data from a Notch1 mutant-driven mouse T-ALL (Ntziachristos et al., 2014). GSEA showed that genes upregulated in human ETP-ALL were also upregulated in DKOITD Mac1⁺ BM cells relative to mouse Notch1 T-ALL (Figure 4K). Downregulated genes also strongly overlapped between these two comparisons (Figure 4K), confirming the relevance of this ETP leukemia mouse model for human ETP ALL.

DKOITD ETPs were more proliferative than WT or DKO ETPs *in vitro* (Figure 5A). While WT ETPs are incapable of long-term reconstitution upon transplantation (Luc et al., 2012), unenriched thymocytes transplanted from DKOITD mice resulted in acute leukemia (n=4; data not shown). We next transplanted purified CD45.2 ETPs, DN2 cells and CD4/CD8 double and/or single positive thymocytes (Figure 5B). Only DKOITD ETPs were capable of engrafting and propagating the leukemia (Figure 5C), when isolated from leukemic (n=1) and pre-leukemic (n=3) mice. Recipients showed the typical leukemic features of primary DKOITD mice with anemia, thrombocytopenia and leucocytosis (Figure 5D), blast and monocyte precursor morphology (Figure S5A) and intracellular CD3 (Figure 5E). Consistent with their ETP rather than HSC origin, transplanted CD45.2 DKOITD ETPs did not contribute to the HSC compartment (Figure 5F), although there was a marked suppression of WT CD45.1 competitor HSCs (x0.035; p=0.0065). In contrast, Lin⁻Sca1⁺Kit⁺Flt3^{high} LMPPs, a thymus-seeding progenitor population closely resembling ETPs (Luc et al., 2012), were expanded and almost exclusively DKOITD ETP-derived (x164; p=0.20). Concurrently, thymic ETPs were exclusively derived from transplanted ETPs, with progressively reduced contribution to downstream thymocytes (Figure S5B).

RNA-sequencing of ETPs from DKOITD mice (GEO: GSE75185) revealed 481 differentially expressed genes in comparison with WT ETPs and 31 in comparison with DKO ETPs (Table S4; Figures 6A-B). In keeping with the small number of differentially expressed genes, unsupervised hierarchical clustering did not clearly separate DKOITD from DKO ETPs (Figure S6A). Unsupervised GSEA showed enrichment of signaling pathway associated gene expression (Table S5) in comparison with WT ETPs. Furthermore, G2M checkpoint genes, thought to limit proliferation of pre-malignant cells (Lobrich and Jeggo, 2007), were markedly downregulated in DKOITD ETPs (Figure 6C and Table S5). QPCR showed further upregulation of signaling (Figure 6D), myeloid (Figure S6B) and HSC (Figure S6C) gene expression in DKOITD cells in comparison to WT and DKO ETPs. PCA of single cell gene expression data showed that the vast majority of DKOITD ETPs clustered together with DKO ETPs but separately

from WT ETPs and LMPPs of all genotypes (Figure S6D), supporting that leukemia-propagating DKOITD ETPs represent thymus-resident progenitors, closely related to DKO ETPs, rather than a population of leukemic cells from DKOITD BM having infiltrated the thymus. WT and DKO HSCs also clustered together, in keeping with the lack of deletion of *Ezh2* and *Runx1* in HSCs (DKOITD HSCs were not analysed owing to their rarity (Figure 5F)). Further, DKO and DKOITD ETPs clustered separately from WT ETPs, in contrast to LMPPs which overlapped in WT, DKO and DKOITD mice (Figure S6D). Importantly, disease propagating DKOITD ETPs showed marked enrichment for signatures characteristic of human ETP-ALL (Figures 6E and S6E).

To further substantiate the importance of RAS pathway signaling, we performed phospho-flow analysis on Lin⁺Kit⁺ BM progenitor cells (ETPs were too rare to be analysed using this method). Phosphorylation of the S6 ribosomal protein, upregulated in response to RAS pathway signaling (Roux et al., 2007), was increased in DKOITD cells (Figure 6F). In contrast, *Flt3-ITD* alone only had a minor effect on the phospho-S6 level. This increased signaling could be reversed using the MEK inhibitor PD-901 (Figure 6G), demonstrating specific enhancement of signaling via the RAS pathway in DKOITD cells. Therefore, deletion of *Ezh2* and *Runx1* act synergistically with a constitutive signaling mutation such as *Flt3-ITD* to increase RAS pathway signaling in an *in vivo* model of ETP ALL.

BET Inhibition Reverses Gene Expression Changes Associated with Loss of PRC2 Function and Inhibits Proliferation of ETP-Propagated Leukemia Cells

A study of peripheral nerve sheath tumors showed that aberrant upregulation of RAS pathway signaling is enhanced by inactivation of PRC2, due to PRC2 inactivation-associated loss of the H3K27me3 repressive histone mark leading to a consequential increase in H3K27ac, and activation of gene transcription via recruitment of the bromodomain and extra terminal (BET) proteins (De Raedt et al., 2014). Such tumors are sensitive to BET protein inhibition. We compared ChIP-seq analysis for H3K27me3 and H3K27ac on BM cells from DKOITD and WT mice (GEO: GSE100693) with

RNA-seq data from Mac1⁺ BM cells (Figures 7A, S7A and Table S6). We first established gene loci that showed significantly increased or decreased presence of H3K27me3 or H3K27ac at the transcription start site in DKOITD relative to WT cells (Table S6). There was an overall loss of H3K27me3 at transcription start sites genome-wide, and genes showing a significant loss of H3K27me3 at the transcription start site showed a reciprocal gain in H3K27ac (Figures 7B and S7B). We compared genes showing both loss of H3K27me3 and gain of H3K27ac in DKOITD compared to WT BM cells with differentially expressed genes by RNA-seq in DKOITD relative to WT BM (Figures 7C-D and S7C). The *Flt3* gene locus showed clear loss of H3K27me3 and gain of H3K27ac (Figure 7D), corresponding to a marked upregulation in *Flt3* gene expression (Figure 4J). This illustrates how loss of H3K27me3 associated gene repression can lead to over-expression of oncogenic mutations, promoting leukemogenesis. Loss of H3K27me3 and gain of H3K27ac was associated with marked upregulation of gene expression across all genes (Figure 7E). Genes showing both reduced H3K27me3 and increased H3K27ac overlapped significantly with genes showing upregulated expression ($p=1.16 \times 10^{-22}$). These results confirm that *EZH2* inactivation-associated epigenetic changes directly lead to aberrant upregulation of relevant gene transcription in this ETP leukemia mouse model.

We next performed RNA-seq and ChIP-seq experiments in the human LOUCY cell line (experimental outline Figure S7D; GSE100694). Although originating from before the disease entity was formally recognised, LOUCY cells show an ETP-ALL gene expression signature and were likely derived from an ETP-ALL patient (Van Vlierberghe et al., 2011). In agreement, we confirmed upregulation of ETP-ALL associated gene expression in LOUCY cells in comparison with the mature T-ALL cell line JURKAT (Figure S7E). Notably, LOUCY cells do not express *EZH2* and show minimal H3K27me3 genome-wide (Figure S7F). RNA-seq analysis demonstrated that LOUCY cells clustered separately from JURKAT cells and that treatment with the BET inhibitors JQ1 and I-BET151 led to similar changes in gene expression, with treated LOUCY cells reproducibly clustering separately from untreated cells (Figure 7F). BET inhibition in LOUCY cells caused marked downregulation of genes showing H3K27ac at the

transcription start site (Figure 7G). Genes downregulated following BET inhibition included MYC, KRAS and JAK-STAT pathways (Figure 7H and Table S7). Genes highly upregulated in DKOITD (ETPs and/or Mac1⁺ BM cells) were also enriched among genes downregulated by BET inhibition in LOUCY cells (Figure 7I). One of these, which was not expressed at all in JURKAT, was the HSC-related gene MPL (Log2FC=-1.91, FDR=4.03x10⁻⁹). This was one of the most significantly upregulated genes in both DKO and DKOITD relative to WT ETPs (Figure 2A and Tables S1 and S4), and was therefore selected for further study in the mouse lympho-myeloid progenitor cell line EML. Using ChIP-qPCR we found that drug-mediated Ezh2 inhibition resulted in loss of H3K27me3 and a corresponding increase in H3K27ac at the *Mpl* locus (Figure 7J). This was associated with increased expression, an effect fully reversed by JQ1 treatment (Figure 7K).

Together, these results establish that upregulated oncogenic gene expression resulting from epigenetic changes induced by loss of *EZH2*, in both mouse and human ETP leukemias, can be reversed by BET inhibition.

We next assessed whether BET inhibitors were effective against DKOITD leukemia. DKOITD leukemia-propagating ETPs were highly sensitive to JQ1 *in vitro* (Figures 8A and S8A). Observed IC₅₀ values were comparable to those for human cell lines reported to be sensitive to JQ1 (NB4, HL-60 and THP-1), in comparison to known resistant cell lines (JURKAT and K562; Figure S8B) (Zuber et al., 2011). The inhibitory effect of both JQ1 (Figure 8B) and I-BET151 (Figure S8C) was significantly greater on Lin⁻Kit⁺ BM progenitors from leukemic DKOITD ETP transplant recipient mice than from WT BM. Mice transplanted with BM cells from DKOITD mice were next treated with JQ1 *in vivo*. JQ1 treatment significantly reduced tumor burden, as measured by peripheral blood leukocyte counts, and BM and spleen cellularity (Figure 8C), findings replicated with I-BET151 (Figure S8D).

LOUCY cells were also highly sensitive to both JQ1 (Figure 8D) and I-BET151 (Figure S8E) treatment. We next tested two ETP-ALL samples derived from separate patients (Maude et al., 2015), both carrying inactivating mutations in PRC2 components, one in *EZH2* as well as *RUNX1* (ETP-ALL 12), and the other in *EED* (ETP-ALL 13) (see STAR Methods). These showed higher sensitivity to both JQ1 (Figure 8E) and I-BET151 (Figure S8F) inhibition *in vitro* compared to the three tested non-ETP T-ALL samples. We transplanted these PRC2-mutant ETP-ALLs into immunodeficient NSG mice, and started treatment with either DMSO or JQ1 *in vivo* upon confirmation of engraftment. JQ1 treatment markedly inhibited progression of *EZH2* and *RUNX1*-mutant ETP leukemia (Figure 8F), with significantly reduced leukocyte counts and human cell chimerism in BM and spleen. This was accompanied by a relative preservation of normal hematopoiesis in BM and spleen, supporting that JQ1 was selectively targeting human ETP leukemia cells whilst preserving normal mouse hematopoietic cells. We obtained similar data from the *EED*-mutant ETP leukemia (Figure 8G), where JQ1 treatment completely halted leukemia progression and strongly reduced human cell composition of the blood leukocytes, BM and spleen.

Collectively, these data support that ETP-propagated PRC2-deficient leukemia is sensitive to BET inhibition, providing experimental support for an approach to treat ETP leukemia associated with loss of PRC2 function.

Discussion

While there is compelling evidence that HSCs, which already possess intrinsic self-renewal potential, might represent the only LSCs in chronic myeloid malignancies (Woll et al., 2014), there is less definitive evidence for the hypothesis that progenitors which normally lack extensive self-renewal potential might be the primary target of recurrent leukemogenic mutations, becoming LSCs, in acute leukemias (Magee et al., 2012).

The hypothesis for an ETP origin and LSC identity in ETP-ALL is primarily based on a similar gene expression signature of leukemic cells from ETP-ALL cases, to that of normal mouse ETPs (Coustan-Smith et al., 2009). However, whether thymus-residing ETPs with sustained lympho-myeloid potential (Bell and Bhandoola, 2008; Luc et al., 2012) are susceptible to transformation by ETP leukemia associated mutations has yet to be established. We herein demonstrate that *Rag1Cre*-mediated targeting of *Ezh2* and *Runx1* inactivation to early lympho-myeloid progenitors, including ETPs (but excluding HSCs and multipotent progenitors), causes a marked expansion of stringently defined ETPs (Luc et al., 2012), with a loss of later stages of thymocyte development. Importantly, inactivation of *Ezh2* or *Runx1* individually had no impact on ETP numbers, helping to explain why the presence of these two mutations is positively correlated in human ETP leukemias (Zhang et al., 2012a). Selectivity of targeting of these mutations to early lympho-myeloid progenitors was confirmed by lack of deletion in HSCs, and by the distinct impact of HSC-targeted deletion of *Ezh2* and *Runx1* using Mx1-Cre, which instead caused a MDS phenotype. In contrast, expanded “pre-leukemic” ETPs in *Rag1Cre*-induced DKO mice showed gene expression changes reminiscent of ETP leukemias, with upregulation of myeloid, HSC and cytokine signaling-associated gene expression. Single-cell gene expression analysis revealed co-expression of lymphoid and myeloid genes, characteristic of ETPs, with aberrant expression of HSC associated genes, helping to explain how inactivation of *Ezh2* and *Runx1* contributes towards establishment of pre-LSC potential in *bona fide* ETPs.

We reasoned that pre-leukemic DKO ETPs might be susceptible to additional mutations causing constitutive activation of signaling pathways, as frequently observed in ETP leukemia (Zhang et al., 2012a). While rare in other T cell leukemias, *FLT3* activating mutations occur quite frequently in ETP leukemias (around 14% of cases) (Zhang et al., 2012a). DKOITD mice developed a highly penetrant, aggressive acute leukemia with co-expression of myeloid and T-lymphoid lineage programs. Exome sequencing analysis, and the high penetrance and short latency of disease, support that the

combination of *Ezh2* and *Runx1* inactivation with *Flt3-ITD* is sufficient to induce this leukemia phenotype. Purified DKOITD ETPs fulfilled the LSC definition, by establishing and propagating the same type of leukemia upon transplantation, whereas other thymic progenitors had no LSC potential. DKOITD ETPs downregulated multiple G2M checkpoint genes that might otherwise have limited the proliferation of pre-malignant DKO ETPs (Lobrich and Jeggo, 2007). DKOITD ETPs also showed aberrant gene expression programmes closely paralleling those seen in human ETP leukemia. These findings provide evidence supporting that ETPs carrying a combination of ETP leukemia-associated mutations can act as LSCs and establish and propagate a lympho-myeloid leukemia *in vivo*.

Phospho-flow analysis established that DKOITD Lin⁻Kit⁺ stem/progenitor cells show greatly enhanced RAS pathway signaling compared to those from DKO and ITD mice. Combined with our gene expression data, these findings suggest that *Ezh2* and *Runx1* deletion establishes an altered transcriptional environment which increases RAS pathway-associated transcription, but only increases RAS signaling to a small extent. The additional hit of *Flt3-ITD* further increases RAS pathway signaling and proliferation, dependent on the altered transcription established by *Ezh2* and *Runx1*. This may help to explain why as many as 67% of ETP-ALLs carry mutations in signaling pathway components such as *FLT3-ITD*, and that these are often combined with mutations in genes involved in epigenetic and transcriptional regulation, such as *EZH2* and *RUNX1* (Zhang et al., 2012a).

Previous mouse models, although displaying some features compatible with ETP-ALL, have not targeted relevant mutations specifically to ETPs rather than HSCs, nor observed the expected expansion of carefully defined ETPs, nor performed the critical experiments to establish the LSC potential of ETPs (Danis et al., 2016; Goossens et al., 2015; Treanor et al., 2014; Yu et al., 2012). In the present studies, when transplanted into recipient mice, ETP-LSCs propagated an aggressive lympho-myeloid leukemia with a severe suppression of normal HSCs and expansion of BM-residing

LMPPs and thymic ETPs. These data provide definitive evidence for the leukemia-*propagating* potential of ETPs targeted with ETP-ALL relevant mutations, and are also compatible with *initiation* of ETP leukemia in the ETP population itself. Initiation of ETP leukemia may also occur in common lymphoid progenitors or the closely-related BM LMPPs, representing thymus-seeding progenitors which upon thymus entry become ETPs (Bell and Bhandoola, 2008; Luc et al., 2012). However, single cell gene expression analysis indicated that the key impact of *Ezh2* and *Runx1* inactivation in our mouse model was on thymus-residing ETPs and not LMPPs, as DKO LMPPs clustered close to WT LMPPs, in contrast to DKO ETPs and WT ETPs which formed highly distinct clusters. While the physiological relevance of the sustained myeloid lineage potential of ETPs and LMPPs remains unclear, our data support the possibility that it underlies the lympho-myeloid phenotype of ETP leukemias. This is also of possible broader relevance for the cell of origin of the distinct clinical entity of biphenotypic leukemias, which also show co-expression of lymphoid and myeloid antigens (Matutes et al., 2011), but for which the cell of origin remains to be established. The myeloid phenotype might also be promoted by mutations such as *FLT3-ITD*, which enhance myeloid differentiation bias of MPPs (Mead et al., 2013).

Our findings also support BET inhibition as a promising therapeutic approach for ETP leukemia. In solid tumors, recent evidence indicates that loss of PRC2 function is associated with aberrant upregulation of RAS pathway signaling, which collaborates with other mutations causing constitutive signaling to promote tumor growth. This renders such tumors sensitive to BET inhibition (De Raedt et al., 2014). Here, we obtained a number of lines of evidence that *Ezh2* mutation-associated loss of H3K27me3 results in the gain of H3K27ac that underlies the aberrant transcriptional programmes in mouse and human PRC2-inactivated ETP leukemia. This aberrant transcription could be reversed with BET inhibitors. Notably, the *Flt3* gene locus showed marked loss of H3K27me3 and gain of H3K27ac in DKOITD BM, which correlated with strongly upregulated *Flt3* expression. This helps to

explain the synergy between DKO and *Flt3-ITD*, as loss of *Ezh2* function in DKO mice drives increased expression of the oncogenic signaling by *Flt3-ITD* in this model.

We further demonstrated that primary mouse DKOITD ETP leukemias, a human ETP leukemia cell line associated with *EZH2* loss of function, as well as patient-derived ETP leukemia xenografts carrying PRC2 loss-of-function mutations were all highly sensitive to BET inhibition both *in vitro* and *in vivo*. Crucially, *in vivo* treatment selectively targeted the ETP leukemia cells whilst leaving normal hematopoietic cells relatively intact. Intriguingly, in an MLL-AF9 driven AML model, it has recently been shown that suppression of the PRC2 complex promotes BET inhibitor resistance in AML (Rathert et al., 2015), suggesting that the cellular context in which PRC2 inactivation occurs might be crucial. For example, whilst *EZH2* inactivating mutations occur in ETP leukemia, MLL associated leukemias frequently overexpress *EZH2* and are susceptible to *EZH2* inhibition (Neff et al., 2012). This clearly illustrates that the impact of *EZH2* inactivation is highly dependent on the targeted cell type and the presence of collaborating mutations, and consequently that findings in one model system cannot be extrapolated to other contexts without careful validation.

In summary, the current work has revealed a pronounced impact of combined inactivating mutations of *Ezh2* and *Runx1* on early thymocyte development, leading to a marked expansion of ETPs and subsequent differentiation block. This, together with a *Flt3-ITD* signaling mutation, results in establishment of ETP-LSCs which can propagate an aggressive lympho-myeloid leukemia. These findings provide new evidence directly linking the phenotype of a malignant disease with the progenitor cell of origin, in this case the development of a lympho-myeloid leukemia due to initiating mutations occurring within a lympho-myeloid progenitor population. In addition, this mouse model also provides support for exploring BET inhibition as a therapeutic strategy in PRC2-inactivated human ETP leukemias, which frequently show resistance to conventional therapeutic approaches.

Acknowledgments

The authors thank the BMS, Oxford University for technical assistance and David Lugo for design, preparation and supply and I-BET151 feed. This work was funded by a Kay Kendall Leukaemia Fund Project Grant (KKL811), a Medical Research Council Senior Clinical Fellowship (MR/L006340/1) to AJM, and a MRC Unit Grant MC_UU_12009/5 and an international recruitment grant from the Swedish Research Council to SEWJ, a MRC-funded Oxford Consortium for Single-cell Biology (MR/M00919X/1) and the Oxford NIHR Biomedical Centre based at Oxford University Hospitals NHS Trust and University of Oxford. The views expressed are those of the author(s) and not necessarily those of the NHS, the NIHR, the Department of Health or the NIH. The authors acknowledge the contributions of the WIMM Flow Cytometry Facility, supported by the MRC HIU; MRC MHU (MC_UU_12009); NIHR Oxford BRC and John Fell Fund (131/030 and 101/517), the EPA fund (CF182 and CF170) and by the WIMM Strategic Alliance awards G0902418 and MC_UU_12025. NA was supported by the Oxford-Wellcome Trust Institutional Strategic Support Fund.

Author Contributions

CAGB performed experiments, analysed the data and helped to write the manuscript. NB analysed and interpreted data. WHN, HB, EJS, AG, NA, JC, LJ, DA and TBJ conducted experiments and analysed data. TAM helped advise on experimental design. DTT provided patient-derived xenograft samples. NF and EP analysed exome sequencing data. GG, RKP and BJPH performed I-BET *in vivo* experiments and helped advise on experimental design. SEWJ and AJM conceived, designed and supervised the research, analysed the data and wrote the manuscript.

Declaration of Interests

The authors declare no competing interests. RKP is an employee and shareholder of GlaxoSmithKline. TAM and SEWJ are founding shareholders of OxStem Oncology, a subsidiary company of OxStem Ltd.

References

- Adolfsson, J., Mansson, R., Buza-Vidas, N., Hultquist, A., Liuba, K., Jensen, C. T., Bryder, D., Yang, L., Borge, O. J., Thoren, L. A., *et al.* (2005). Identification of Flt3+ lympho-myeloid stem cells lacking erythro-megakaryocytic potential: a revised road map for adult blood lineage commitment. *Cell* **121**, 295-306.
- Bell, J. J., and Bhandoola, A. (2008). The earliest thymic progenitors for T cells possess myeloid lineage potential. *Nature* **452**, 764-767.
- Boiers, C., Carrelha, J., Lutteropp, M., Luc, S., Green, J. C., Azzoni, E., Woll, P. S., Mead, A. J., Hultquist, A., Swiers, G., *et al.* (2013). Lymphomyeloid contribution of an immune-restricted progenitor emerging prior to definitive hematopoietic stem cells. *Cell Stem Cell* **13**, 535-548.
- Coustan-Smith, E., Mullighan, C. G., Onciu, M., Behm, F. G., Raimondi, S. C., Pei, D., Cheng, C., Su, X., Rubnitz, J. E., Basso, G., *et al.* (2009). Early T-cell precursor leukaemia: a subtype of very high-risk acute lymphoblastic leukaemia. *Lancet Oncol* **10**, 147-156.
- Danis, E., Yamauchi, T., Echanique, K., Zhang, X., Haladyna, J. N., Riedel, S. S., Zhu, N., Xie, H., Orkin, S. H., Armstrong, S. A., *et al.* (2016). Ezh2 Controls an Early Hematopoietic Program and Growth and Survival Signaling in Early T Cell Precursor Acute Lymphoblastic Leukemia. *Cell Rep* **14**, 1953-1965.
- De Raedt, T., Beert, E., Pasmant, E., Luscan, A., Brems, H., Ortonne, N., Helin, K., Hornick, J. L., Mautner, V., Kehrer-Sawatzki, H., *et al.* (2014). PRC2 loss amplifies Ras-driven transcription and confers sensitivity to BRD4-based therapies. *Nature* **514**, 247-251.
- Della Gatta, G., Palomero, T., Perez-Garcia, A., Ambesi-Impiombato, A., Bansal, M., Carpenter, Z. W., De Keersmaecker, K., Sole, X., Xu, L., Paietta, E., *et al.* (2012). Reverse engineering of TLX oncogenic transcriptional networks identifies RUNX1 as tumor suppressor in T-ALL. *Nat Med* **18**, 436-440.
- Dorantes-Acosta, E., and Pelayo, R. (2012). Lineage switching in acute leukemias: a consequence of stem cell plasticity? *Bone Marrow Res* **2012**, 406796.

Drynan, L. F., Pannell, R., Forster, A., Chan, N. M., Cano, F., Daser, A., and Rabbitts, T. H. (2005). Mll fusions generated by Cre-loxP-mediated de novo translocations can induce lineage reassignment in tumorigenesis. *EMBO J* 24, 3136-3146.

Goardon, N., Marchi, E., Atzberger, A., Quek, L., Schuh, A., Soneji, S., Woll, P., Mead, A., Alford, K. A., Rout, R., *et al.* (2011). Coexistence of LMPP-like and GMP-like leukemia stem cells in acute myeloid leukemia. *Cancer Cell* 19, 138-152.

Goossens, S., Radaelli, E., Blanchet, O., Durinck, K., Van der Meulen, J., Peirs, S., Taghon, T., Tremblay, C. S., Costa, M., Farhang Ghahremani, M., *et al.* (2015). ZEB2 drives immature T-cell lymphoblastic leukaemia development via enhanced tumour-initiating potential and IL-7 receptor signalling. *Nat Commun* 6, 5794.

Growney, J. D., Shigematsu, H., Li, Z., Lee, B. H., Adelsperger, J., Rowan, R., Curley, D. P., Kutok, J. L., Akashi, K., Williams, I. R., *et al.* (2005). Loss of Runx1 perturbs adult hematopoiesis and is associated with a myeloproliferative phenotype. *Blood* 106, 494-504.

Ichikawa, M., Asai, T., Saito, T., Seo, S., Yamazaki, I., Yamagata, T., Mitani, K., Chiba, S., Ogawa, S., Kurokawa, M., and Hirai, H. (2004). AML-1 is required for megakaryocytic maturation and lymphocytic differentiation, but not for maintenance of hematopoietic stem cells in adult hematopoiesis. *Nat Med* 10, 299-304.

Kiel, M. J., Yilmaz, O. H., Iwashita, T., Terhorst, C., and Morrison, S. J. (2005). SLAM family receptors distinguish hematopoietic stem and progenitor cells and reveal endothelial niches for stem cells. *Cell* 121, 1109-1121.

Laiosa, C. V., Stadtfeld, M., Xie, H., de Andres-Aguayo, L., and Graf, T. (2006). Reprogramming of committed T cell progenitors to macrophages and dendritic cells by C/EBP alpha and PU.1 transcription factors. *Immunity* 25, 731-744.

Lee, B. H., Tothova, Z., Levine, R. L., Anderson, K., Buza-Vidas, N., Cullen, D. E., McDowell, E. P., Adelsperger, J., Frohling, S., Huntly, B. J., *et al.* (2007). FLT3 mutations confer enhanced proliferation

and survival properties to multipotent progenitors in a murine model of chronic myelomonocytic leukemia. *Cancer Cell* 12, 367-380.

Lobrich, M., and Jeggo, P. A. (2007). The impact of a negligent G2/M checkpoint on genomic instability and cancer induction. *Nat Rev Cancer* 7, 861-869.

Luc, S., Luis, T. C., Boukarabila, H., Macaulay, I. C., Buza-Vidas, N., Bouriez-Jones, T., Lutteropp, M., Woll, P. S., Loughran, S. J., Mead, A. J., *et al.* (2012). The earliest thymic T cell progenitors sustain B cell and myeloid lineage potential. *Nat Immunol* 13, 412-419.

Magee, J. A., Piskounova, E., and Morrison, S. J. (2012). Cancer stem cells: impact, heterogeneity, and uncertainty. *Cancer Cell* 21, 283-296.

Margueron, R., and Reinberg, D. (2011). The Polycomb complex PRC2 and its mark in life. *Nature* 469, 343-349.

Matutes, E., Pickl, W. F., van't Veer, M., Morilla, R., Swansbury, J., Strobl, H., Attarbaschi, A., Hopfinger, G., Ashley, S., Bene, M. C., *et al.* (2011). Mixed-phenotype acute leukemia: clinical and laboratory features and outcome in 100 patients defined according to the WHO 2008 classification. *Blood* 117, 3163-3171.

Maude, S. L., Dolai, S., Delgado-Martin, C., Vincent, T., Robbins, A., Selvanathan, A., Ryan, T., Hall, J., Wood, A. C., Tasian, S. K., *et al.* (2015). Efficacy of JAK/STAT pathway inhibition in murine xenograft models of early T-cell precursor (ETP) acute lymphoblastic leukemia. *Blood* 125, 1759-1767.

McCormack, M. P., Forster, A., Drynan, L., Pannell, R., and Rabbitts, T. H. (2003). The LMO2 T-cell oncogene is activated via chromosomal translocations or retroviral insertion during gene therapy but has no mandatory role in normal T-cell development. *Mol Cell Biol* 23, 9003-9013.

Mead, A. J., Kharazi, S., Atkinson, D., Macaulay, I., Pecquet, C., Loughran, S., Lutteropp, M., Woll, P., Chowdhury, O., Luc, S., *et al.* (2013). FLT3-ITDs instruct a myeloid differentiation and transformation bias in lymphomyeloid multipotent progenitors. *Cell Rep* 3, 1766-1776.

Milne, T. A., Zhao, K., and Hess, J. L. (2009). Chromatin immunoprecipitation (ChIP) for analysis of histone modifications and chromatin-associated proteins. *Methods Mol Biol* 538, 409-423.

Neff, T., Sinha, A. U., Kluk, M. J., Zhu, N., Khattab, M. H., Stein, L., Xie, H., Orkin, S. H., and Armstrong, S. A. (2012). Polycomb repressive complex 2 is required for MLL-AF9 leukemia. *Proc Natl Acad Sci U S A* 109, 5028-5033.

Niebuhr, B., Kriebitzsch, N., Fischer, M., Behrens, K., Gunther, T., Alawi, M., Bergholz, U., Muller, U., Roscher, S., Ziegler, M., *et al.* (2013). Runx1 is essential at two stages of early murine B-cell development. *Blood* 122, 413-423.

Ntziachristos, P., Tsirigos, A., Welstead, G. G., Trimarchi, T., Bakogianni, S., Xu, L., Loizou, E., Holmfeldt, L., Strikoudis, A., King, B., *et al.* (2014). Contrasting roles of histone 3 lysine 27 demethylases in acute lymphoblastic leukaemia. *Nature* 514, 513-517.

Picelli, S., Faridani, O. R., Björklund, Å. K., Winberg, G., Sagasser, S., and Sandberg, R. (2014). Full-length RNA-seq from single cells using Smart-seq2. *Nat Protocols* 9, 171-181.

Rathert, P., Roth, M., Neumann, T., Muerdter, F., Roe, J. S., Muhar, M., Deswal, S., Cerny-Reiterer, S., Peter, B., Jude, J., *et al.* (2015). Transcriptional plasticity promotes primary and acquired resistance to BET inhibition. *Nature* 525, 543-547.

Riemke, P., Czeh, M., Fischer, J., Walter, C., Ghani, S., Zepper, M., Agelopoulos, K., Lettermann, S., Gebhardt, M. L., Mah, N., *et al.* (2016). Myeloid leukemia with transdifferentiation plasticity developing from T-cell progenitors. *EMBO J* 35, 2399-2416.

Roux, P. P., Shahbazian, D., Vu, H., Holz, M. K., Cohen, M. S., Taunton, J., Sonenberg, N., and Blenis, J. (2007). RAS/ERK signaling promotes site-specific ribosomal protein S6 phosphorylation via RSK and stimulates cap-dependent translation. *J Biol Chem* 282, 14056-14064.

Sanjuan-Pla, A., Macaulay, I. C., Jensen, C. T., Woll, P. S., Luis, T. C., Mead, A., Moore, S., Carella, C., Matsuoka, S., Bouriez Jones, T., *et al.* (2013). Platelet-biased stem cells reside at the apex of the haematopoietic stem-cell hierarchy. *Nature* 502, 232-236.

Sashida, G., Harada, H., Matsui, H., Oshima, M., Yui, M., Harada, Y., Tanaka, S., Mochizuki-Kashio, M., Wang, C., Saraya, A., *et al.* (2014). Ezh2 loss promotes development of myelodysplastic syndrome but attenuates its predisposition to leukaemic transformation. *Nat Commun* 5, 4177.

Schlenner, S. M., and Rodewald, H. R. (2010). Early T cell development and the pitfalls of potential. *Trends Immunol* 31, 303-310.

Shlush, L. I., Zandi, S., Mitchell, A., Chen, W. C., Brandwein, J. M., Gupta, V., Kennedy, J. A., Schimmer, A. D., Schuh, A. C., Yee, K. W., *et al.* (2014). Identification of pre-leukaemic haematopoietic stem cells in acute leukaemia. *Nature* 506, 328-333.

Su, I. H., Basavaraj, A., Krutchinsky, A. N., Hobert, O., Ullrich, A., Chait, B. T., and Tarakhovsky, A. (2003). Ezh2 controls B cell development through histone H3 methylation and Igh rearrangement. *Nat Immunol* 4, 124-131.

Su, I. H., Dobenecker, M. W., Dickinson, E., Oser, M., Basavaraj, A., Marqueron, R., Viale, A., Reinberg, D., Wulfig, C., and Tarakhovsky, A. (2005). Polycomb group protein ezh2 controls actin polymerization and cell signaling. *Cell* 121, 425-436.

Treanor, L. M., Zhou, S., Janke, L., Churchman, M. L., Ma, Z., Lu, T., Chen, S. C., Mullighan, C. G., and Sorrentino, B. P. (2014). Interleukin-7 receptor mutants initiate early T cell precursor leukemia in murine thymocyte progenitors with multipotent potential. *J Exp Med* 211, 701-713.

Van Dongen, J. J., Krissansen, G. W., Wolvers-Tettero, I. L., Comans-Bitter, W. M., Adriaansen, H. J., Hooijkaas, H., Van Wering, E. R., and Terhorst, C. (1988). Cytoplasmic expression of the CD3 antigen as a diagnostic marker for immature T-cell malignancies. *Blood* 71, 603-612.

Van Vlierberghe, P., Ambesi-Impimbato, A., Perez-Garcia, A., Haydu, J. E., Rigo, I., Hadler, M., Tosello, V., Della Gatta, G., Paietta, E., Racevskis, J., *et al.* (2011). ETV6 mutations in early immature human T cell leukemias. *J Exp Med* 208, 2571-2579.

Woll, Petter S., Kjällquist, U., Chowdhury, O., Doolittle, H., Wedge, David C., Thongjuea, S., Erlandsson, R., Ngara, M., Anderson, K., Deng, Q., *et al.* (2014). Myelodysplastic Syndromes Are Propagated by Rare and Distinct Human Cancer Stem Cells In Vivo. *Cancer Cell* 25, 794-808.

Wu, J. Q., Seay, M., Schulz, V. P., Hariharan, M., Tuck, D., Lian, J., Du, J., Shi, M., Ye, Z., Gerstein, M., *et al.* (2012). Tcf7 is an important regulator of the switch of self-renewal and differentiation in a multipotential hematopoietic cell line. *PLoS Genet* 8, e1002565.

Yu, S., Zhou, X., Steinke, F. C., Liu, C., Chen, S. C., Zagorodna, O., Jing, X., Yokota, Y., Meyerholz, D. K., Mullighan, C. G., *et al.* (2012). The TCF-1 and LEF-1 transcription factors have cooperative and opposing roles in T cell development and malignancy. *Immunity* 37, 813-826.

Zhang, J., Ding, L., Holmfeldt, L., Wu, G., Heatley, S. L., Payne-Turner, D., Easton, J., Chen, X., Wang, J., Rusch, M., *et al.* (2012a). The genetic basis of early T-cell precursor acute lymphoblastic leukaemia. *Nature* 481, 157-163.

Zhang, J. A., Mortazavi, A., Williams, B. A., Wold, B. J., and Rothenberg, E. V. (2012b). Dynamic transformations of genome-wide epigenetic marking and transcriptional control establish T cell identity. *Cell* 149, 467-482.

Zuber, J., Shi, J., Wang, E., Rappaport, A. R., Herrmann, H., Sison, E. A., Magoon, D., Qi, J., Blatt, K., Wunderlich, M., *et al.* (2011). RNAi screen identifies Brd4 as a therapeutic target in acute myeloid leukaemia. *Nature* 478, 524-528.

Figure Legends

Figure 1: Inactivation of Ezh2 and Runx1 Targeted to Early Lymphoid Progenitors Collaborate to Cause a Marked Expansion of ETPs

(A) Experimental design. DKO = double knockout. (B) Hematological parameters, 6-8 week old mice (WT n=25, Ezh2 KO n=13, Runx1 KO n=6, DKO n=12). FC; Fold Change. (C) FACS analysis of absolute numbers of CD19⁺ (B cell), CD4⁺ and/or CD8⁺ (T cells) and Mac1⁺ (myeloid cells) cells per ml blood (WT n=9, Ezh2 KO n=4, Runx1 KO n=4, DKO n=5). (D) Total thymus cellularity (WT n=26, Ezh2 KO n=9, Runx1 KO n=10, DKO n=18). (E) Representative FACS plots. Figures represent mean percentage of total thymocytes falling into each gate across all experiments. (F) FACS analysis of absolute numbers of Lin⁻CD4⁻CD8⁻CD44⁺CD25⁻Kit⁺Flt3⁺ ETPs per thymus (WT n=26, Ezh2 KO n=9, Runx1 KO n=10, DKO n=18). (G) Line chart illustrating relative proportion of indicated thymocyte progenitor populations relative to WT mice. (H) Leukemia-free survival curves for WT, Ezh2 KO, Runx1 KO and DKO mice. X-axis represents age of the mice. Significance tested by log-rank test. p values by ANOVA (B-F),

* $p < 0.05$, ** $p < 0.01$ and *** $p < 0.001$. n.s.; not significant ($p > 0.05$). Bars and horizontal lines show mean \pm SEM. See also Figure S1.

Figure 2: Disrupted Gene Expression Signatures in DKO ETPs Recapitulate Features of ETP Leukemia

(A) Hierarchical clustering and heatmap showing expression levels, scaled per gene, of the 50 most significantly differentially expressed genes between WT and DKO ETPs (WT $n=4$, DKO $n=4$). Each replicate represents 100 purified ETPs from individual mice at 6-8 weeks of age. (B) GSEA comparing WT and DKO ETPs for PRC2 target genes. (C-E) Expression relative to WT of HSC (C), myeloid (D) and lymphoid-associated genes (E) in DKO ETPs by RNA-sequencing. (F-H) GSEA plots comparing WT and DKO ETPs for Il2-Stat5 signaling genes (F), Il6-Jak-Stat3 signaling genes (G) and Kras signaling genes (H) (upregulated genes top panel and downregulated genes bottom panel). (I-K) Relative expression of indicated genes in 100 ETPs from Ezh2 KO, Runx1 KO and DKO mice, relative to gene expression in WT ETPs by qPCR (WT $n=8$, Ezh2 KO $n=6$, Runx1 KO $n=5$, DKO $n=7$). Box plots show median, lower and upper quartiles. Replicates shown as dots when outside 1.5 times the inter-quartile range. See also Figure S2 and Tables S1 and S2.

Figure 3: HSC and Myeloid Genes are Co-Expressed with Lymphoid Genes within Single DKO ETPs.

(A) Heatmap showing co-expression of indicated genes within single WT ($n=129$) and DKO ($n=91$) ETPs, by single-cell qPCR. Expression levels are scaled per gene. Single ETPs were collected from 12 WT and 9 DKO mice. FDR q values are by Kolmogorov-Smirnov test based on expression levels, * $p < 0.05$, ** $p < 0.01$ and *** $p < 0.001$. (B-C) Scatter plots showing level of co-expression of lymphoid with HSC (B) and myeloid genes (C) within single WT ($n=129$) and DKO ($n=91$) ETPs. Each dot represents a single cell, for which are plotted the number of genes showing detectable expression from the panel of HSC-, myeloid- and lymphoid-associated genes shown in (A). See also Figure S3.

Figure 4: Activating Flt3 Mutation Collaborates with Inactivating Ezh2 and Runx1 Mutations Targeted to Early Lymphoid Progenitors to Cause Acute Leukemia

(A) Total thymus cellularity and FACS analysis of absolute numbers of ETPs per thymus in 6-8 week old mice (WT n=26, DKO n=18, ITD n=6, DKOITD n=16). Horizontal lines show mean \pm SEM. (B) Leukemia-free survival curves for WT, DKO, ITD and DKOITD mice. X-axis represents age of the mice. Significance tested by log-rank test. (C) Hematological parameters from moribund DKOITD (n=12) and ITD littermate control (n=4) mice. Horizontal lines show mean \pm SEM. (D) Representative images of blood smears and BM cytopsins from leukemic DKOITD mice. Scale bars represent 20 μ m. (E) FACS analysis of absolute numbers of CD19⁺ (B cells), CD4⁺ and/or CD8⁺ (T cells) and Mac1⁺ (myeloid cells) per ml blood (WT n=9, DKO n=5, ITD n=4, DKOITD n=4). Bars show mean \pm SEM. (F) Representative images of histological sections of BM stained for hematoxylin and eosin (H&E), CD3 or TdT. Scale bar represents 100 μ m and pertains to all panels. (G-H) GSEA plots comparing WT and leukemic DKOITD Mac1⁺ BM cells for myeloid (G) and early T cell progenitor-associated expression signatures (H). (I-J) Expression in leukemic DKOITD Mac1⁺ BM cells relative to WT of lymphoid-associated (I) and stem/progenitor-associated genes (J) (WT n=3, DKOITD n=4). (K) GSEA plots comparing Notch1 mouse T-ALL and leukemic DKOITD Mac1⁺ BM cells for genes upregulated (top panel) or downregulated (bottom panel) in human ETP-ALL relative to non-ETP T-ALL. p values by ANOVA (A), log-rank test (B) or T-test (C), *p<0.05, **p<0.01 and ***p<0.001. n.s.; not significant (p>0.05). See also Figure S4 and Table S3.

Figure 5: Leukemia Induced by Activating Flt3 Mutation Combined with Inactivating Ezh2 and Runx1 Mutations can be Propagated by ETPs

(A) *In vitro* granulocyte-monocyte assay of myeloid proliferative potential of ETPs from WT (n=5), DKO (n=4) and DKOITD (n=3) mice. 60 wells per plate were seeded with single ETPs and proliferation was measured following 8 days of culture. p values by T-test comparing number of wells per plate showing high proliferation (>50 cells). (B) Experimental design showing thymocyte population

sorting strategy from DKOITD (CD45.2) mice for transplantation into CD45.1 mice. (C) FACS analysis of level of CD45.2 chimerism of total white blood cells, myeloid (Mac1⁺), B (CD19⁺) and T (CD4⁺ and/or CD8⁺) cells in peripheral blood of CD45.1 recipient mice post-transplantation of FACS-purified CD45.2 DKOITD thymocyte populations with CD45.1 support BM cells (DP/SP n=7, DN2 n=5, ETP n=13). (D) Hematological parameters from mice transplanted with FACS-purified DKOITD ETPs: 16 weeks post-transplantation for recipient mice showing no CD45.2 engraftment (n=3), and upon development of leukemia for recipient mice showing CD45.2 engraftment (n=4). (E) Representative images of histological sections of BM from transplant recipient mice stained for hematoxylin and eosin (H&E) or CD3. Scale bar represents 100 μ m and pertains to all panels. (F) Representative FACS plots showing relative contribution of CD45.1 and CD45.2 cells to HSCs (Lin⁻Sca1⁺Kit⁺CD48⁻CD150⁺) and LMPPs (Lin⁻Sca1⁺Kit⁺Flt3^{high}) in recipient mice transplanted with DKOITD ETPs. Figures represent mean percentage of total BM mononuclear cells falling into each gate across all replicates (non-engrafted recipient mice n=3, leukemic recipient mice n=4). p values by T-test, *p<0.05, **p<0.01 and ***p<0.001. n.s.; not significant (p>0.05). Bars and horizontal lines show mean \pm SEM. See also Figure S5.

Figure 6: Activating Flt3 Mutation Augments Upregulation of Signaling Pathway-Associated Transcription and Suppresses G2M Checkpoint Genes in DKO ETPs

(A) Significantly differentially expressed genes between WT, DKO and DKOITD ETPs by RNA-sequencing (top), and overlap of genes within each pairwise comparison (bottom) (WT n=4, DKO n=4, DKOITD n=4). (B) Hierarchical clustering and heatmap showing expression levels, scaled per gene, of all significantly differentially expressed genes between WT, DKO and DKOITD ETPs (WT n=4, DKO n=4, DKOITD n=4). Each replicate represents 100 purified ETPs from individual mice at 6-8 weeks of age. (C) GSEA plot comparing DKO and DKOITD ETPs for G2M checkpoint-associated gene expression. (D) Expression relative to WT of signaling pathway-associated genes in DKO and DKOITD ETPs by qPCR (WT n=8, DKO n=7, DKOITD n=6). Box plots show median, lower and upper quartiles.

Replicates shown as dots when outside 1.5 times the inter-quartile range. (E) GSEA comparing WT DP thymocytes and DKOITD ETPs for genes upregulated in human ETP-ALL relative to non-ETP T-ALL. (F) FACS analysis of phospho-S6 level in WT, DKO, ITD and DKOITD Lin⁻Kit⁺ BM cells. Representative histograms (left), median phospho-S6 fluorescence intensities normalised to WT from 3 experiments (right). Bars show mean \pm SEM. (G) FACS analysis of phospho-S6 in ITD and DKOITD Lin⁻Kit⁺ BM cells treated for 2 hr with DMSO or 2.5 μ M PD-901 (MEK inhibitor). Representative histograms (left), median phospho-S6 fluorescence intensities normalised to WT from 3 experiments (right). Bars show mean \pm SEM. p values by ANOVA, *p<0.05, **p<0.01 and ***p<0.001. n.s.; not significant (p>0.05). See also Figure S6 and Tables S4 and S5.

Figure 7: BET Inhibition Reverses Gene Expression Changes Associated with Loss of PRC2 Function

(A) Experimental design for ChIP-seq and RNA-seq experiments in WT and DKOITD BM cells. WT ChIP-seq n=3 (5 million Kit-enriched cells/sample), DKOITD ChIP-seq n=5 (5 million unsorted cells/sample), WT RNA-seq n=3 (100 Mac1⁺ cells/sample), DKOITD RNA-seq n=4 (100 Mac1⁺ cells/sample). (B) Normalised read density within 2 kb of the transcription start site for H3K27me3 at all genes (top) and H3K27ac at genes showing significantly decreased H3K27me3 in DKOITD relative to WT BM cells (n=520) (bottom). (C) Venn diagram showing overlap of genes displaying increased H3K27ac (H3K27ac Up), decreased H3K27me3 (H3K27me3 Down), and up- or downregulation of gene expression in DKOITD relative to WT BM. (D) Genome browser tracks showing H3K27me3 and H3K27ac at the *Flt3* locus in WT and DKOITD BM cells. Fold change refers to gene expression in DKOITD relative to WT Mac1⁺ BM cells. (E) GSEA comparing WT and DKOITD Mac1⁺ BM cells for genes which lose H3K27me3 and gain H3K27ac (n=235) in DKOITD relative to WT BM cells. (F) Multidimensional scaling analysis of RNA-seq data from untreated LOUCY and JURKAT cells (n=6 per cell line) and DMSO, JQ1 and I-BET151-treated LOUCY cells (n=4 per condition). LOUCY cells treated for 24 hr with 0.05% DMSO, 250 nM JQ1 or 500 nM I-BET151. Each point represents one replicate sample. (G-I) GSEA comparing DMSO and JQ1-treated LOUCY cells for genes (n=793) showing

H3K27ac at the transcription start site in LOUCY but not JURKAT cells (G), genes associated with upregulation of KRAS signaling (H), and genes upregulated in DKOITD relative to WT ETPs (left) ($\log_{2}FC > 2$; $n=262$ genes) and DKOITD relative to WT Mac1⁺ BM cells (right) ($\log_{2}FC > 8$; $n=219$ genes) (I). (J) ChIP-qPCR for H3K27me3 and H3K27ac at the *Mpl* locus in DMSO and UNC1999 (Ezh2 inhibitor) treated EML cells ($n=3$ for each condition). (K) qPCR expression analysis of *Mpl* mRNA in EML cells treated with DMSO, UNC1999, JQ1 or UNC1999 and JQ1 ($n=3$ for each condition). Bars show mean \pm SD. p values by T-test, * $p < 0.05$, ** $p < 0.01$ and *** $p < 0.001$. See also Figure S7 and Tables S6 and S7.

Figure 8: BET Inhibition Selectively Targets Proliferation of ETP Propagated Leukemia Cells

(A) MTS proliferation assay of DKOITD ETPs cultured with increasing concentrations of JQ1, relative to DMSO control ($n=3$ for each concentration). (B) Single-cell proliferation assay of CD45.2 Lin⁺ Kit⁺ BM progenitor cells from mice transplanted with WT BM or DKOITD ETP cells and cultured with increasing concentrations of JQ1. Frequency of clones showing high proliferation at each concentration is shown relative to DMSO control (WT $n=3-8$ and DKOITD $n=4-10$ for each concentration). Cells were collected from three WT BM and four DKOITD ETP recipient mice. (C) White blood cell counts and total BM and spleen cellularity of WT mice transplanted with DKOITD BM and treated with 45 mg/kg/day JQ1 or DMSO for 28 days. DMSO $n=8$, JQ1 $n=10$. One JQ1 mouse was excluded due to weight loss. (D) MTS proliferation assay of K562, LOUCY and THP-1 leukemia cell lines with increasing concentrations of JQ1, relative to DMSO control ($n=6$ for each concentration). Data collected from two independent experiments. (E) MTS proliferation assay of T-ALL and ETP-ALL patient-derived xenografts cultured with increasing concentrations of JQ1, relative to DMSO control ($n=3$ for each concentration). See STAR Methods for mutations carried by ETP-ALL samples. (F-G) Peripheral blood chimerism curves (left panels) and white blood cell counts, BM and spleen cellularities and human cell composition at end of treatment period (right panels) for NSG mice transplanted with human PRC2-mutant ETP-ALLs and treated with 45 mg/kg/day JQ1 or DMSO for 36 days. Sample ETP-ALL 12: *EZH2* and *RUNX1* mutant, DMSO $n=8$, JQ1 $n=8$ (F). Sample ETP-ALL

13: *EED* mutant, DMSO n=8, JQ1 n=9 (G). In right panels, fold changes and p values compare absolute numbers of human cells. p values by F-test (B, E) or T-test (C, F-G), *p<0.05, **p<0.01 and ***p<0.001. Bars and horizontal lines show mean \pm SEM. See also Figure S8.

STAR Methods

CONTACT FOR REAGENT AND RESOURCE SHARING

Further information and requests for resources and reagents should be directed to and will be fulfilled by the Lead Contact, Adam Mead (adam.mead@imm.ox.ac.uk).

EXPERIMENTAL MODEL AND SUBJECT DETAILS

Animal models

All animal protocols were approved by the UK Home Office. Mice were maintained in individually ventilated cages in a specific-pathogen-free facility. *Ezh2^{fl/+}*, *Runx1^{fl/+}*, *Rag1Cre⁺* and *Flt3^{ITD/+}* mice have been previously described (Growney et al., 2005; Lee et al., 2007; McCormack et al., 2003; Su et al., 2003). *Mx1Cre⁺* and NSG mice were obtained from the Jackson Laboratory. All mice, except NSG recipients, were on a pure C57BL/6 background. Phenotypic analysis was performed on mice aged 6-8 weeks unless otherwise stated. Males and females were assigned randomly to control and experimental groups. For survival curves, mice that were not analysed were counted as an event.

Patient-derived xenografts

T-ALL and ETP leukemia patient-derived xenograft samples have been previously described (Maude et al., 2015). Genetic lesions carried by ETP leukemia samples:

| Sample no. | ID, USI/SJCRH | Age (years) | Gender | WBC ($\times 10^9$ /L) | Genetic Lesions |
|------------|------------------|----------------|--------|----------------------------|-----------------|
| | | | | | |

| | | | | | |
|------------|-----------|----|---|------|---|
| ETP-ALL 12 | SJTALL165 | 16 | M | 251 | EZH2 S651L, <i>RUNX1</i> T148fs, NOTCH1 S2492*, <i>IKZF1</i> SV, PHF6 N147fs, SUZ12 C350R, WT1 C350R L564_S568, <i>SH2B3</i> SV |
| ETP-ALL 13 | SJTALL004 | 3 | M | 21.5 | EED S259F |

Cell lines

EML cells (established from mouse bone marrow) were purchased from ATCC (ATCC number: CRL-11691). EML cells were cultured in IMDM (Gibco) supplemented with 20% FCS (HyClone), 200 ng/ml mSCF (Peprotech) and 1% penicillin/streptomycin (PAA Laboratories). LOUCY cells (established from peripheral blood of a 38-year old female) were purchased from ATCC (ATCC number: CRL-2629).

JURKAT cells (established from peripheral blood of a 14-year old male) were purchased from ATCC (ATCC number: TIB-152). LOUCY and JURKAT cells were cultured in RPMI-1640 (Gibco) supplemented with 10% FCS (HyClone) and 1% penicillin/streptomycin (PAA Laboratories).

METHOD DETAILS

Induction of Mx1Cre

For Mx1Cre-induced deletion of *Ezh2* and *Runx1*, *Ezh2^{fl/fl}Runx1^{fl/fl}Mx1Cre⁺* mice and *Ezh2^{fl/fl}Runx1^{fl/fl}Mx1Cre⁻* littermate controls were treated at 6-8 weeks of age with 3 doses of 200 µg of Poly(IC) (GE Healthcare) at 2-day intervals by intra-peritoneal injection.

RNA sequencing

ETPs were prepared for RNA-seq using the SMARTer Ultra Low RNA kit for Illumina Sequencing (Clontech). One hundred cells were sorted directly into lysis buffer supplemented with RNase Inhibitor (Clontech), before preparation of cDNA libraries as directed using 15 cycles of amplification. Amplified cDNA libraries were sheared using the Covaris AFA system. The NEBNext DNA Library Prep Reagent Set for Illumina (New England Biolabs) was then used to repair ends, adenylate 3' ends,

ligate genomic adaptors and amplify fragments with Genomic DNA Sample Prep oligos (Illumina). Samples were sequenced using the Illumina HiSeq 2000 platform, generating 50 bp single-end reads.

Mac1⁺ BM cells were prepared for RNA-seq using Smart-Seq2 as previously described (Picelli et al., 2014). One hundred cells were sorted directly into 4 µl of lysis buffer containing 0.2% Triton X-100 (Sigma-Aldrich), RNase inhibitor (Clontech), 2.5 mM dNTPs (Thermo Fisher) and 2.5 µM oligo-dT30VN primer (Biomers.net). cDNA was generated using SuperScript II (Invitrogen), pre-amplified using KAPA HiFi HotStart ReadyMix (KAPA Biosystems) and purified using Agencourt AMPure XP (Beckman Coulter). Tagmentation and library preparation was performed using the Nextera XT DNA Library Preparation Kit (Illumina). Samples were sequenced using the Illumina NextSeq 500 platform, generating 75 bp paired-end reads.

LOUCY and JURKAT RNA was extracted from 500,000 cells per sample using the RNeasy Mini Kit (Qiagen). Ten nanograms of RNA per sample was then prepared for sequencing using Smart-Seq2 as for Mac1⁺ BM cells above, but generating 75 bp single-end reads. For RNA-seq following inhibitor treatment, 500,000 cells per sample were first cultured for 24 hours with either 0.05% DMSO, 250 nM JQ1 (MedChem Express) or 500 nM I-BET151 (Sigma-Aldrich). Cells were cultured in RPMI-1640 (Gibco) supplemented with 10% FCS (HyClone) and 1% penicillin/streptomycin (PAA Laboratories).

RNA-seq data analysis

Mouse ETP and Mac1⁺ BM cell RNA-sequencing reads were aligned to the mouse genome (mm10) using Tophat2 (version 2.0.10) (RRID:SCR_013035) and Bowtie2 (version 2.1.00) (RRID:SCR_005476) as the underlying aligner. Non-uniquely mapping reads were filtered using samtools (version 0.1.19) (RRID:SCR_002105). Read alignments were summarized to gene identifiers using the htseq-count tool (version 0.5.4p5) (RRID:SCR_005514) against the mm10 UCSC transcriptome annotation.

Differential expression analysis was performed using the generalized linear model function of edgeR

(version 3.10.4) (RRID:SCR_012802). Genes with fewer than 2 reads in at least 3 samples were excluded from subsequent analysis. RPKM value calculation was performed using the `rpkm` function of edgeR.

LOUCY and JURKAT reads were aligned to the human genome (hg38) using STAR (version 2.5.1b) (RRID:SCR_004463). Reads mapping to gene exons were counted using the Subread (version 1.4.5-p1) `featureCounts` tool (RRID:SCR_009803) and UCSC hg38 annotation. Analysis was performed using edgeR (version 3.10.5) (RRID:SCR_012802). Only genes detected at greater than 1 count per million (cpm) in at least 4 samples were used for analysis.

Gene set enrichment analysis

Gene set enrichment analysis was performed using GSEA software (v 2.2.0) (RRID:SCR_003199). The Hallmark gene sets were obtained from MSigDB (RRID:SCR_003199) and converted to mouse gene identifiers using the Biomart (RRID:SCR_006442) R package prior to analysis. ETP-ALL gene sets were derived from the top 500 up- or downregulated genes in ETP-ALL relative to non-ETP T-ALL (Zhang et al., 2012a), converted to mouse gene identifiers using Biomart. For ETP-ALL GSEA, previously published RNA-seq data was obtained from mouse Notch1 T-ALL (Ntziachristos et al., 2014) and wild-type mouse DP thymocytes (Zhang et al., 2012b), and compared to DKOITD Mac1⁺ BM cells or DKOITD ETPs respectively. Custom gene expression signatures for early T cells, myeloid cells and HSCs were generated as follows. Previously published data (Luc et al., 2012) (<https://gexc.riken.jp/>) were used to perform differential expression comparisons between ETPs and HSCs, and DN2 and HSC (Luc et al., 2012), and between DN1 and HSCs, and GMPs and HSCs (<https://gexc.riken.jp/>). Gene sets up-regulated to each of the following cell types were generated by combining genes from the above comparisons as follows: early T cells (ETP against HSC, DN2 against HSC and DN1 against HSC); Myeloid (GMPs against HSCs). The early T cell gene set consisted of all genes upregulated in early T cells but not myeloid cells, while the myeloid gene set consisted of all genes upregulated in

myeloid cells but not early T cells. The HSC gene set consisted of all genes upregulated in HSCs relative to any other cell type, and not present in the early T cell or myeloid sets. The PRC2 target gene set (De Raedt et al., 2014), Pre-GM and Pre-MegE gene sets (Sanjuan-Pla et al., 2013) have been previously described.

Multiplex qPCR

Multiplex quantitative real time PCR analysis was performed using the BioMark 96.96 Dynamic Array platform (Fluidigm) and TaqMan gene expression assays (Life Technologies; see Table S8 for full list of assays used). CellsDirect One-Step qRT-PCR kit (Invitrogen) was used for cDNA synthesis and pre-amplification of target genes. Cells were FACS-sorted directly into 5 μ l (single cells) or 10 μ l (bulk; 50 cells) of lysis/pre-amplification buffer. Ten microliters of this buffer consisted of: 2.5 μ l Taqman assay mix containing all assays at 0.2x dilution, 5 μ l CellsDirect 2x Reaction mix (Invitrogen), 1.2 μ l CellsDirect RT/Taq mix (Invitrogen), 1.2 μ l TE buffer and 0.1 μ l SUPERase-In RNase Inhibitor (Ambion). Reverse transcription and target pre-amplification were performed as follows: 50°C for 15 min; 95°C for 2 min; 22 cycles of 95°C for 15 s and 60°C for 4 min. Pre-amplified product was diluted 1:5 in TE buffer and analyzed using the default M96 RT-PCR protocol.

Single cell qPCR analysis

Single cell qPCR data analysis was performed in R (version 3.2.2). Cells were filtered so as to only retain cells that expressed Actb, B2M, Gapdh and Hprt with Ct values lower than 21. Furthermore at least 70 assays were required to result in amplification per cell for it to be included in the analysis. Cells with consistently low amplification (mean non drop-out Ct > 20) were excluded from the analysis. Absolute expression was calculated as 2^{-Ct} . Ct values were standardized per gene, after excluding measurements that did not give rise to any amplification, for the purposes of visualization. Significance of differential expression was assessed by means of the Kolmogorov-Smirnov non-parametric test on the raw Ct values after FDR multiple testing correction.

Bulk qPCR analysis

Bulk qPCR analysis was performed in R (version 3.2.2). Assays with Ct values over 30 and reactions that failed quality control by the instrument were excluded. Assays with undetermined values in more than two samples were excluded from the analysis. The mean Ct value of technical replicates was obtained and used for further analysis. Delta Ct normalization was performed using Gapdh as reference.

Whole exome sequencing

Genomic DNA was extracted from bone marrow cells using the DNeasy Blood & Tissue Kit (Qiagen). DNA was prepared for sequencing using the SureSelectXT Mouse All Exon Kit (Agilent). Sequencing was performed using the Illumina HiSeq 4000 platform, generating 2x70 bp paired-end reads and an average coverage of 103X.

The raw whole-exome sequence data was aligned to GRCm38/mm10 mouse reference genome using the BWA-MEM algorithm (v. 0.7.12-r1039) (<http://bio-bwa.sourceforge.net/bwa.shtml>), and data quality was assessed using MultiQC software (v. 1.2) (RRID:SCR_014982). Candidate substitutions and insertions/deletions in 8 DKOITD and 10 wild-type control mice were called using the CaVEMan (v. 1.7.2) (<http://cancerit.github.io/CaVEMan/>) and PINDEL (v. 1.5.4) (RRID:SCR_000560) algorithms. Orthologous human genes to coding variants identified using this method were determined using the Ensembl database (v. 78) (RRID:SCR_002344). The list of orthologous human genes to each mouse variant was generated using the “getLDS” function from the biomaRt package (v. 2.30.0) (RRID:SCR_006442). The Cancer Gene Census database was used to identify variants in DKOITD leukemic mice for which mutations have been causally implicated in cancer for their orthologous pair (<http://cancer.sanger.ac.uk/census>).

Copy number alterations were identified using the CNVkit software (v. 0.8.5) (<http://cnvkit.readthedocs.io/en/stable/>) and the “bin-level log2 ratios” (.cnr) and “segmented log2 ratios” (.cns) results of CNVkit. Segments with log2-ratio $\geq +0.2$ or ≤ -0.25 were selected as candidate copy number gains or losses, respectively. These thresholds are sensitive enough to detect single-copy gain or loss in a diploid tumor with as low as 30% sub-clonality (or purity). Genes potentially affected by candidate copy number variations were mapped to human orthologs using the same approach as for substitutions and insertions/deletions. Using the Cancer Gene Census database as for substitutions and insertions/deletions, none of these were identified as causally implicated in cancer.

Chromatin immunoprecipitation (ChIP)

EML cells (ATCC) were cultured in IMDM (Gibco) supplemented with 20% FCS (HyClone), 200 ng/ml mSCF (Peprotech) and 1% penicillin/streptomycin (PAA Laboratories). For H3K27me3 and H3K27ac ChIP, cells were fixed with 1% formaldehyde for 10 min. Fixed chromatin samples were fragmented using an S220 Focused-ultrasonicator (Covaris) to an average size of 200-500 bp.

Immunoprecipitation was then performed using a mixture of Protein A and Protein G Dynabeads (Life Technologies). Antibodies used were: anti-H3K27me3 (07-449, Merck MilliPore) and anti-H3K27ac (C15410196, Diagenode). ChIP samples were quantified relative to inputs as previously described (Milne et al., 2009). Three replicate samples were used for ChIP-qPCR. See Key Resources Table for primer sequences used.

For WT and DKOITD bone marrow ChIP-seq, three samples of WT and five samples of DKOITD, each sample consisting of cells from separate mice, were used. WT samples were first enriched for Kit expressing cells using CD117 microbeads and LS columns (Miltenyi Biotec) as directed. 5 million cells per sample were used for ChIP-seq, which was performed using conditions and antibodies as for H3K27ac and H3K27me3 ChIP in EML cells (above). One input control sample was used for each

genotype. Samples were prepared for sequencing using the NEBNext Ultra II DNA Library Prep Kit for Illumina, with NEBNext Multiplex Oligos for Illumina (New England BioLabs) as directed. Sequencing was performed using the Illumina NextSeq 500 platform, generating 40 bp paired-end reads.

For ChIP-qPCR and gene expression analysis of EML C1 cells, cells were treated with DMSO or 5 μ M UNC1999 (Cambridge Bioscience) and/or 250 nM JQ1 (MedChem Express) for 48 hr before harvesting. RNA was extracted using RNeasy Mini Kit (Qiagen), and cDNA generated using SuperScript II (Invitrogen) as directed. Expression of *Mpl* was quantified and shown normalised to *Actb* using custom primers (see Key Resources Table) and SYBR Green (Thermo-Fisher) and the ddCt method.

ChIP-seq data analysis

For WT and DKOITD ChIP-seq analysis, reads were aligned to the mouse genome (mm10) using Bowtie2 (version 2.2.5) (RRID:SCR_005476). Peak calling was performed using Macs2 (version 2.0.10) (RRID:SCR_013291) and the broad peak calling parameter. DiffBind (version 1.14.6) (RRID:SCR_012918) was used to identify regions under peaks called by Macs2 which were associated with significantly different levels of H3K27ac and H3K27me3 in DKOITD versus WT samples. Tracks for genome visualisation were generated using the Macs2 bdgcmp function and the UCSC genome browser (<http://genome.ucsc.edu/>). Identified peaks and regions showing differential H3K27ac and H3K27me3 were mapped to nearby transcription start sites (within 2.5kb in either direction) using Homer (version 4.7) (RRID:SCR_010881). Normalised read density histograms and heatmaps were generated using Homer, by pooling reads from replicate WT and DKOITD samples. Genes showing reduced H3K27me3 in DKOITD were obtained from the DiffBind analysis of individual samples.

For LOUCY and JURKAT ChIP-seq analysis, reads were aligned to the human genome (hg38) using Bowtie2 (version 2.2.5) (RRID:SCR_005476). Peak calling was performed using Macs2 (version 2.0.10)

(RRID:SCR_013291) and the broad peak calling parameter. Identified peaks were mapped to nearby transcription start sites (within 1kb in either direction) using Homer (version 4.7) (RRID:SCR_010881) and hg38 annotation data (NCBI RefSeq Curated) downloaded from the UCSC Table Browser (RRID:SCR_005780).

Histology and immunohistochemistry

Mouse tissue was fixed in neutral buffered formalin and processed to paraffin using standard techniques. Three-micron sections were cut and stained with hematoxylin and eosin. Serial sections were immunostained for CD3 using polyclonal rabbit serum raised against a synthetic peptide corresponding to a region showing 100% homology between mouse and human CD3 ϵ at the manufacturer's "ready-to-use" concentration (IR503; Dako). Immunostaining for TdT was performed using polyclonal rabbit anti-TdT (ab85148; Abcam) at a 1:200 dilution. Staining was performed on a Ventana Discovery Ultra Immunostainer (Ventana Medical Systems). Briefly, following deparaffinisation, sections were heated to 95°C for 36 min in CC1 solution (a tris-based buffer with slightly alkaline pH) and incubated in primary antibody at 36°C for 32 min. Bound rabbit antibody was detected using the Omnimap anti-rabbit DAB kit. All reagents apart from the primary antibody were obtained from Ventana Medical Systems and used according to the manufacturer's instructions. Immunostaining of WT mouse thymus was used as a positive control for both CD3 and TdT. Rabbit anti-FITC antibody (71-1900; Life Technologies) was used as a negative control on representative histological sections. Stained sections were photographed with a Nikon DS-F11 camera with a Nikon DS-L2 control unit and an Olympus BX40 microscope.

Phospho-flow cytometry

Unfractionated bone marrow cells were cultured in Opti-MEM (Gibco), 5 million cells per ml, without serum or cytokines for 2 hours. For MEK inhibitor experiments, either 0.05% DMSO or 2.5 μ M PD-901 (PD0325901; Cambridge Biosciences) were added to the media. Cells were then fixed with 1.5%

paraformaldehyde (Electron Microscopy Sciences) for 10 minutes at 22°C. Fixed cells were treated with Fc block and stained for Sca1 (Pacific Blue conjugate), then permeabilised with ice-cold acetone for 15 minutes before staining for phospho-S6 (APC), Kit (APC-eF780) and lineage markers (B220, Ter119, Mac1 and Gr1, all conjugated to PE-Cy5). Lin⁻Kit⁺ cells were gated for analysis of phospho-S6.

In vitro proliferation assays

For granulocyte-monocyte assays, 75 ETPs were sorted into 1.5 ml of X-Vivo 15 (SLS Life Science) supplemented with 10% FCS (HyClone), 10⁻⁴ M 2-mercaptoethanol (Sigma-Aldrich), 1% penicillin/streptomycin (PAA Laboratories) and the following cytokines: 2 ng/ml murine stem cell factor (mSCF; PeproTech), 5 ng/ml human FLT3 ligand (hFL; Immunex), 5 ng/ml human thrombopoietin (hTPO; PeproTech), 5 ng/ml murine interleukin 3 (mIL-3; PeproTech), 10 ng/ml human granulocyte colony-stimulating factor (G-CSF; Neopogen) and 10 ng/ml murine granulocyte-macrophage colony-stimulating factor (mGM-CSF; Immunex). Twenty microliters were transferred to each well of a 60-well Terasaki plate (VWR), seeding on average one cell per well by Poisson distribution. Density of cell growth in each well was evaluated after 8 days of culture.

For colony assays, single cells were sorted directly into 60-well Terasaki plates containing media as defined above and including either 0.05% DMSO or equivalent volumes of JQ1 (MedChem Express) or I-BET151 (Sigma-Aldrich) to final concentrations as indicated. Density of cell growth in each well was evaluated after 8 days of culture, with each well containing a colony derived from a single cell. Colonies of 50 cells or more were defined as highly proliferative. The proportion of wells containing highly proliferative colonies for one 60-well plate was used as a single replicate.

For MTS assays, 500 cells (ETPs), 20,000 cells (cell lines) or 250,000 cells (patient-derived xenografts) were cultured in 100 µl of media (see below) in 96-well plates for 72 hours (ETPs and cell lines) or 48 hours (xenografts) before measuring proliferation using the CellTiter 96 AQueous Non-Radioactive

Cell Proliferation Assay (Promega) as directed. For ETPs, media consisted of Opti-MEM (Gibco) supplemented with 10% FCS (HyClone), 10^{-4} M 2-mercaptoethanol (Sigma-Aldrich), 1% penicillin/streptomycin (PAA Laboratories) and the following cytokines: 10 ng/ml mSCF (PeproTech), 5 ng/ml hFL (Immunex), 10 ng/ml hTPO (PeproTech), 20 ng/ml mL-3 (PeproTech), 20 ng/ml hG-CSF (Neopogen), 20 ng/ml mGM-CSF (Immunex) and 10 ng/ml human colony stimulating factor 1 (hCSF1; Cetus). For cell lines, media consisted of RPMI-1640 (Gibco) supplemented with 10% FCS (HyClone) and 1% penicillin/streptomycin (PAA Laboratories). For patient-derived xenografts, media consisted of RPMI-1640 (Gibco) supplemented with 10% FCS (HyClone), 1% penicillin/streptomycin (PAA Laboratories), 10 ng/ml hSCF (PeproTech), 10 ng/ml hFL (Immunex), 10 ng/ml hTPO (PeproTech), 10 ng/ml hG-CSF (Neopogen), 10 ng/ml hGM-CSF (Berlex), 10 ng/ml hIL-6 (PeproTech) and 10 ng/ml hIL-7 (PeproTech). Either 0.05% DMSO or equivalent volumes of JQ1 (MedChem Express) or I-BET151 (Sigma-Aldrich) were added to final concentrations as indicated.

Patient-derived xenograft cells were obtained from spleens of leukemic recipient mice (Maude et al., 2015). FACS analysis was used to confirm >85% human chimerism of CD45⁺ cells before cells were used for MTS assays.

In vivo experiments

For thymocyte transplantation experiments, C57BL/6 CD45.1 recipient mice were lethally irradiated (10 Gy, split dose) before intra-venous transplantation of total numbers of each specified population in the thymus: ETPs (range 413-6880 cells), DN2 (range 557-8005 cells) or DP/SP (range 412-1462 cells) with 250,000 CD45.1 unfractionated bone marrow support cells. Analysis of hematological parameters was performed using a Sysmex KX-21N analyser. Presence of leukemia was arbitrarily defined as a white blood cell count $> 50 \times 10^9/L$ in the peripheral blood or blast percentage in the peripheral blood and/or bone marrow greater than 20%.

In vivo administration of JQ1

C57BL/6 CD45.1 recipient mice were lethally irradiated (10 Gy, split dose) before intra-venous transplantation of 2 million DKOITD bone marrow cells with 500,000 CD45.1 unfractionated bone marrow support cells. NSG mice were sublethally irradiated (2.5 Gy, split dose) before injection of 2-2.5 million ETP-ALL xenograft spleen cells. For *in vivo* treatment, a 100 mg/ml stock of JQ1 (MedChem Express) in DMSO was diluted 1/20 into 10% 2-hydroxypropyl- β -cyclodextrin (Cambridge Bioscience), and administered daily by intra-peritoneal injection at a dose of 45 mg/kg. Control mice received a similar volume of diluted DMSO. Each mouse received a maximum of 36 intra-peritoneal injections as specified by Home Office approvals. Analysis of hematological parameters was performed using a Sysmex KX-21N analyser.

In vivo administration of I-BET151

C57BL/6 CD45.1 recipient mice were sub-lethally irradiated (a single dose of 5.5 Gy) before intra-venous transplantation of approximately 1.8 million DKOITD bone marrow cells re-suspended in Hanks' Balanced Salt Solution (Sigma). Peripheral blood was collected from the saphenous vein into EDTA-coated tubes (Sarstedt). Analysis of hematological parameters was performed using a Vet abc counter (Scil Animal Care). These *in vivo* studies used a modified murine feed containing 0.018% (180ppm) I-BET151 (or control feed). All mice had ad libitum access to feed.

QUANTIFICATION AND STATISTICAL ANALYSIS

Details of statistical tests are indicated in the Figure Legends. Statistical analyses were performed using GraphPad Prism v7.00 or R v3.2.2. Survival curves were compared using the log-rank test. The T-test or ANOVA followed by multiple comparisons testing were used to compare experimental groups as indicated in the Figure Legends. Sensitivity of experimental groups to JQ1 and I-BET151 in *in vitro* proliferation assays was compared using the F-test after fitting curves to the data. Numbers of replicates for each experiment are indicated in the Figure Legends.

Significance of overlap of genes showing reduced H3K27me3 and increased H3K27ac with genes showing upregulated expression was assessed using the R “phyper” function. The number of genes detected in either genotype by RNA-sequencing (11,172) was used as the total number of genes.

DATA AND SOFTWARE AVAILABILITY

GEO codes: GSE75185 (ETP RNA-seq), GSE75187 (bone marrow Mac1⁺ cell RNA-seq), GSE100693 (bone marrow and human cell line ChIP-seq), GSE100694 (human cell line RNA-seq).

Supplemental Tables

Table S1, Related to Figure 2. ETP RNA-seq data for DKO vs WT (RPKMs, fold changes and significance). Provided as an Excel file.

Table S2, Related to Figure 2. Hallmark GSEA for DKO ETPs. Provided as an Excel file.

Table S3, Related to Figure 4. Cancer-associated substitutions and insertions/deletions, and copy number variants detected by exome sequencing of DKOITD leukemia samples. Provided as an Excel file.

Table S4, Related to Figure 6. ETP RNA-seq data for DKOITD vs WT and DKOITD vs DKO (RPKMs, fold changes and significance). Provided as an Excel file.

Table S5, Related to Figure 6. Hallmark GSEA for DKOITD ETPs. Provided as an Excel file.

Table S6, Related to Figure 7. Overlaps of genes showing differential H3K27ac and H3K27me3 with differential expression in DKOITD relative to WT bone marrow cells. Provided as an Excel file.

Table S7, Related to Figure 7. Hallmark GSEA for LOUCY cells: JQ1 vs DMSO and I-BET151 vs DMSO.

Provided as an Excel file.

Table S8, Related to STAR Methods. List of Taqman probes used for gene expression analysis of ETPs.

| REAGENT or RESOURCE | SOURCE | IDENTIFIER |
|---------------------|------------------|---------------------------------|
| Antibodies | | |
| B220 APC | BioLegend | Clone RA3-6B2, Cat# 103211 |
| B220 PE-Cy5 | BioLegend | Clone RA3-6B2, Cat# 103209 |
| B220 PE-Texas Red | Becton Dickinson | Clone RA3-6B2, Cat# 551489 |
| CD11c APC | eBioscience | Clone N418, Cat# 17-0114-81 |
| CD150 PE-Cy7 | BioLegend | Clone TC15-12F12.2, Cat# 115913 |
| CD19 APC | eBioscience | Clone 1D3, Cat# 17-0193-82 |
| CD19 PE-Cy7 | eBioscience | Clone 1D3, Cat# 25-0193-82 |
| CD25 PerCP-Cy5.5 | BioLegend | Clone PC61, Cat# 102029 |
| CD3e APC | eBioscience | Clone 145-2C11, Cat# 17-0031-82 |
| CD4 AF700 | eBioscience | Clone RM4-5, Cat# 56-0042-82 |
| CD4 APC-eF780 | eBioscience | Clone RM4-5, Cat# 47-0042-82 |
| CD4 PE-Cy5 | BioLegend | Clone RM4-5, Cat# 100513 |
| CD44 FITC | eBioscience | Clone IM7, Cat# 11-0441-82 |
| CD45.1 FITC | BioLegend | Clone A20, Cat# 110705 |
| CD45.2 AF700 | BioLegend | Clone 104, Cat# 109821 |

| | | |
|--------------------|------------------|-------------------------------|
| CD48 APC | BioLegend | Clone HM48-1, Cat# 103411 |
| CD5 FITC | Becton Dickinson | Clone 53-7.3, Cat# 553024 |
| CD5 PE-Cy5 | BioLegend | Clone 53-7.3, Cat# 100609 |
| CD8a APC-eF780 | eBioscience | Clone 53-6.7, Cat# 47-0081-82 |
| CD8a PE-Cy7 | eBioscience | Clone 53-6.7, Cat# 25-0081-82 |
| CD8a PE-Cy5 | BioLegend | Clone 53-6.7, Cat# 100709 |
| Flt3 PE | BioLegend | Clone A2F10, Cat# 135305 |
| Gr1 Pacific Orange | Invitrogen | Clone RB6-8C5, Cat# RM3030 |
| Gr1 PE-Cy5 | BioLegend | Clone RB6-8C5, Cat# 108409 |
| Gr1 APC | BioLegend | Clone RB6-8C5, Cat# 108411 |
| Human CD45 AF700 | BioLegend | Clone HI30, Cat# 304023 |
| Kit APC | eBioscience | Clone 2B8, Cat# 17-1171-82 |
| Kit APC-eF780 | eBioscience | Clone 2B8, Cat# 47-1171-82 |
| Mac1 AF700 | eBioscience | Clone M1/70, Cat# 56-0112-82 |
| Mac1 APC | BioLegend | Clone M1/70, Cat# 101211 |
| Mac1 FITC | eBioscience | Clone M1/70, Cat# 11-0112-82 |

| | | |
|---|---|------------------------------|
| Mac1 PE | eBioscience | Clone M1/70, Cat# 12-0112-82 |
| Mac1 PE-Cy5 | BioLegend | Clone M1/70, Cat# 101209 |
| Mouse CD45 PE-Texas Red | Invitrogen | Clone 30-F11, Cat# MCD4517 |
| NK1.1 APC | eBioscience | Clone PK136, Cat# 17-5941-82 |
| NK1.1 Pacific Blue | BioLegend | Clone PK136, Cat# 108721 |
| Phospho-S6 APC | Cell Signaling | Clone D57.2.2E, Cat# 14733 |
| Sca1 BV605 | BioLegend | Clone D7, Cat# 108133 |
| Sca1 Pacific Blue | BioLegend | Clone E13-161.7, Cat# 122519 |
| Ter119 PE-Cy5 | BioLegend | Clone TER-119, Cat# 116209 |
| H3K27me3 (ChIP) | Merck MilliPore | Cat# 07-449 |
| H3K27ac (ChIP) | Diagenode | Cat# C15410196 |
| CD3 (Immunohistochemistry) | Dako | Cat# IR503 |
| TdT (Immunohistochemistry) | Abcam | Cat# ab85148 |
| Bacterial and Virus Strains | | |
| Biological Samples | | |
| Patient-derived xenografts | Laboratory of David T. Teachey (Maude et al., 2015) | N/A |
| Chemicals, Peptides, and Recombinant Proteins | | |
| Poly(IC) | GE Healthcare | Cat# 27-4732-01 |
| PD-901 | Cambridge Bioscience | Cat# SM26 |
| JQ1 | MedChem Express | Cat# HY-13030 |

| | | |
|--|--------------------------|------------------------|
| I-BET151 | Sigma-Aldrich | Cat# SML0666 |
| 2-hydroxypropyl- β -cyclodextrin | Cambridge Bioscience | Cat# CAY16169 |
| Critical Commercial Assays | | |
| SMARTer Ultra Low RNA kit for Illumina Sequencing | Clontech | Cat# 634936 |
| NEBNext DNA Library Prep Reagent Set for Illumina | New England Biolabs | Cat# E6000 |
| Nextera XT DNA Library Preparation Kit | Illumina | Cat# FC-131 |
| CellsDirect One-Step qRT-PCR kit | Invitrogen | Cat# 11753100 |
| SureSelectXT Mouse All Exon Kit | Agilent | Cat# 5190-4641 |
| NEBNext Ultra II DNA Library Prep Kit for Illumina | New England BioLabs | Cat# E7645 |
| Deposited Data | | |
| ETP RNA-seq | This paper | GSE75185 |
| Mac1 ⁺ bone marrow RNA-seq | This paper | GSE75187 |
| Mouse bone marrow, LOUCY and JURKAT ChIP-seq | This paper | GSE100693 |
| LOUCY and JURKAT RNA-seq | This paper | GSE100694 |
| Experimental Models: Cell Lines | | |
| Mouse: EML | ATCC | ATCC number: CRL-11691 |
| Human: LOUCY | ATCC | ATCC number: CRL-2629 |
| Human: JURKAT | ATCC | ATCC number: TIB-152 |
| Experimental Models: Organisms/Strains | | |
| Mouse: C57BL/6 Ezh2 ^{fl/+} | (Su et al., 2003) | N/A |
| Mouse: C57BL/6 Runx1 ^{fl/+} | (Growney et al., 2005) | N/A |
| Mouse: C57BL/6 Mx1Cre | The Jackson Laboratory | Cat# 003556 |
| Mouse: C57BL/6 Rag1Cre | (McCormack et al., 2003) | N/A |

| | | |
|--|---|-----------------|
| Mouse: C57BL/6 Flt3 ^{ITD/+} | (Lee et al., 2007) | N/A |
| Mouse: NSG | The Jackson Laboratory | Cat# 005557 |
| Oligonucleotides | | |
| EML cell H3K27ac and H3K27me3 ChIP-qPCR: Mpl forward primer: GCAACGTGGAGTGGGTCT | This paper | N/A |
| EML cell H3K27ac and H3K27me3 ChIP-qPCR: Mpl reverse primer: GCTGTGTGTGTGTCCTCGT | This paper | N/A |
| EML cell gene expression qPCR: Mpl forward primer: CTGTATGCCTACCGAGGAGAG | This paper | N/A |
| EML cell gene expression qPCR: Mpl reverse primer: TCTGGTTGAGGGACACATTCTT | This paper | N/A |
| EML cell gene expression qPCR: Actin forward primer: GGCTGTATTCCCCTCCATCG | This paper | N/A |
| EML cell gene expression qPCR: Actin reverse primer: CCAGTTGGTAACAATGCCATGT | This paper | N/A |
| For Taqman probes used for gene expression analysis see Table S8. | N/A | N/A |
| Recombinant DNA | | |
| Software and Algorithms | | |
| Flowjo | Treestar | RRID:SCR_008520 |
| Tophat2 | John Hopkins University | RRID:SCR_013035 |
| Bowtie2 | University of California Santa Cruz | RRID:SCR_005476 |
| Samtools | Wellcome Trust Sanger Institute | RRID:SCR_002105 |
| HTseq | EMBL Heidelberg | RRID:SCR_005514 |
| edgeR | Walter and Eliza Hall Institute of Medical Research | RRID:SCR_012802 |

| | | |
|------------------------------|---|--|
| STAR | Cold Spring Harbor Laboratory | RRID:SCR_004463 |
| Subread | Walter and Eliza Hall Institute of Medical Research | RRID:SCR_009803 |
| Gene set enrichment analysis | Broad Institute | RRID:SCR_003199 |
| MSigDB | Broad Institute | RRID:SCR_003199 |
| Gene expression commons | Stanford University | https://gexc.riken.jp / |
| BWA-MEM | Broad Institute | http://bio-bwa.sourceforge.net /bwa.shtml |
| MultiQC | Stockholm University | RRID:SCR_014982 |
| CaVEMan | Wellcome Trust Sanger Institute | http://cancerit.github.io/CaVEMan/ |
| PINDEL | Wellcome Trust Sanger Institute | RRID:SCR_000560 |
| Ensembl database | EMBL-EBI | RRID:SCR_002344 |
| Bioconductor BiomaRt | Lawrence Berkeley National Laboratory | RRID:SCR_006442 |
| Cancer Gene Census | Wellcome Trust Sanger Institute | http://cancer.sanger.ac.uk/census |
| CNVkit | University of California San Francisco | http://cnvkit.readthedocs.io/en/stable/ |
| Macs2 | Dana Farber Cancer Institute | RRID:SCR_013291 |
| DiffBind | University of Cambridge | RRID:SCR_012918 |
| Homer | Salk Institute | RRID:SCR_010881 |
| UCSC Table Browser | University of California Santa Cruz | RRID:SCR_005780 |

| |
|-------|
| Other |
|-------|

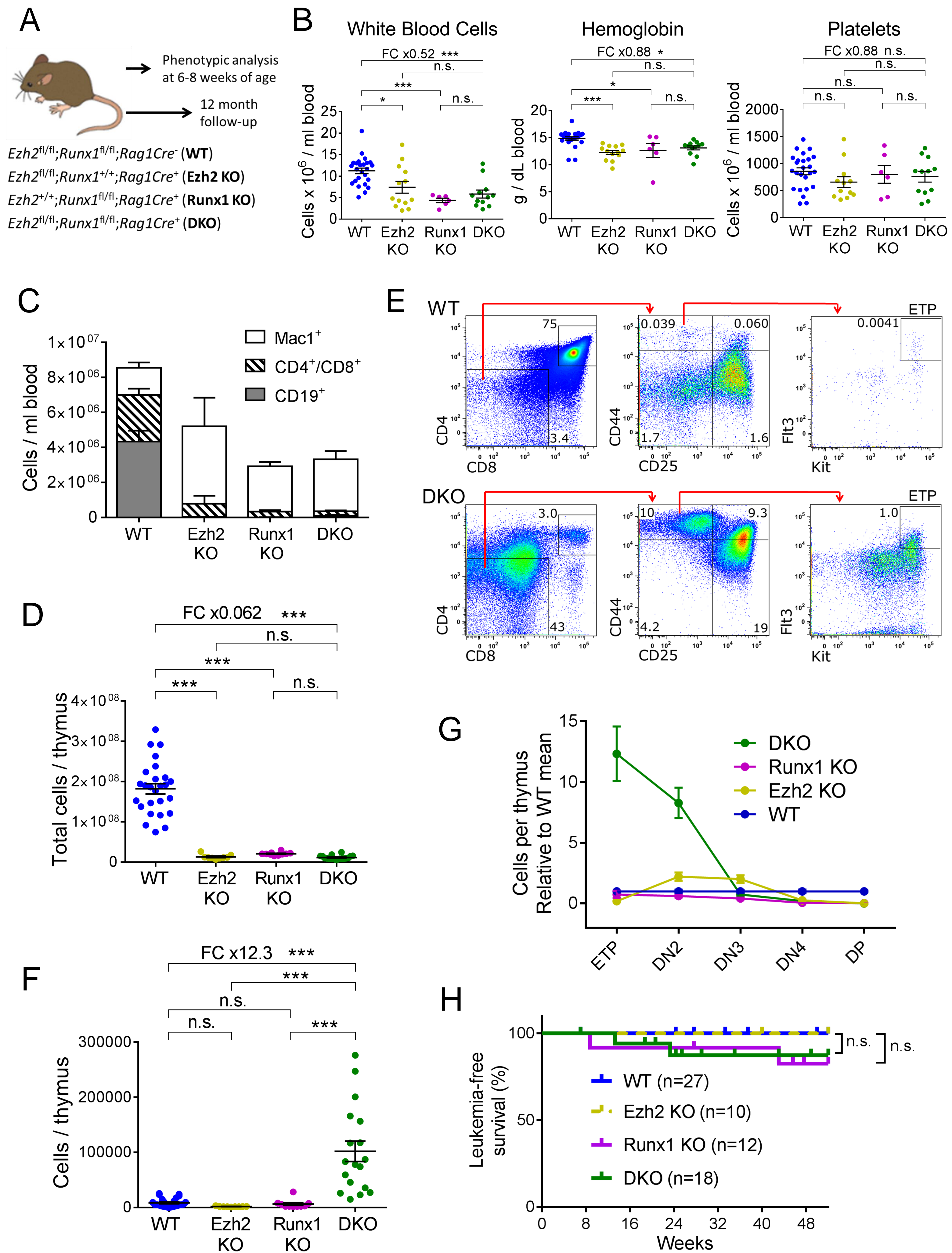


Figure 2

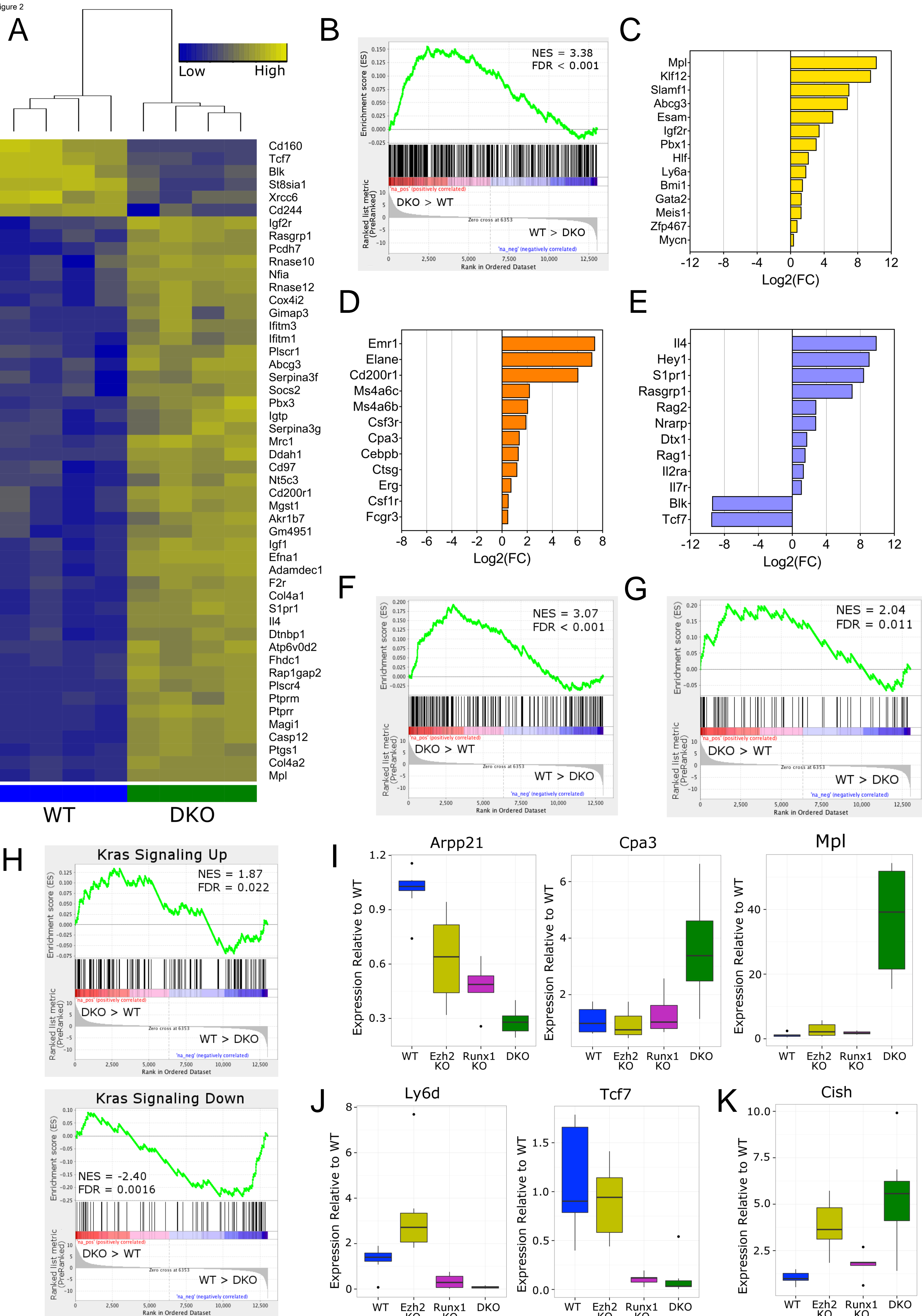
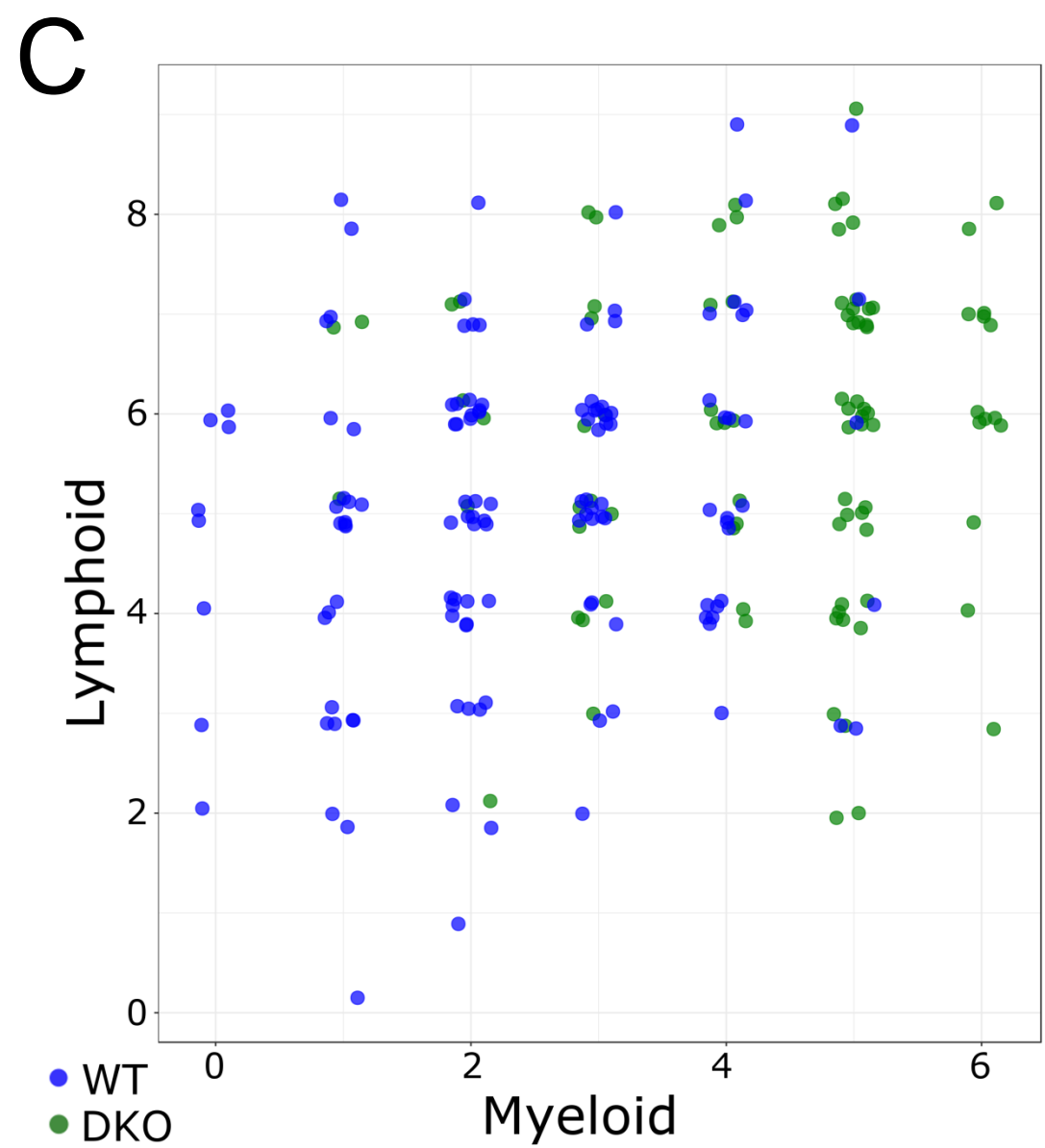
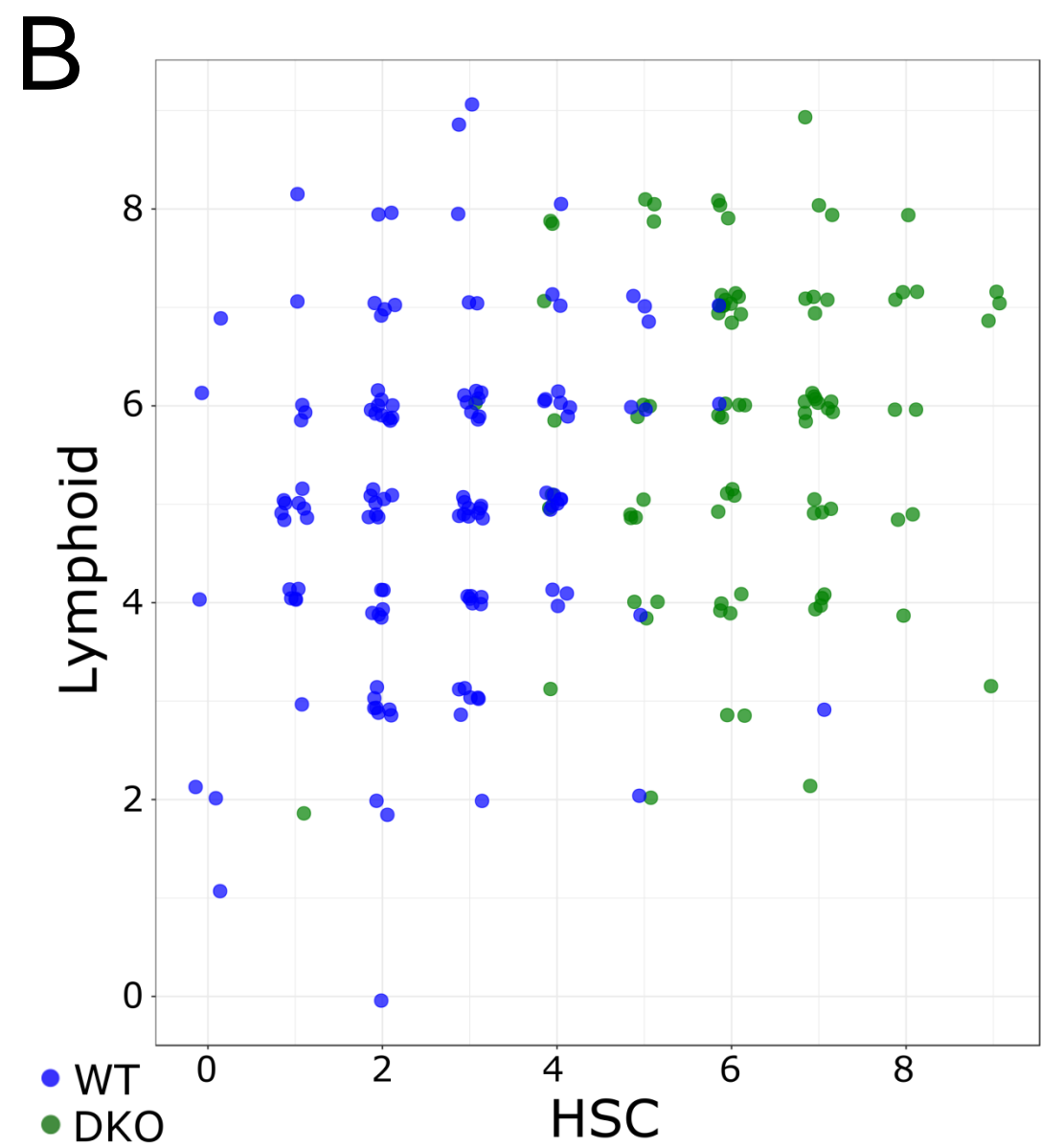
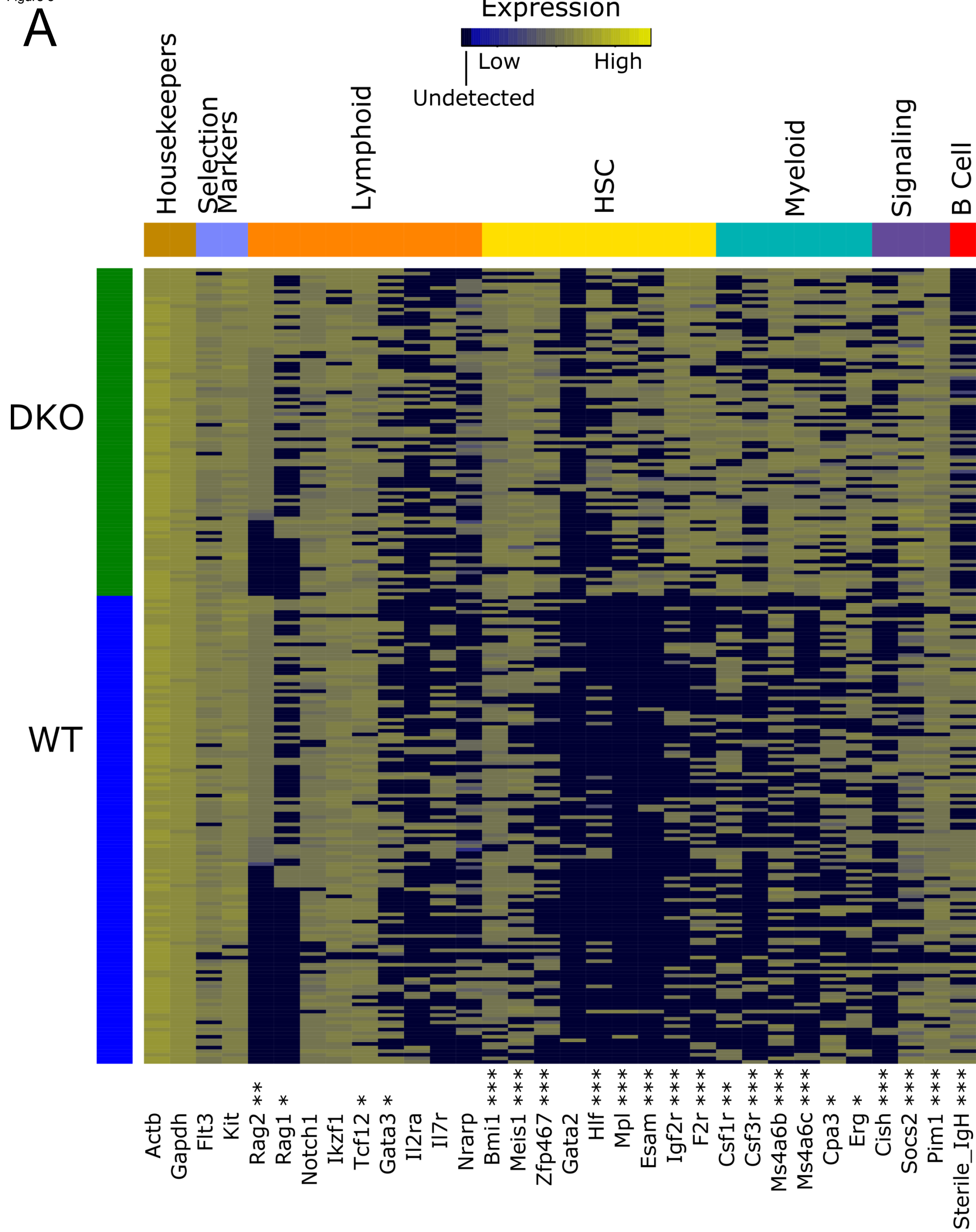
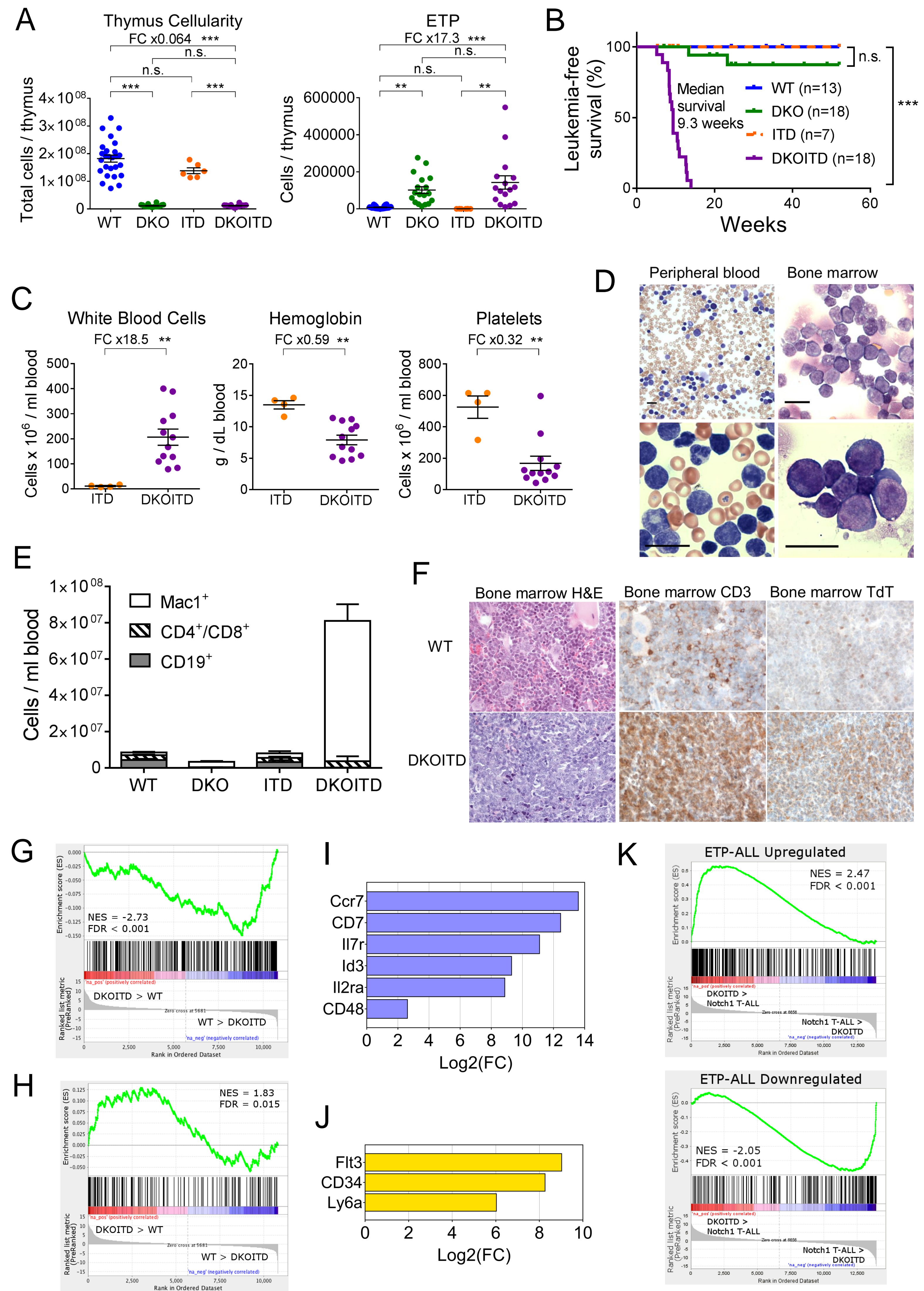


Figure 3





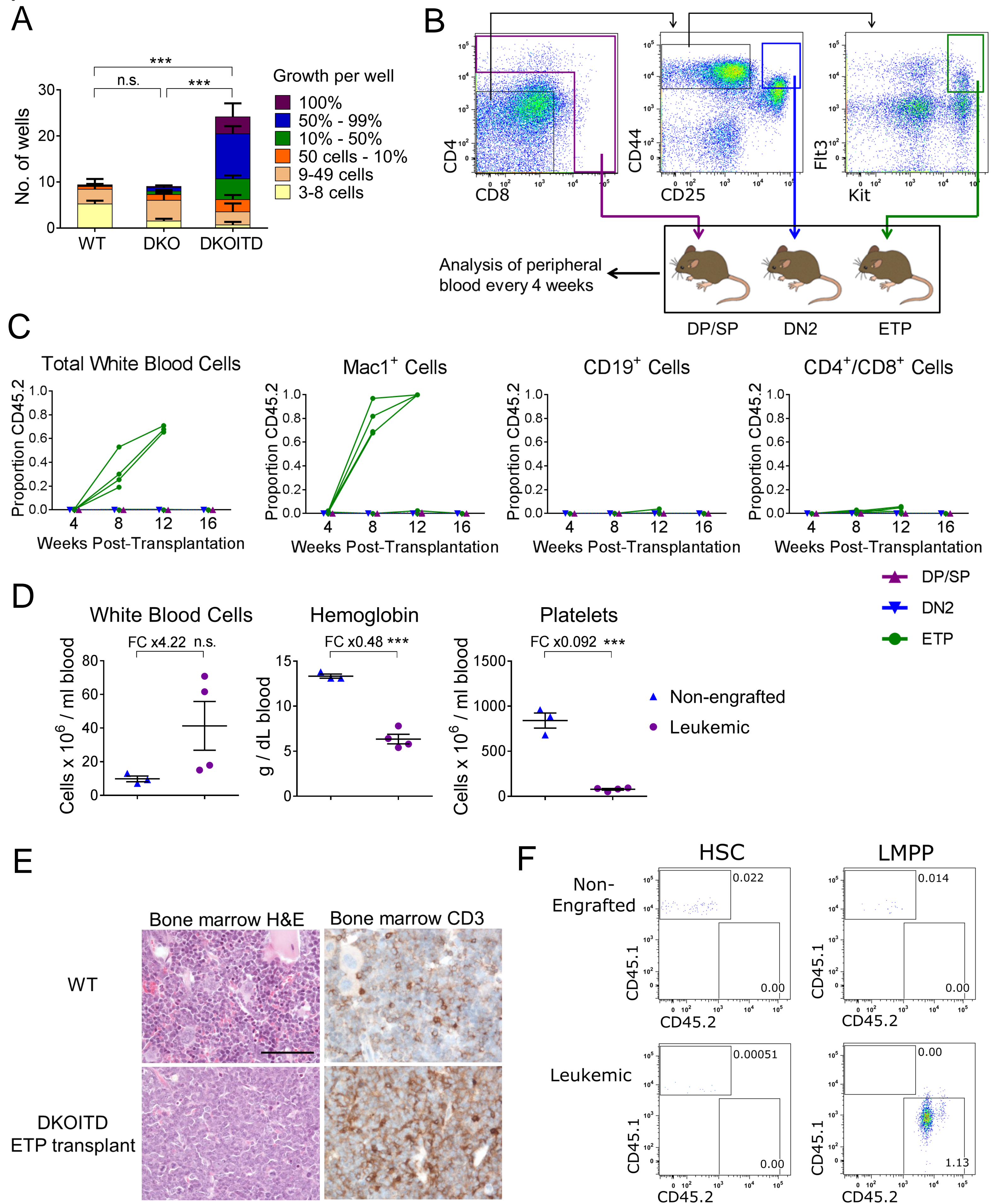


Figure 6

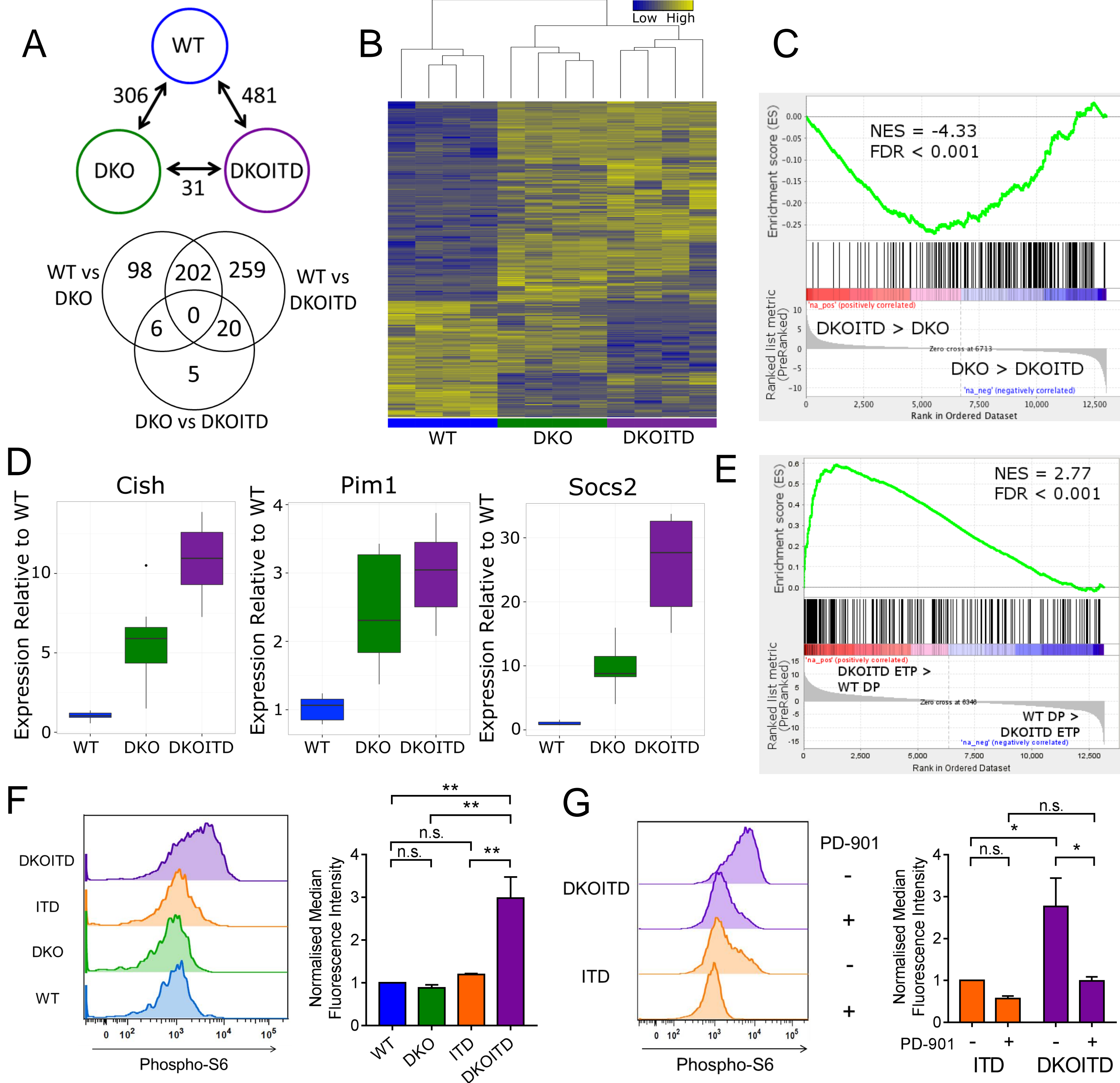
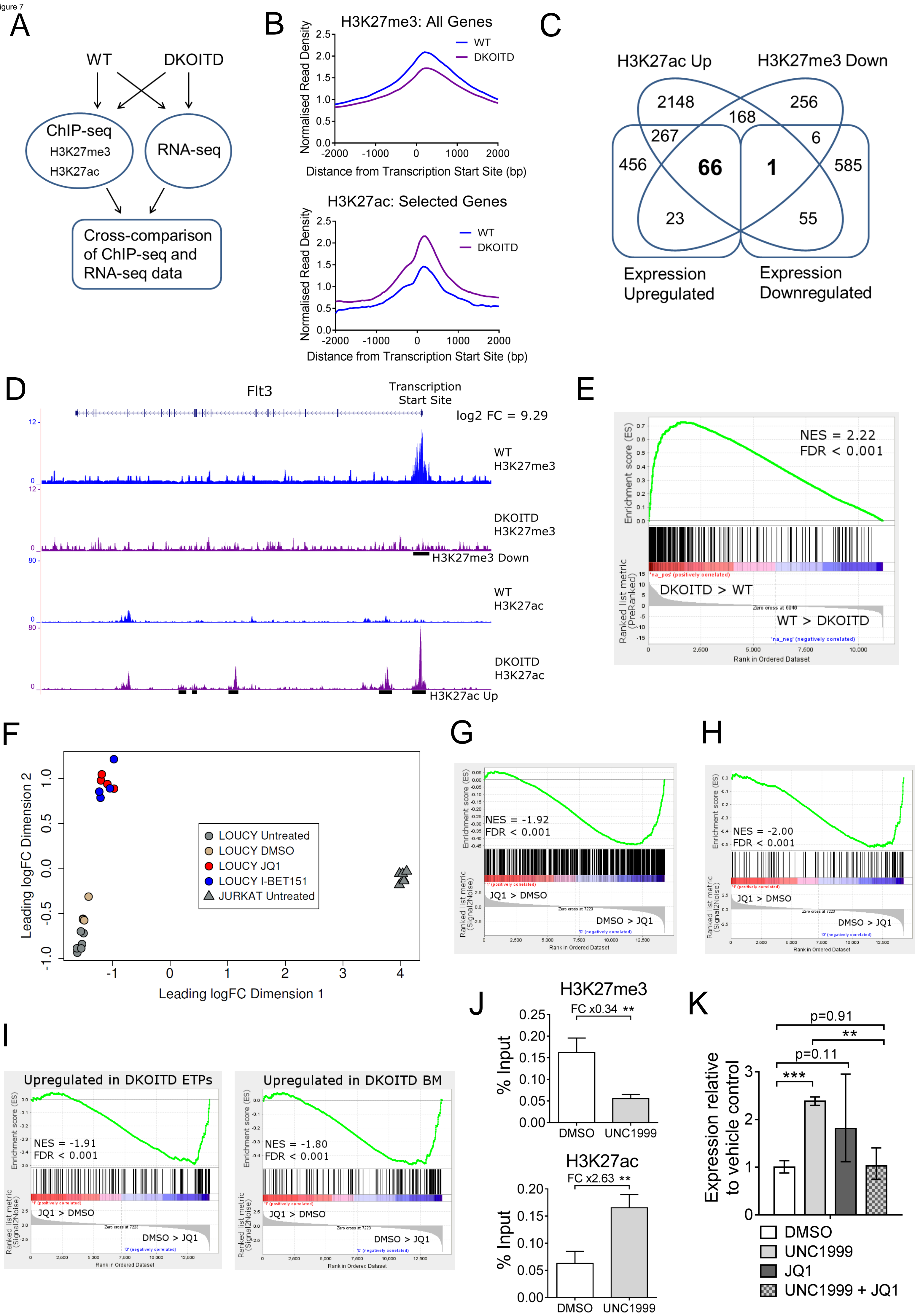
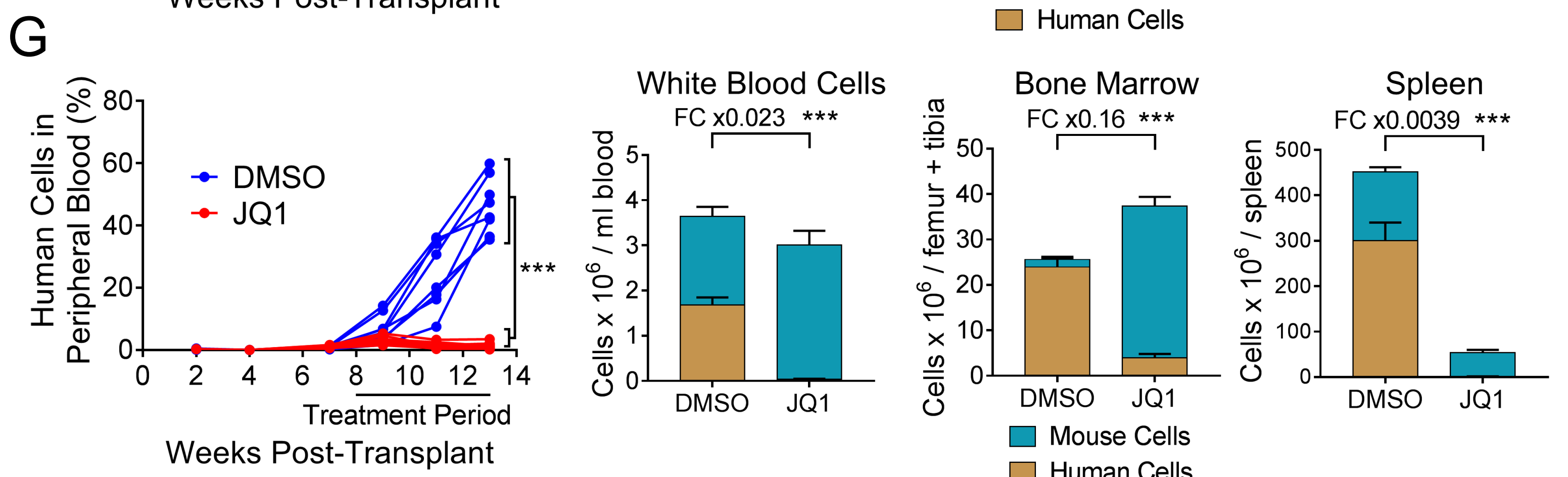
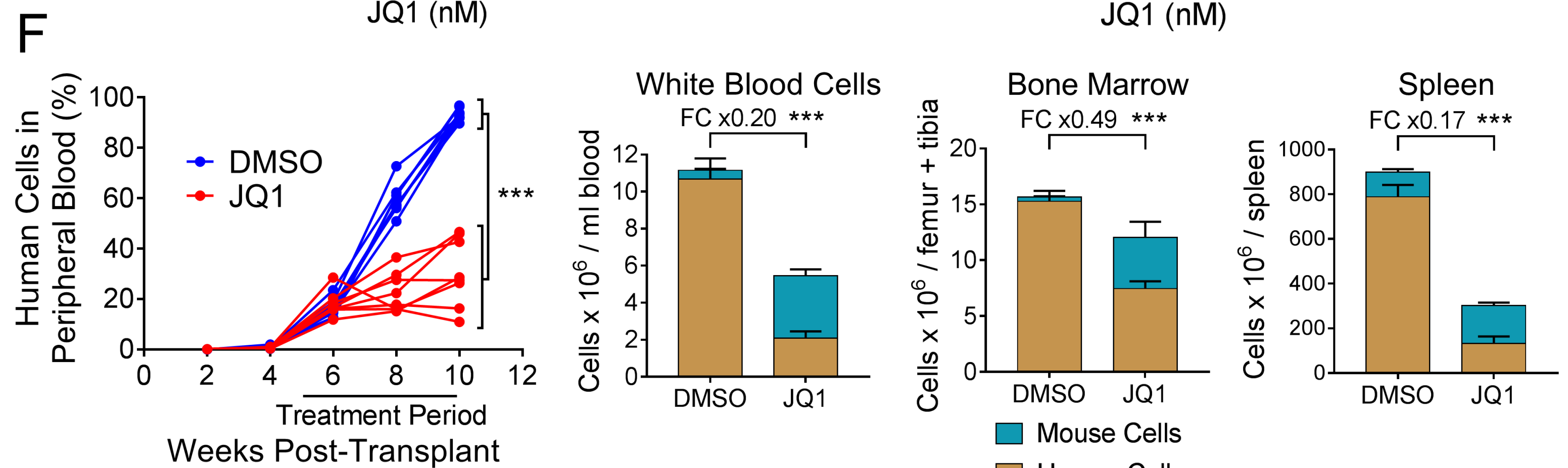
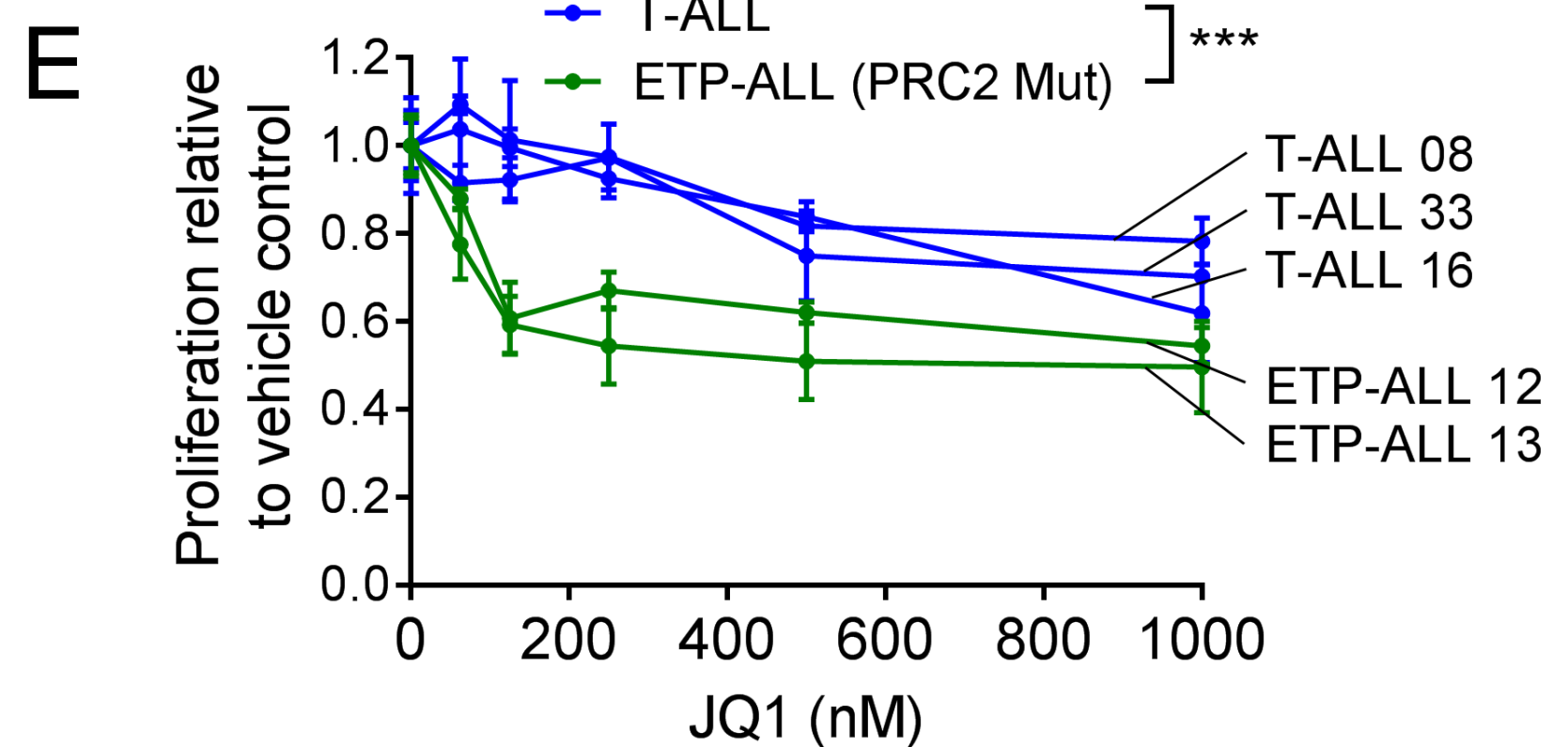
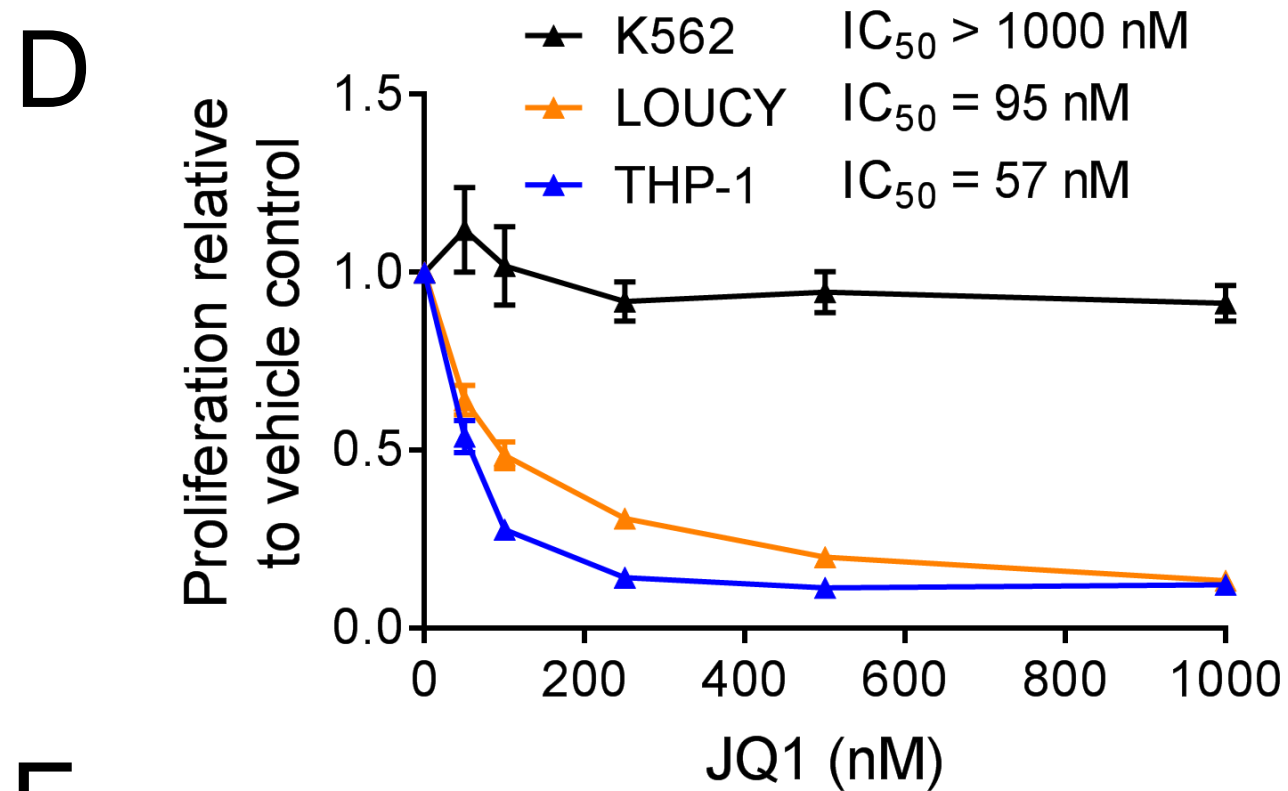
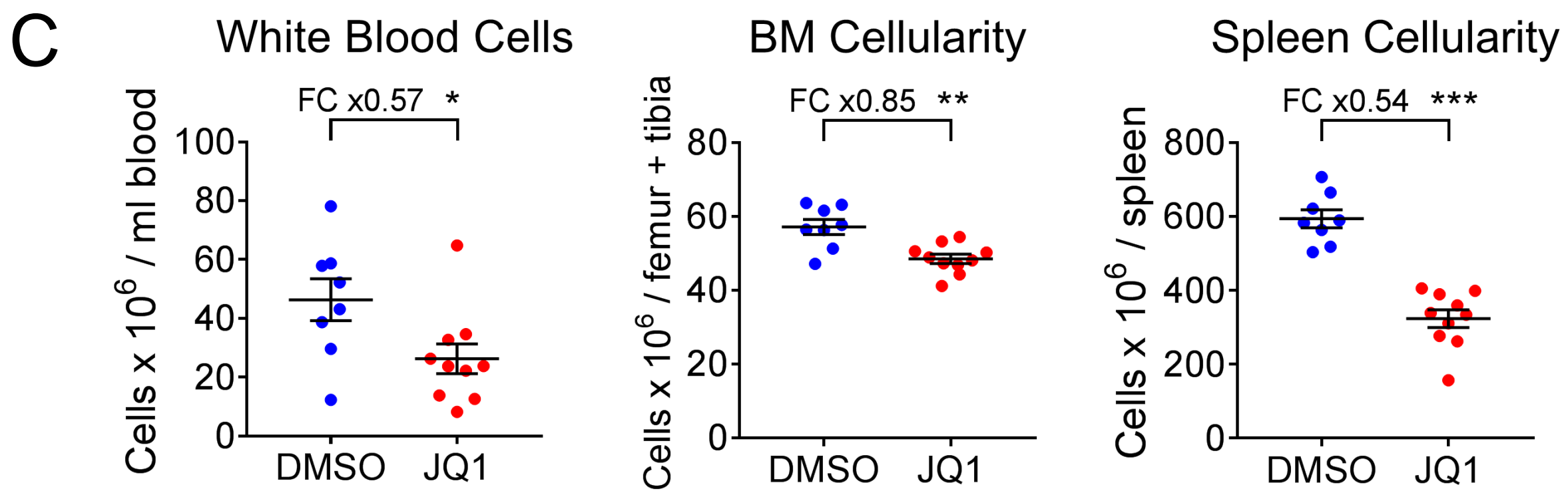
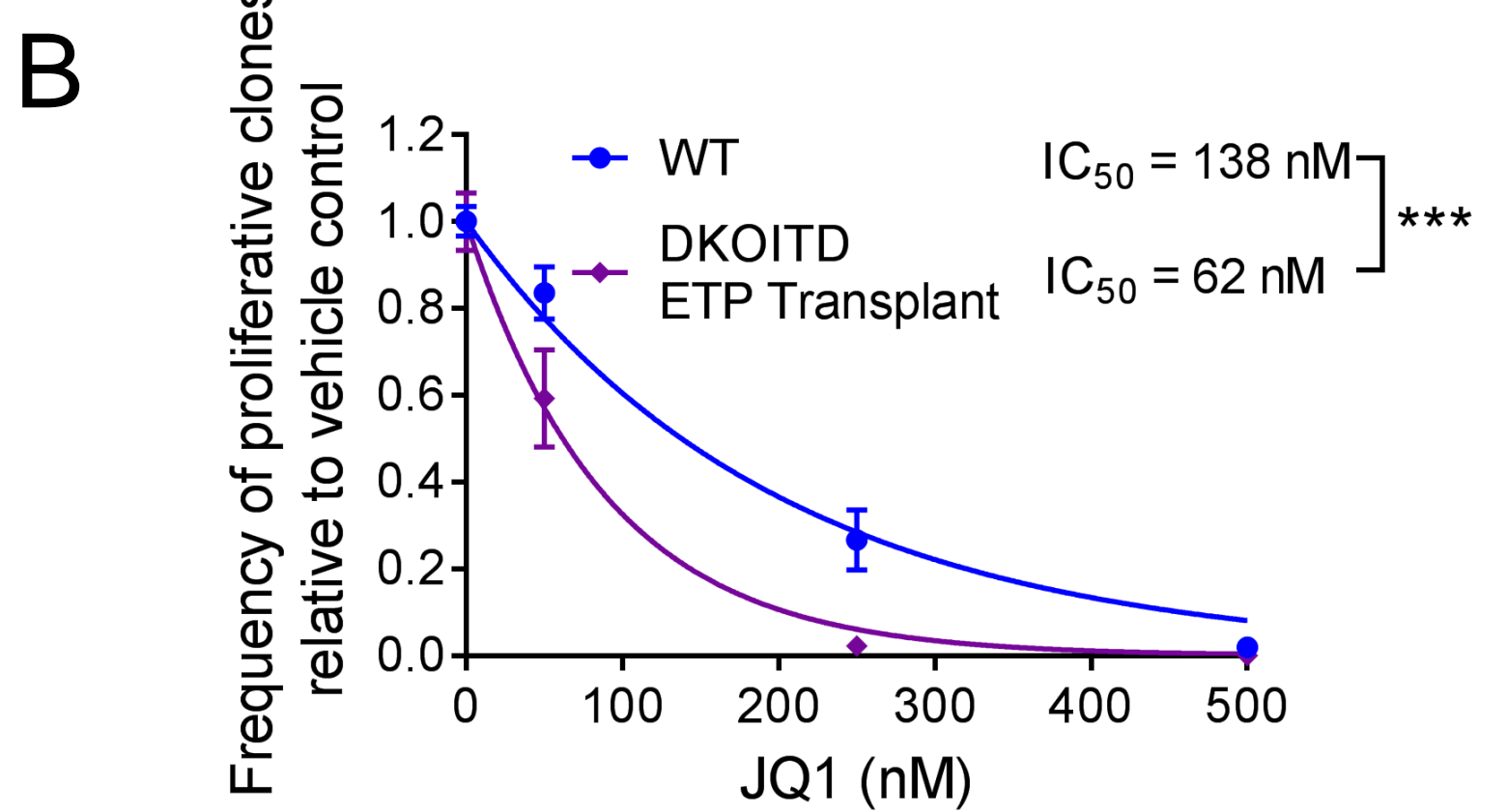
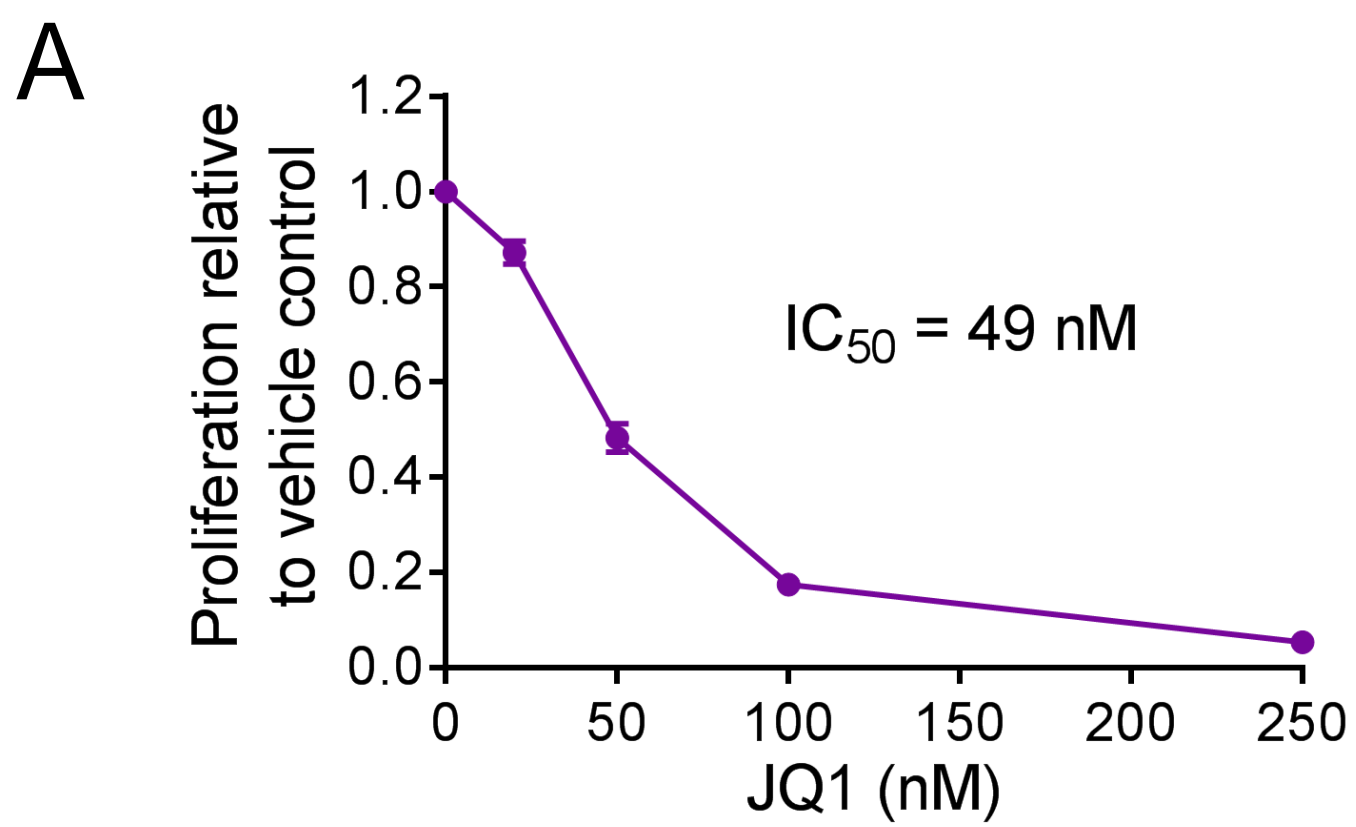


Figure 7





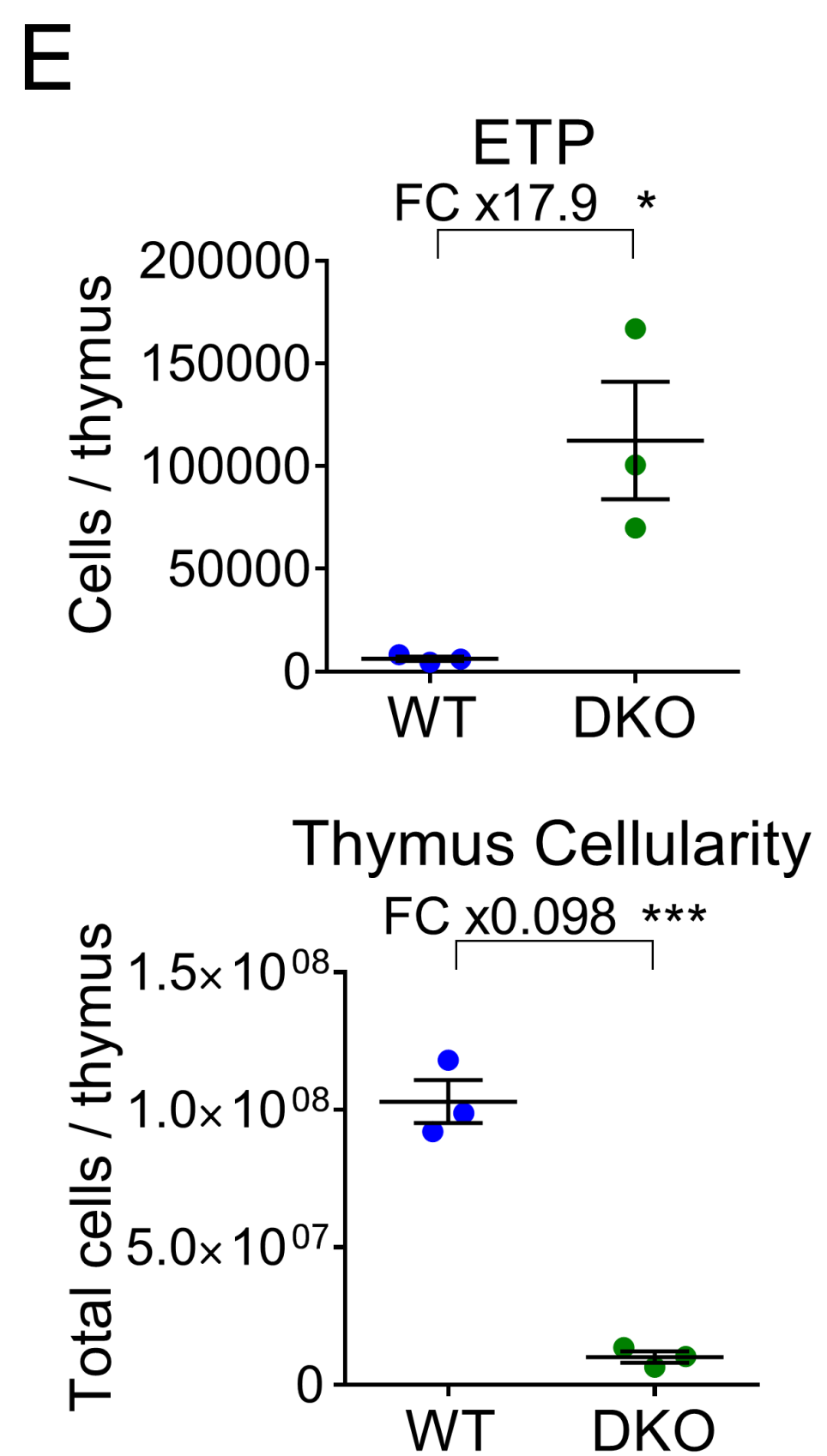
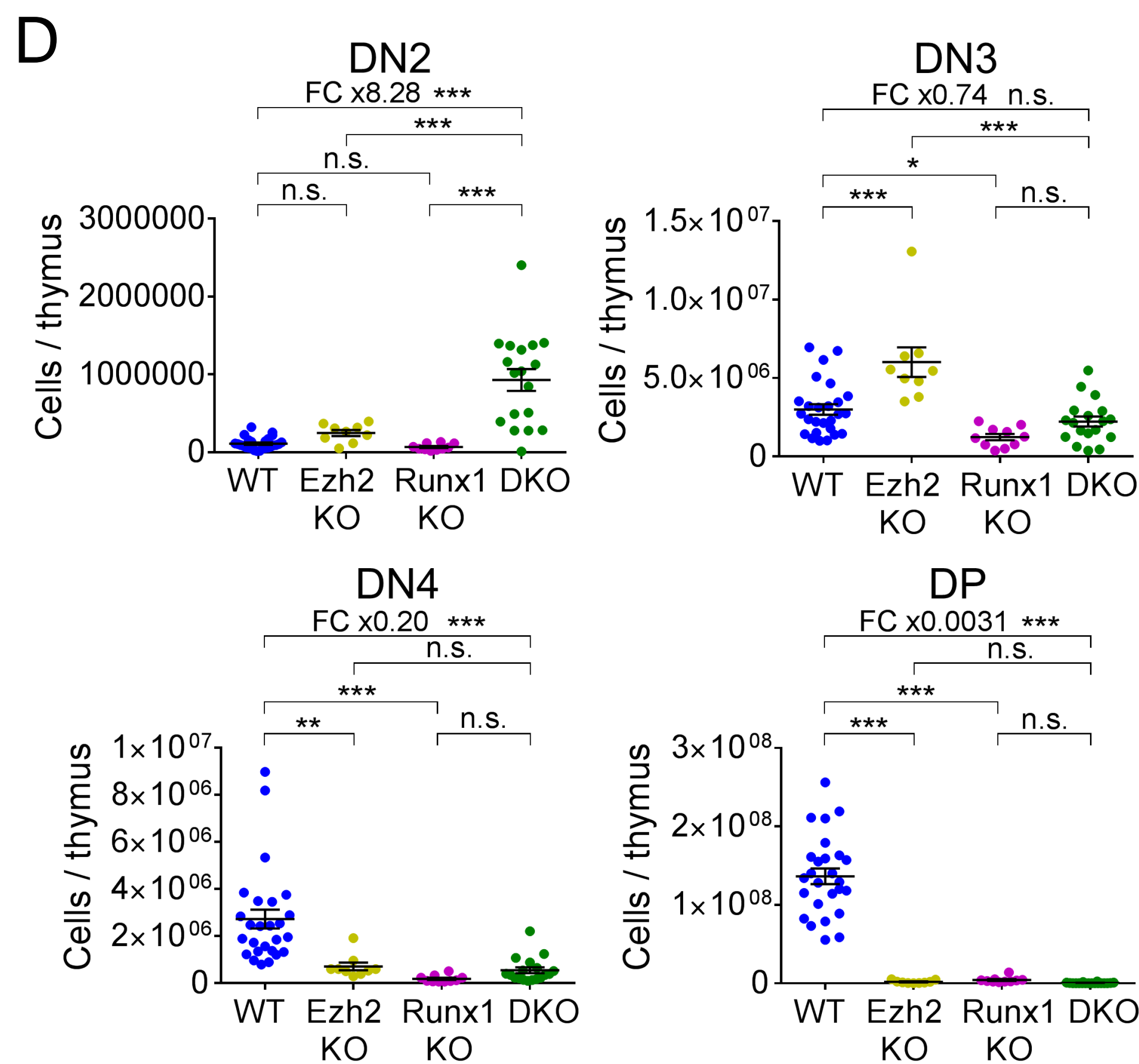
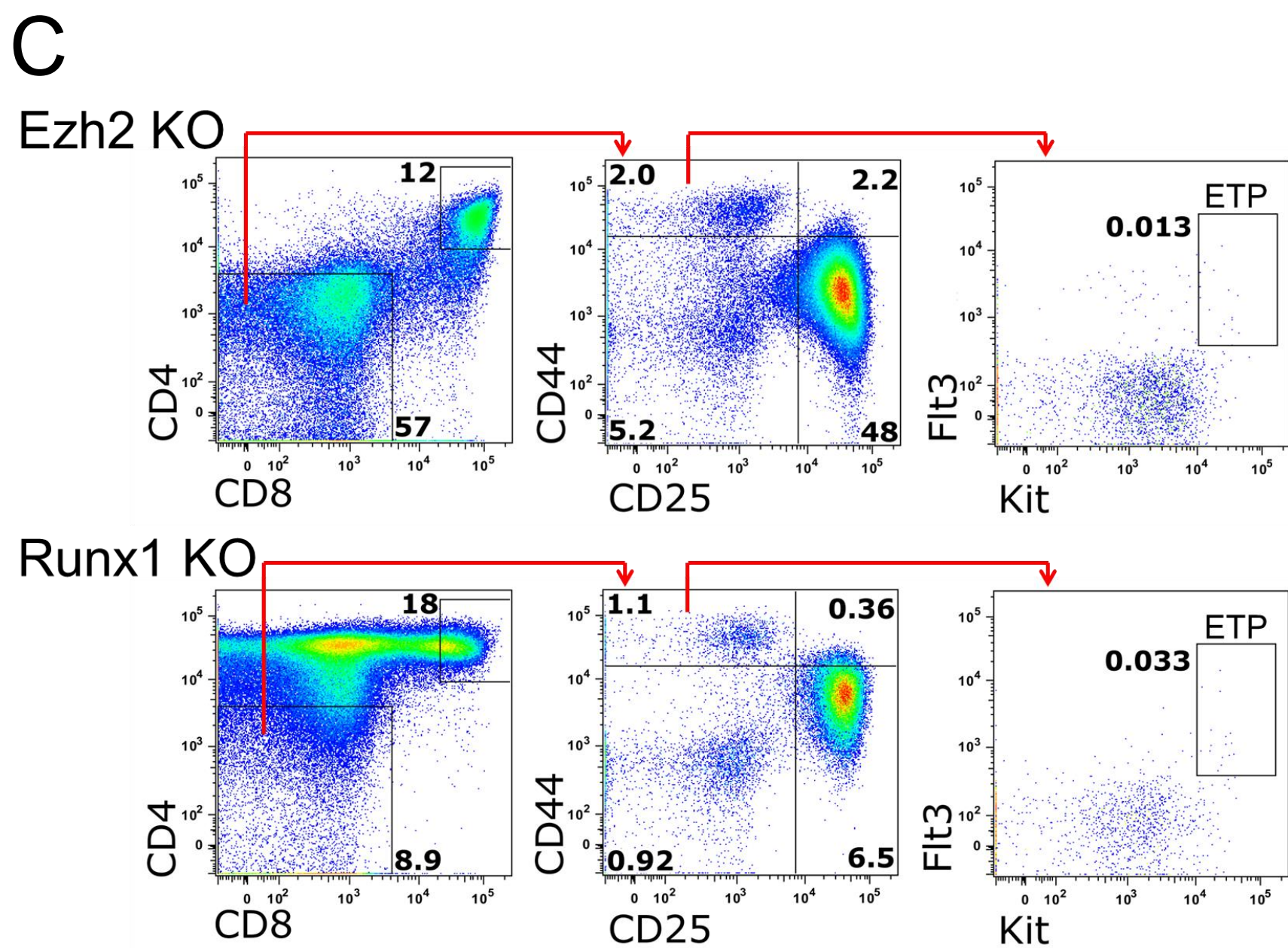
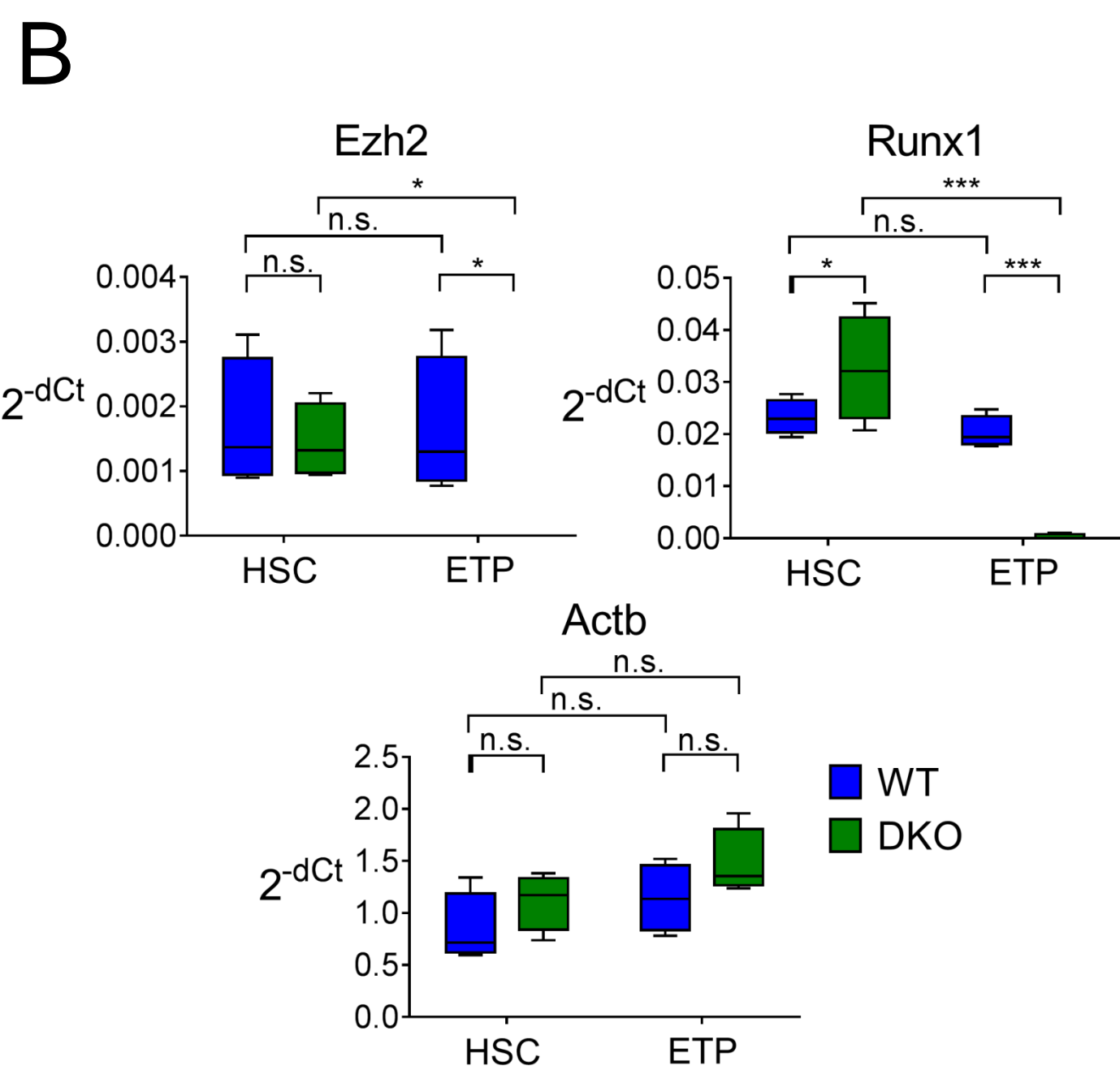
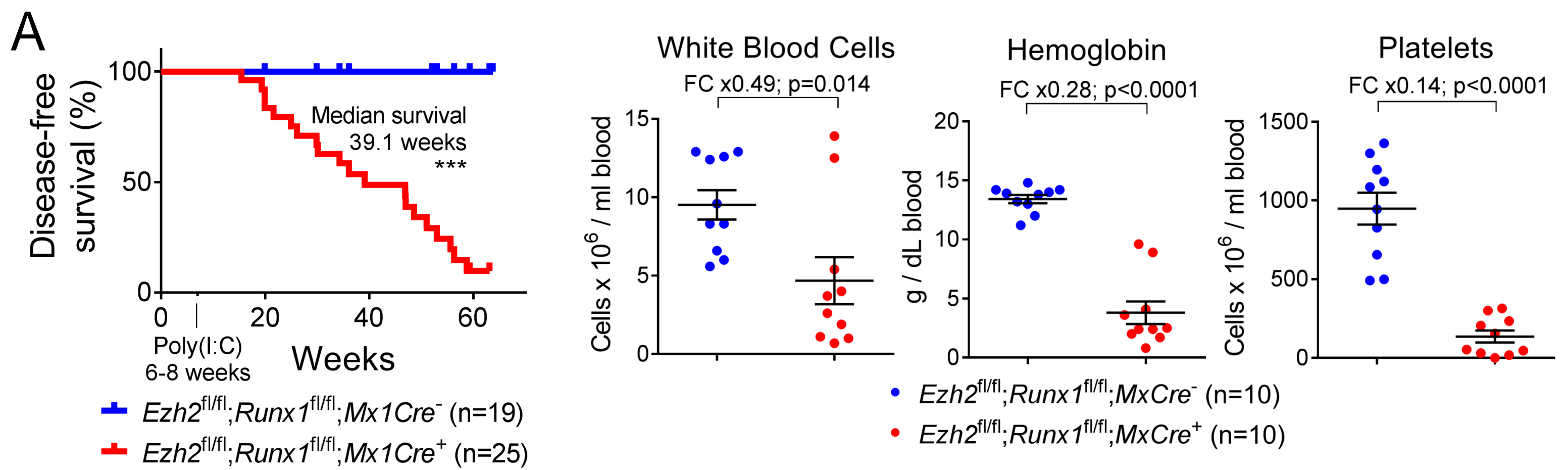


Figure S1, Related to Figure 1. Inactivation of Ezh2 and Runx1 Targeted to Early Lymphoid Progenitors

Collaborate to Cause a Marked Expansion of ETPs

(A) Disease-free survival curves (left) and hematological parameters of peripheral blood at time of culling (right) for *Ezh2^{fl/fl}Runx1^{fl/fl}Mx1Cre⁻* and *Ezh2^{fl/fl}Runx1^{fl/fl}Mx1Cre⁺* mice treated with Poly(IC) to activate Mx1Cre at 6-8 weeks of age. Time on the x-axis represents age of the mice. Significance was tested using the log-rank test (left) or T-test (right). Hematological parameters from one mouse are excluded; this mouse developed a CD19⁺Mac1⁺ leukemia at 42 weeks of age. (B) Determination of efficiency of deletion by Rag1Cre of conditionally targeted *Ezh2* and *Runx1* alleles, in Lin⁻Kit⁺Sca1⁺CD150⁺CD48⁻ HSCs and Lin⁻CD4⁻CD8⁻CD44⁺CD25⁻Kit⁺Flt3⁺ ETPs from 6-8 week old WT and DKO mice. Relative expression levels of *Ezh2* and *Runx1* mRNA are shown; Ct values were normalised to *Gapdh*. Amplicons were designed to target exons removed by Rag1Cre recombination. The bottom panel shows expression of *Actb* normalised to *Gapdh*. n=4 for each cell type; each replicate represents a sample of 50 cells. Box plots show median, upper and lower quartiles. (C) Representative FACS plots showing ETP gating strategy for Ezh2-KO and Runx1-KO thymuses. Figures represent mean percentage of total thymocytes falling into each gate across all experiments. (D) FACS analysis of absolute numbers of DN2, DN3, DN4 and DP cells per thymus in 6-8 week old mice (WT n=26, Ezh2-KO n=9, Runx1-KO n=10, DKO n=18). (E) FACS analysis of absolute numbers of ETPs per thymus (top) and total thymus cellularity (bottom) in 6 month old mice (WT n=3, DKO n=3). p values are by T-test (A, E), or ANOVA (B, D), *p<0.05, **p<0.01 and ***p<0.001. n.s.; not significant (p>0.05). Horizontal lines show mean ± SEM (A, D-E).

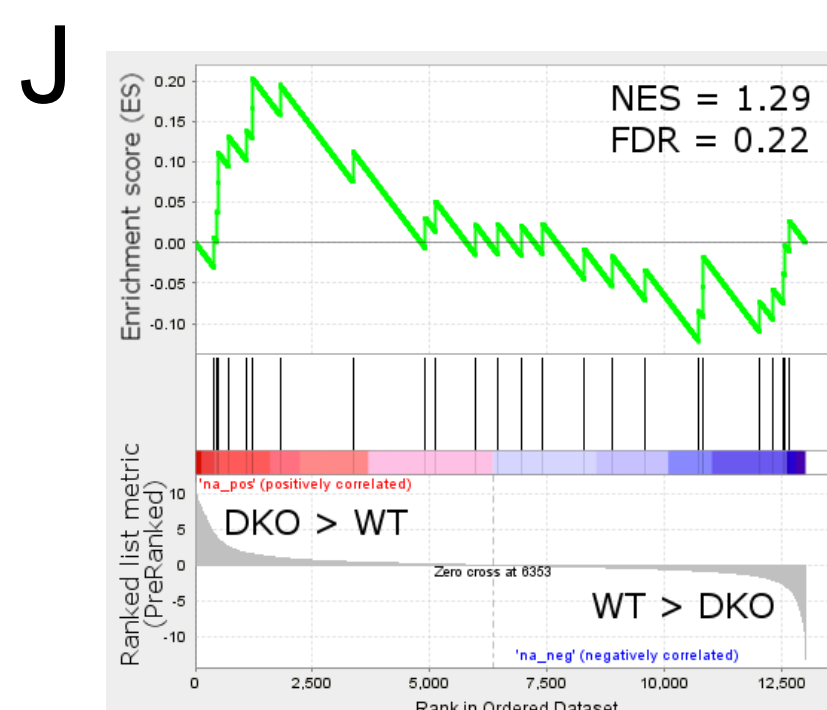
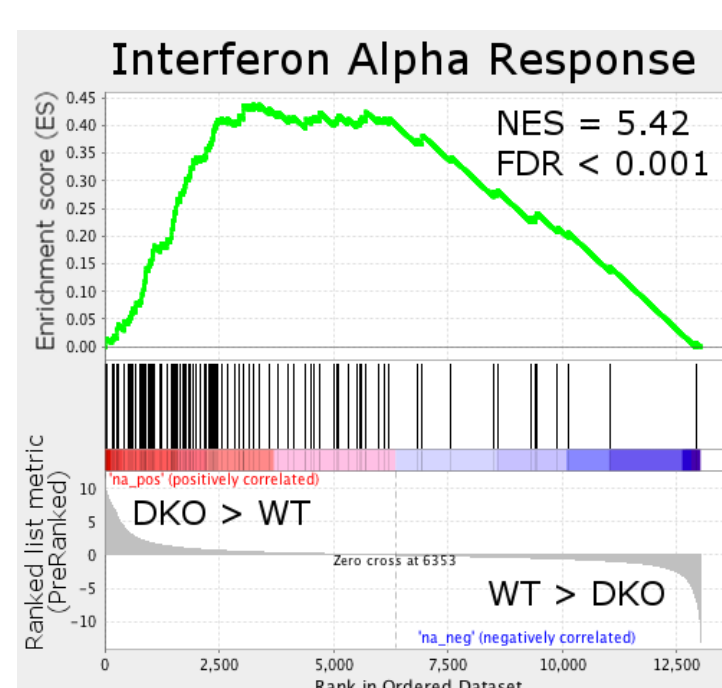
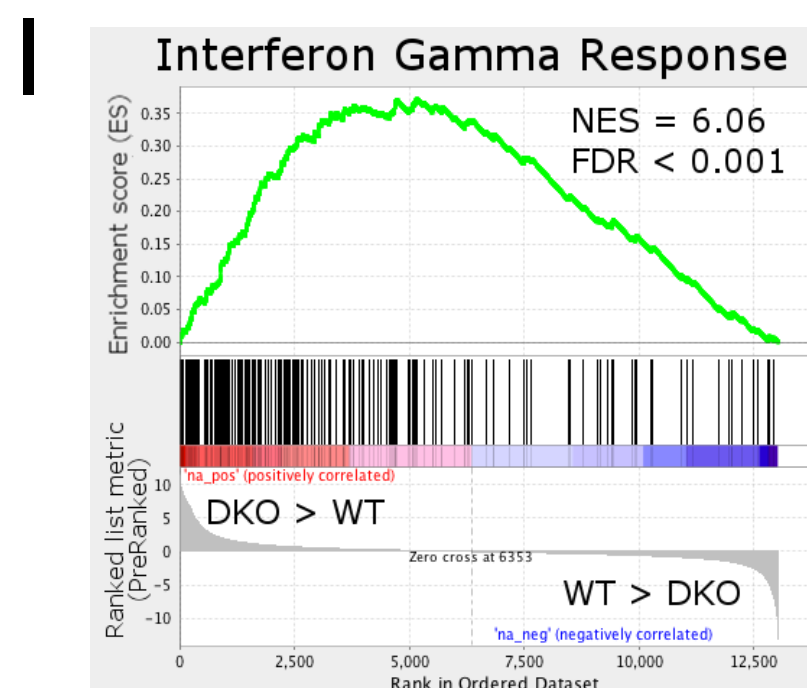
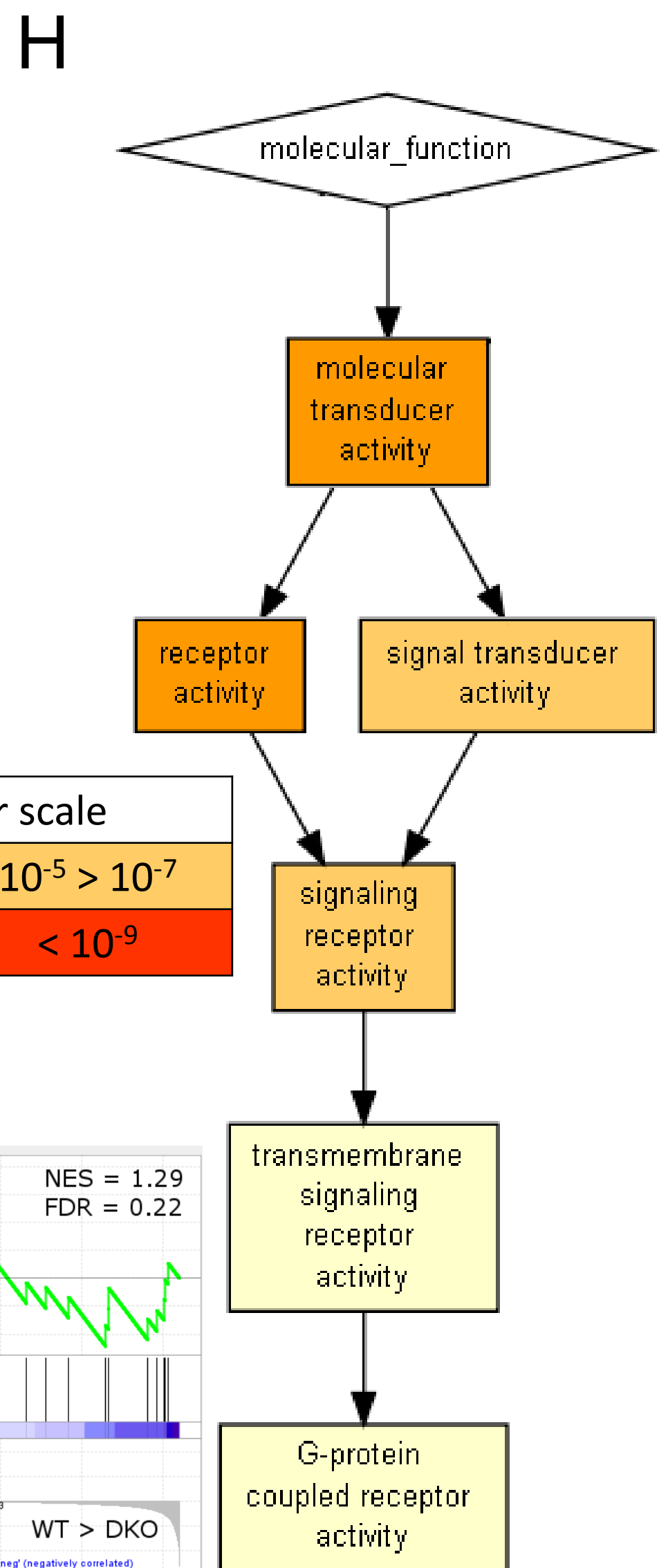
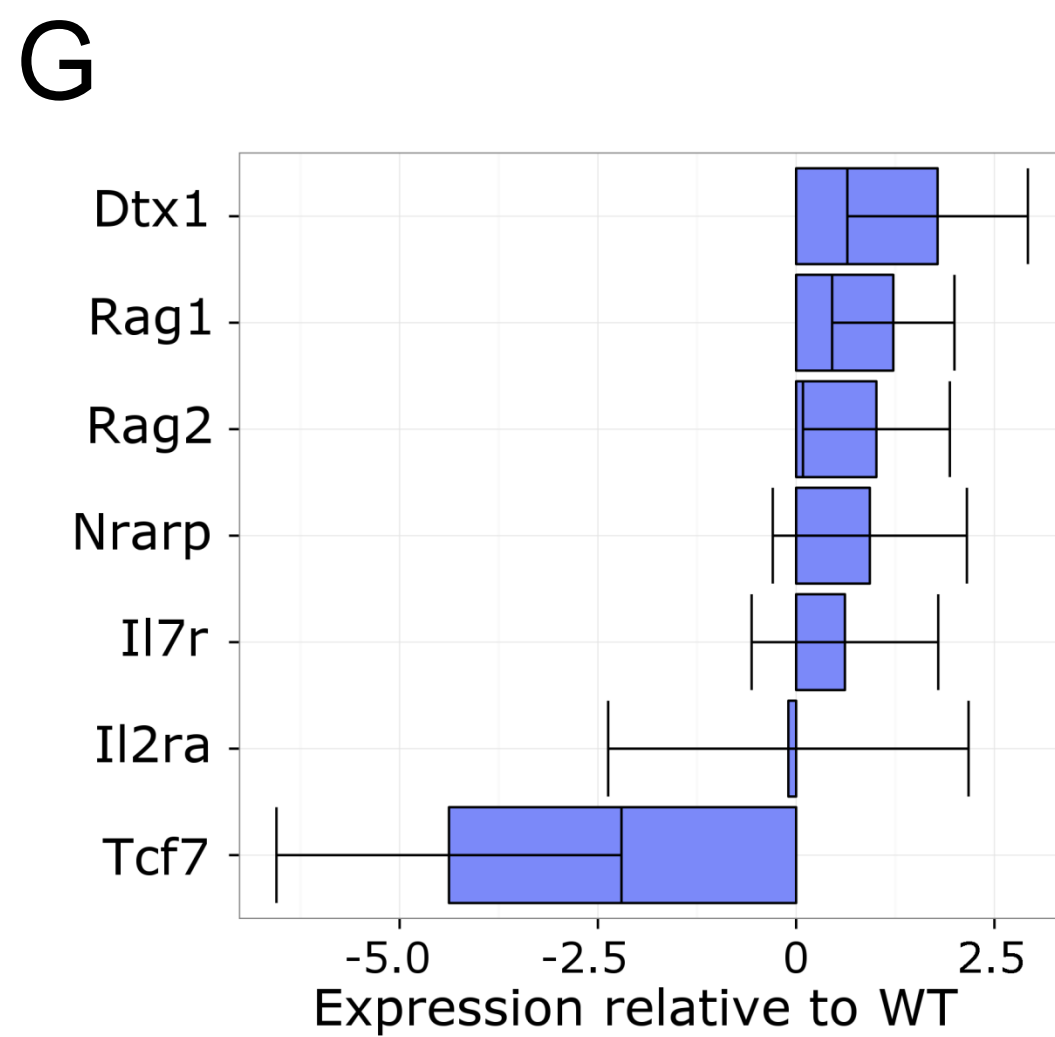
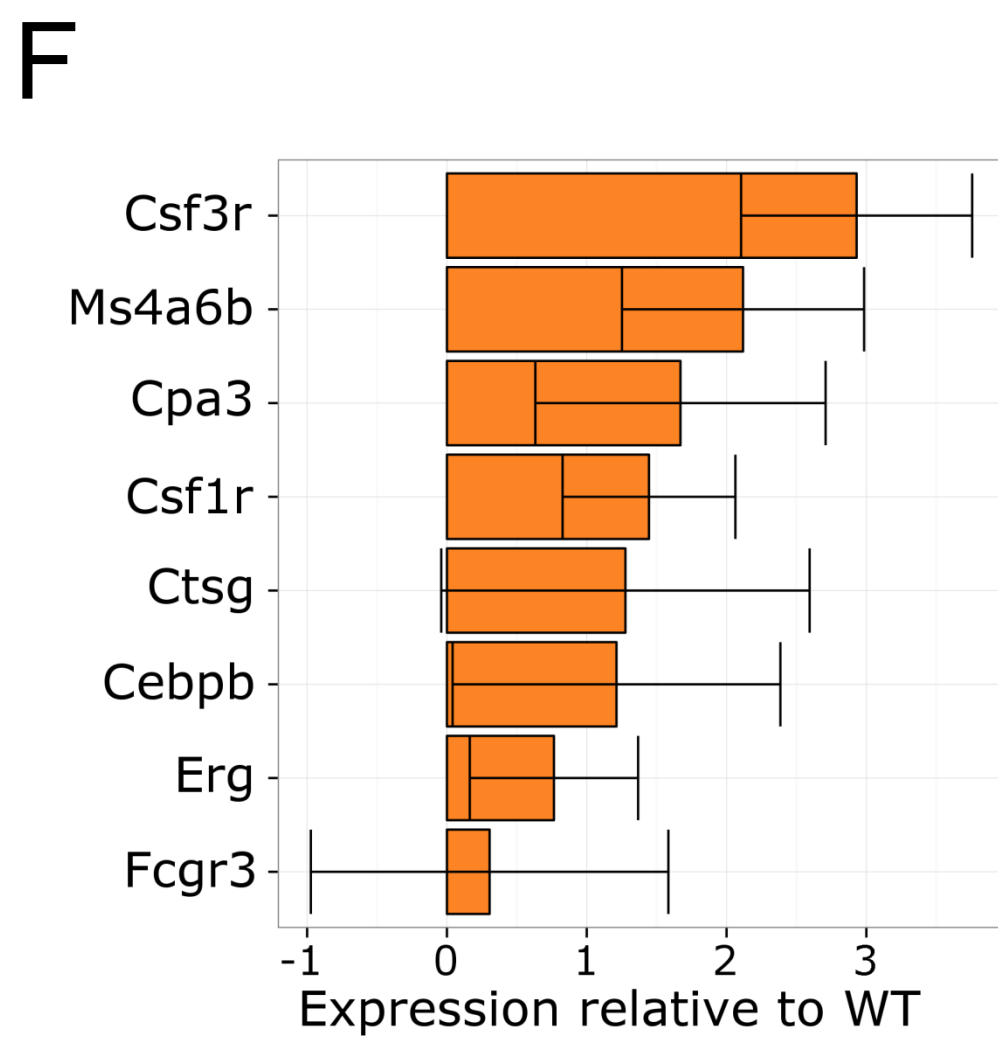
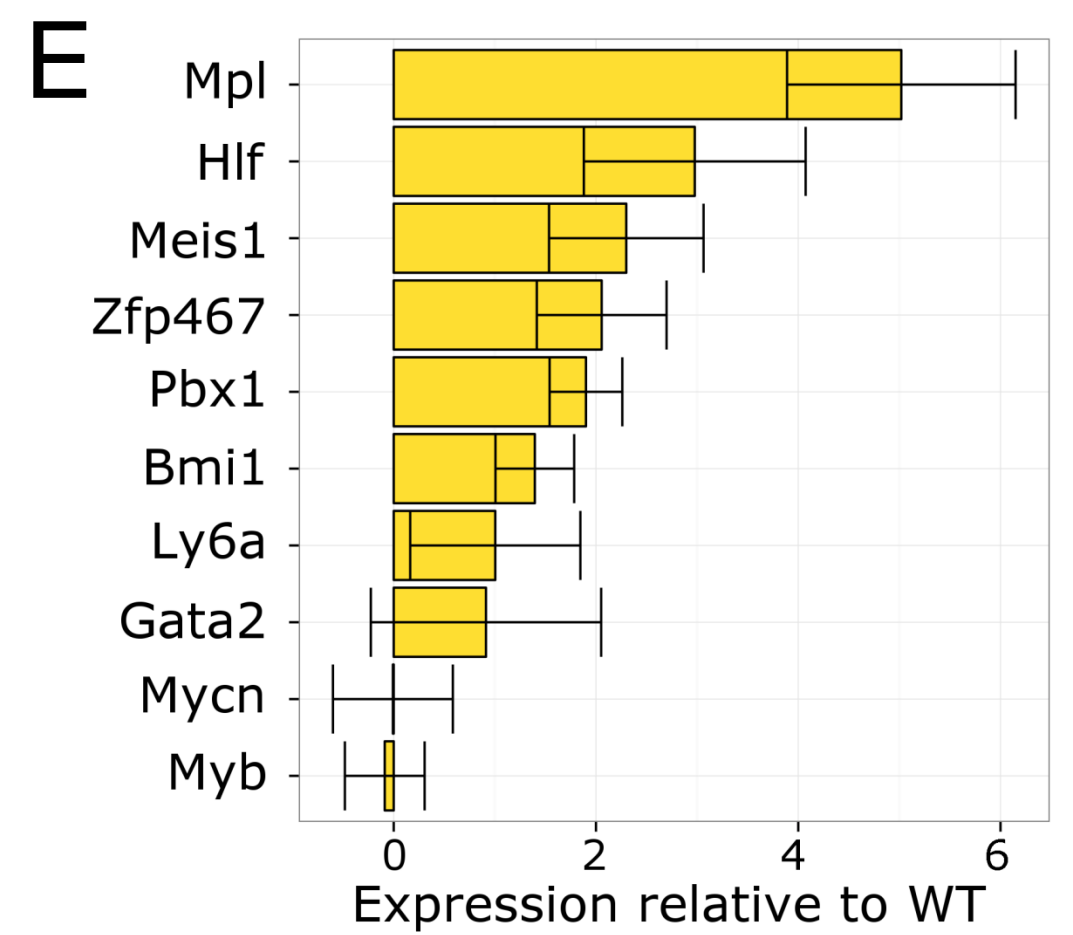
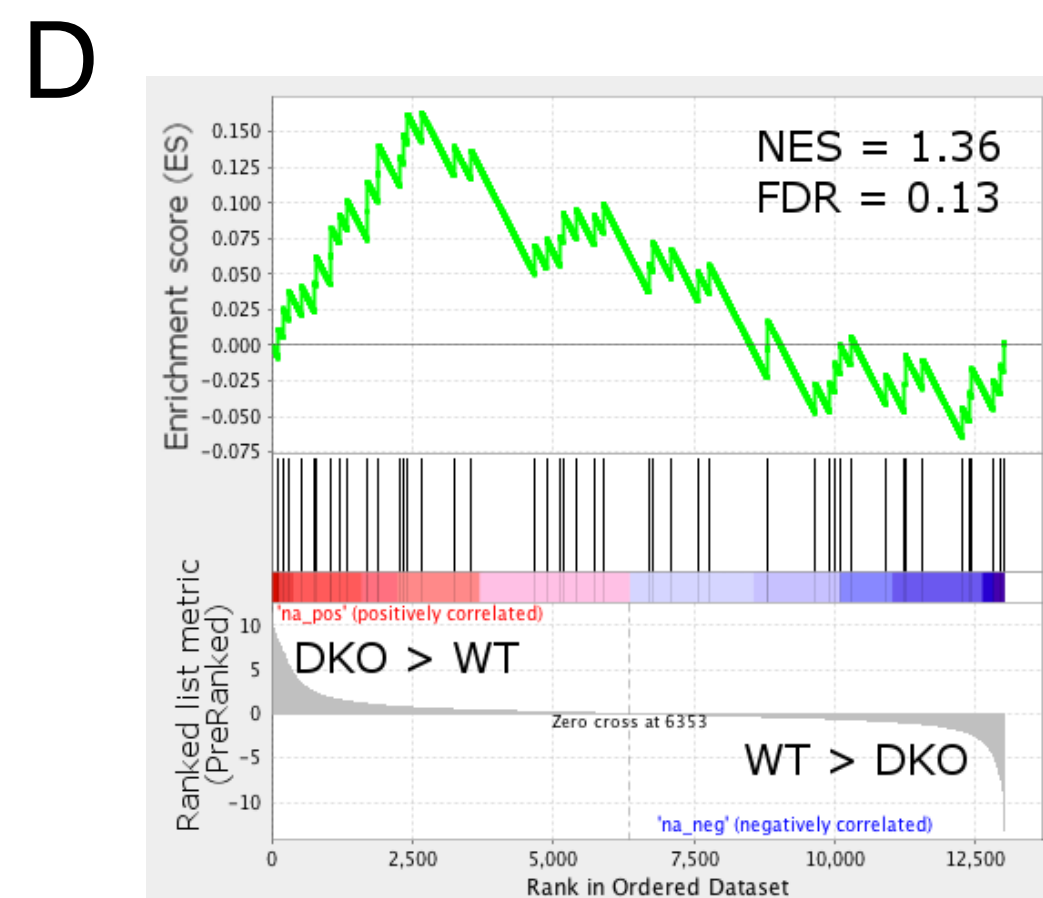
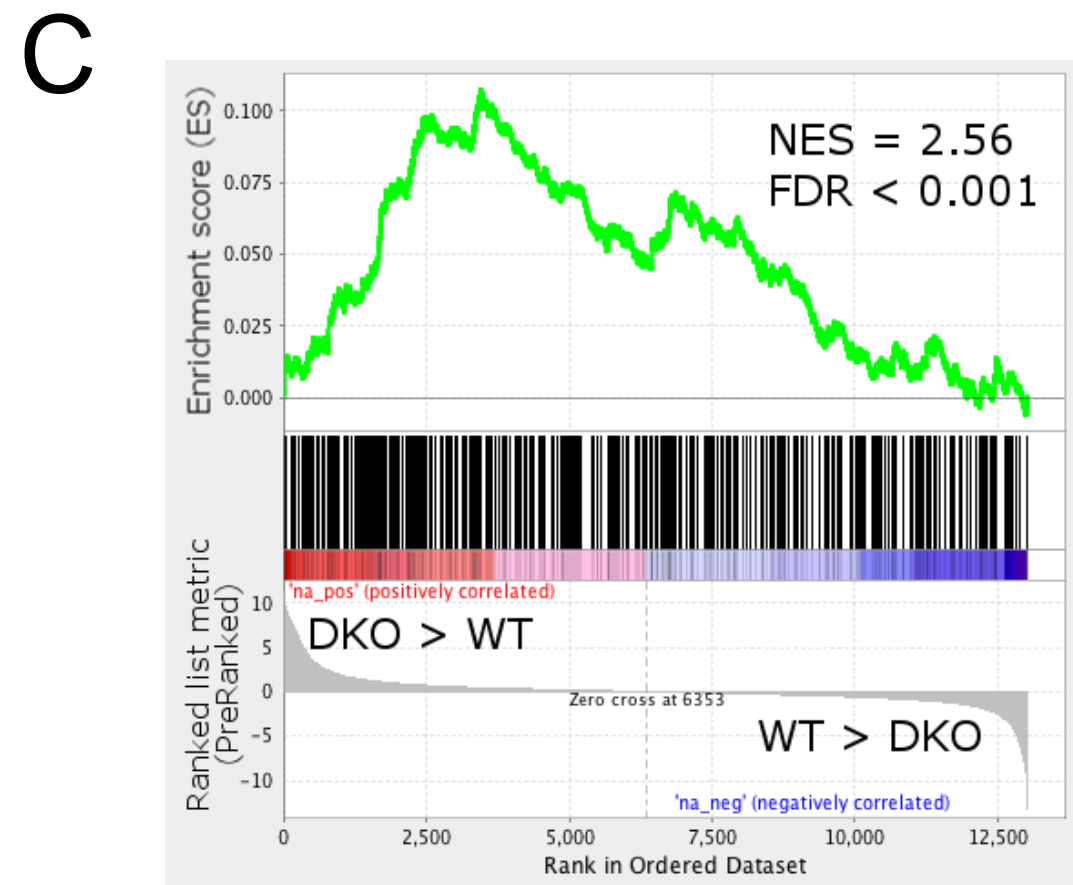
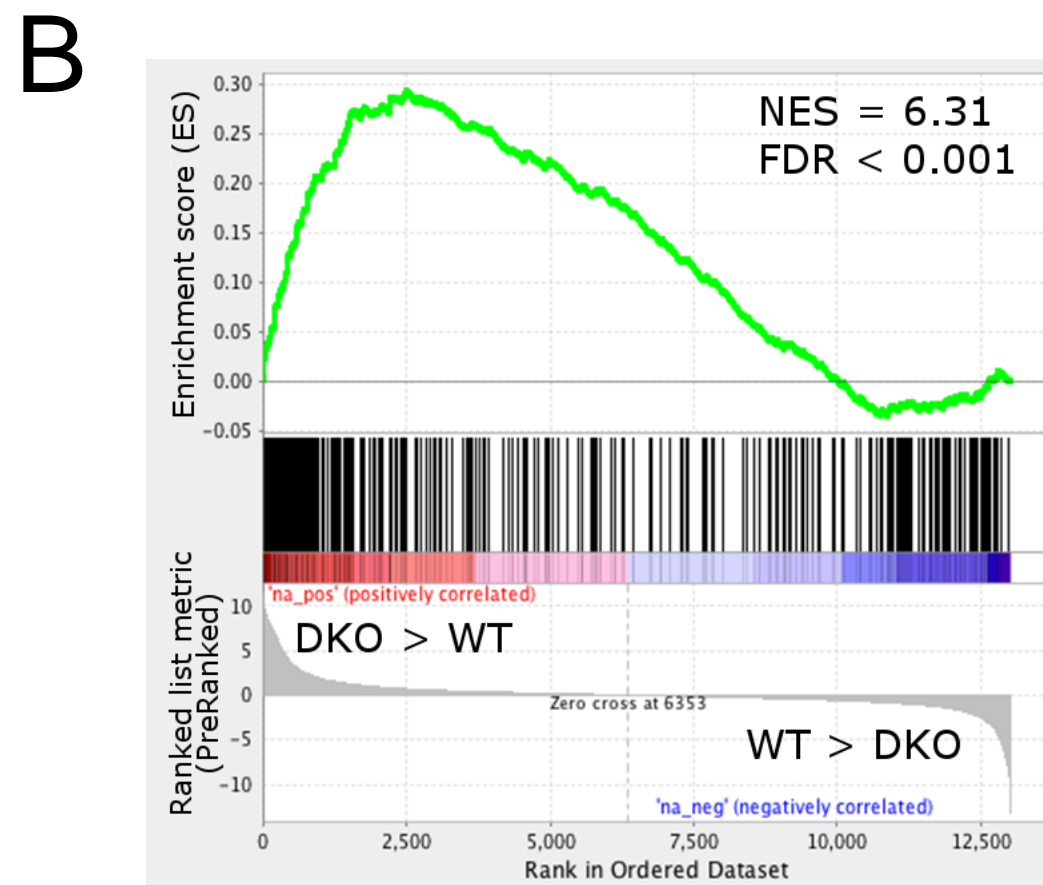
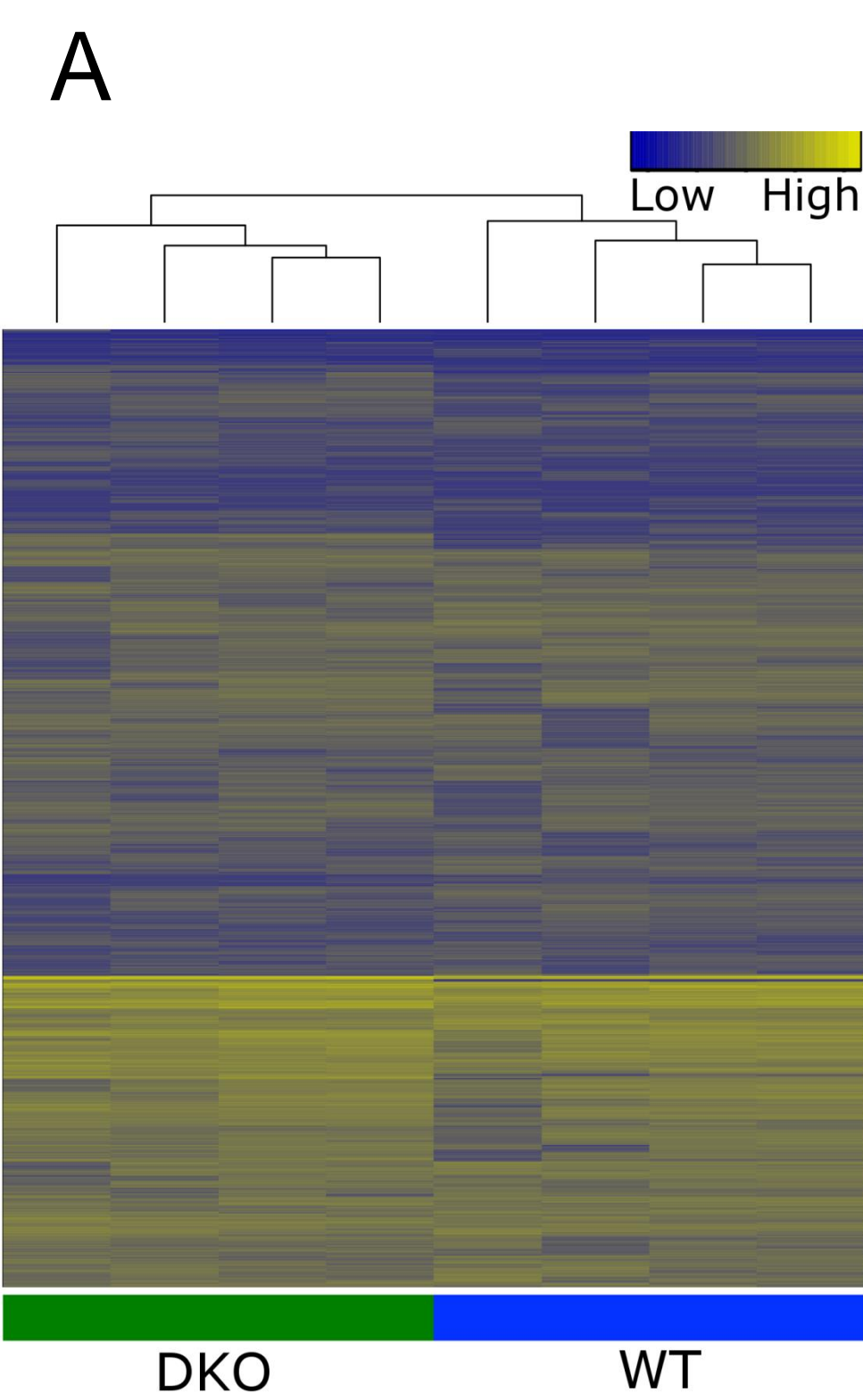


Figure S2, Related to Figure 2. Disrupted Gene Expression Signatures in DKO ETPs Recapitulate Features of ETP Leukemia

(A) Hierarchical clustering and heatmap showing expression levels, scaled per gene, of the 3000 most variable genes between WT and DKO ETPs (WT n=4, DKO n=4). Each replicate represents 100 purified ETPs from individual mice at 6-8 weeks of age. (B-D) GSEA plots of HSC (B), Pre-GM (C) and Pre-MegE gene expression programs (D) comparing WT and DKO ETPs. (E-G) Relative expression level of HSC (E), myeloid (F) and lymphoid-associated genes (G) in DKO ETPs expressed relative to the level in WT ETPs (log2 scale) as determined by qPCR (WT n=8, DKO n=7). Each replicate represents 50 purified ETPs from individual mice at 6-8 weeks of age. Bars show mean \pm SD. (H) Gene ontology diagram showing pathways enriched in DKO relative to WT ETPs. (I-J) GSEA plots comparing WT and DKO ETPs for Interferon signaling target genes (I) (Interferon gamma left panel and Interferon alpha right panel) and Notch1 target genes (J).

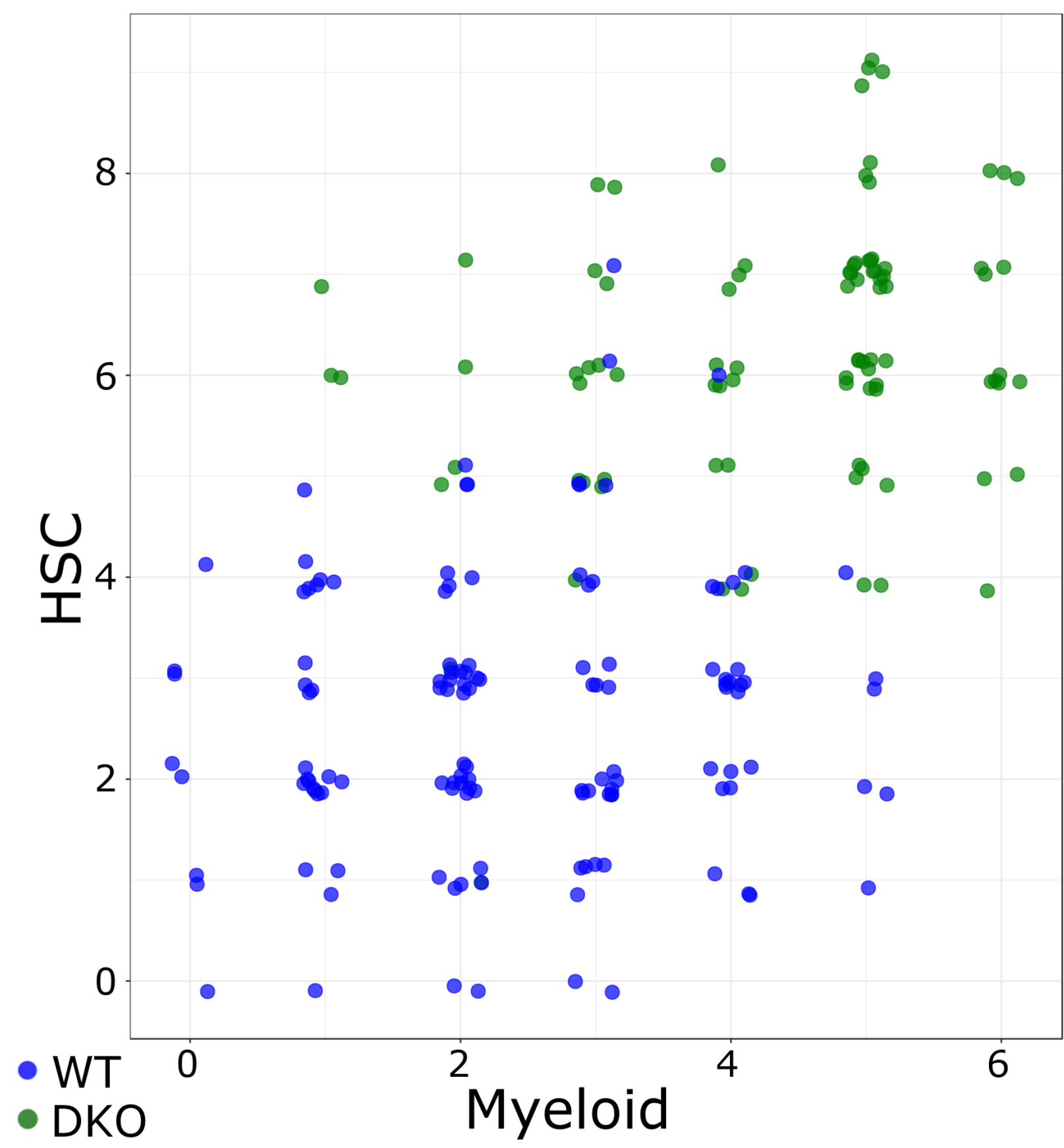


Figure S3, Related to Figure 3. HSC and Myeloid Genes are Co-Expressed within Single DKO ETPs.

Scatter plot showing level of co-expression of HSC and myeloid genes within single WT (n=129) and DKO (n=91) ETPs. Each dot represents a single cell, for which are plotted the number of genes showing detectable expression from the panel of HSC- and myeloid-associated genes shown in Figure 3A.

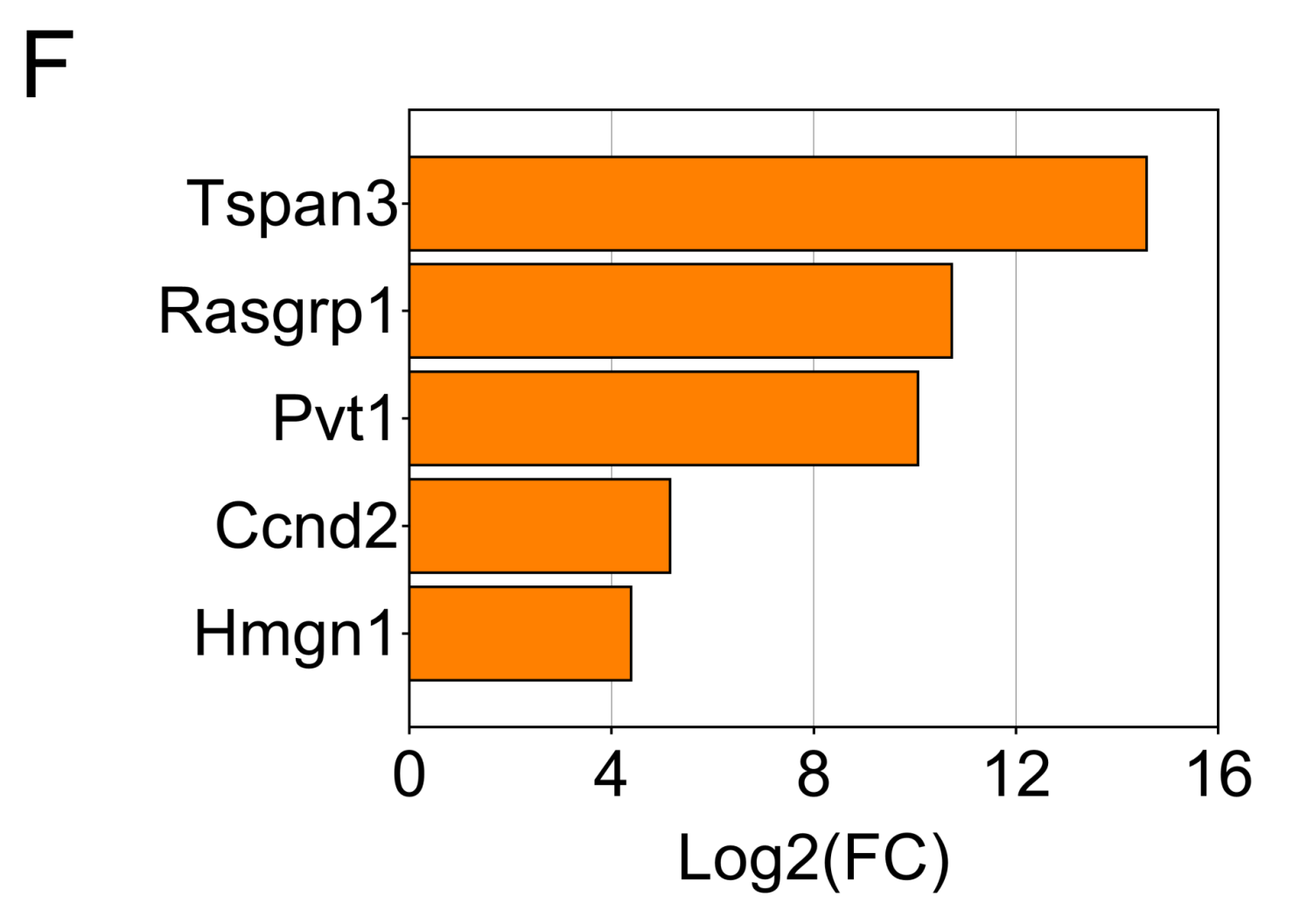
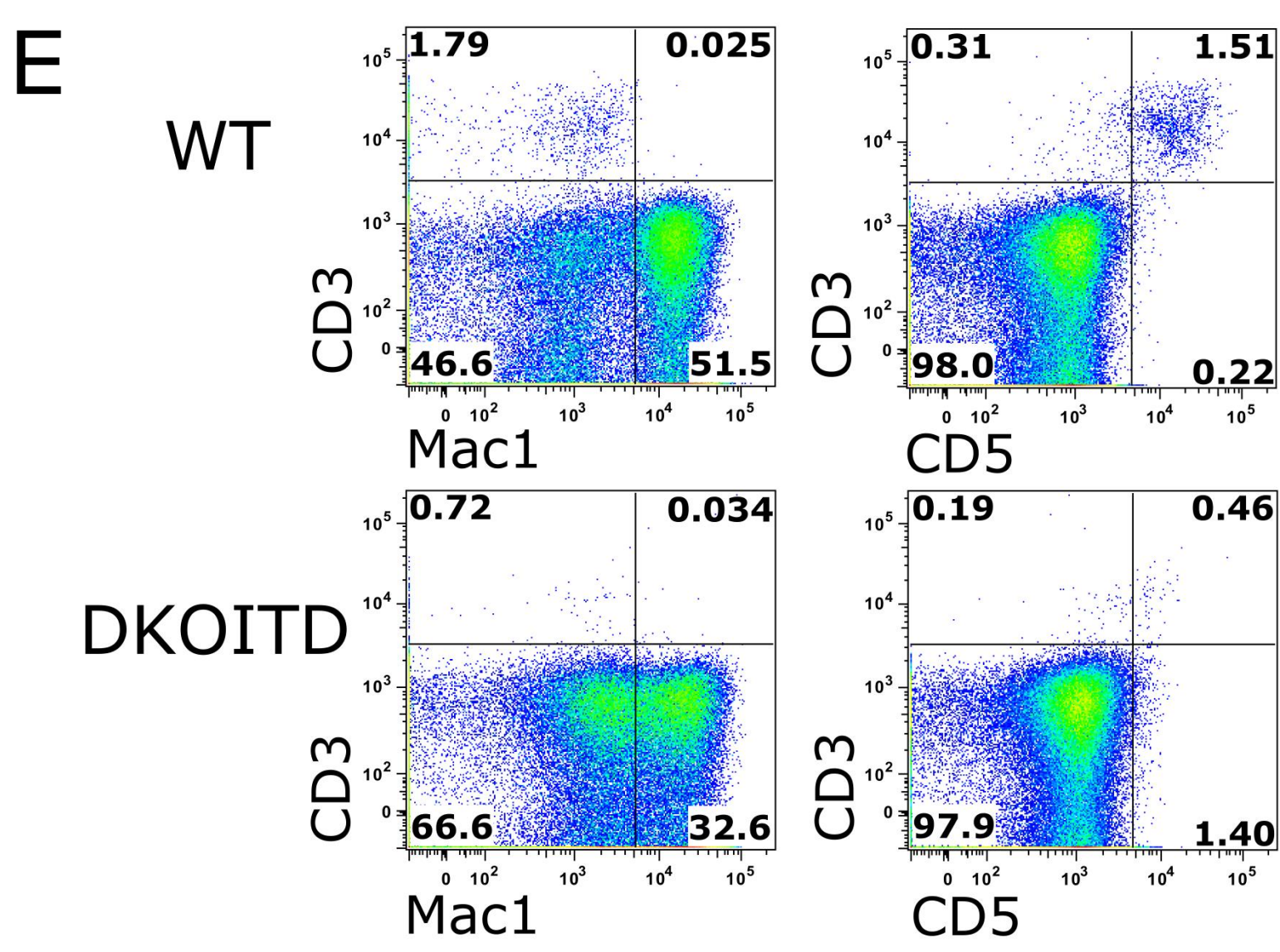
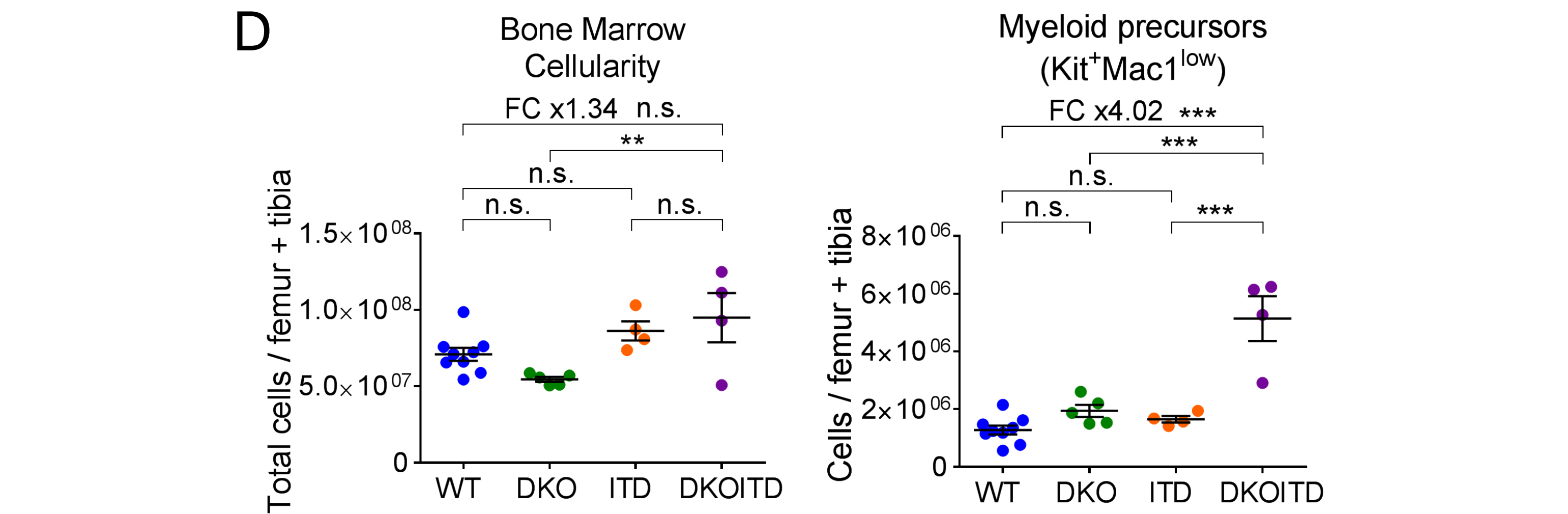
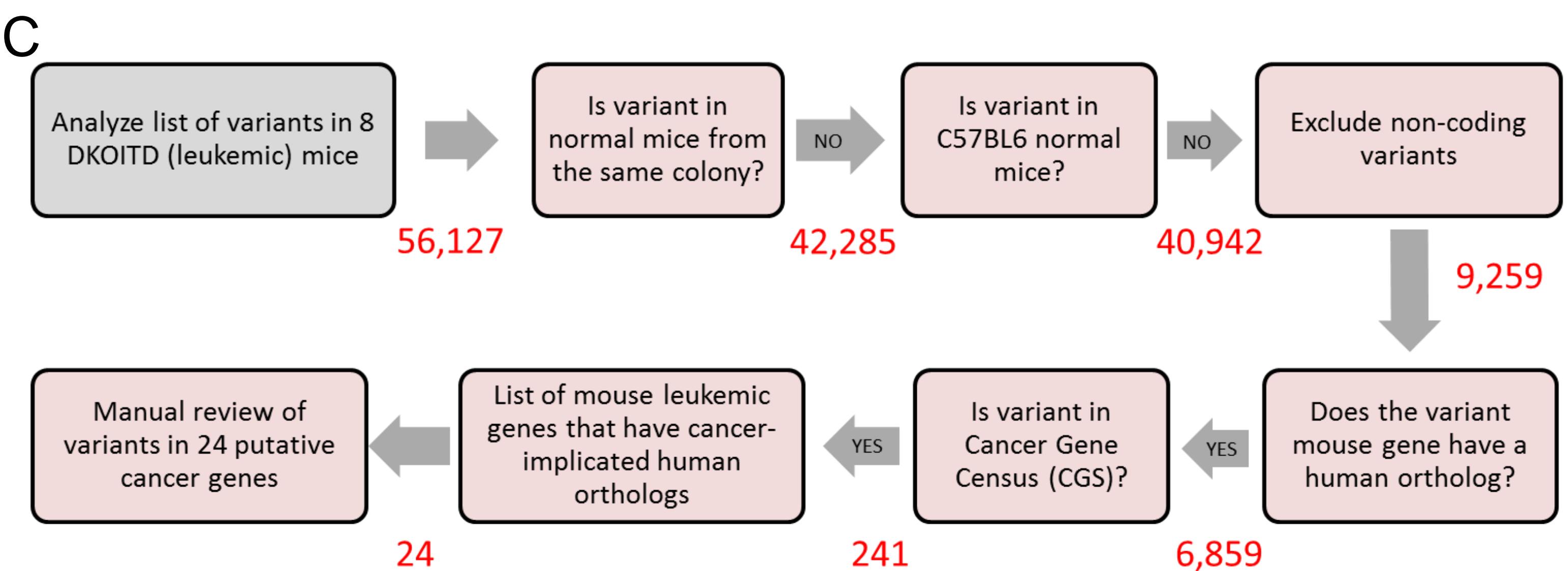
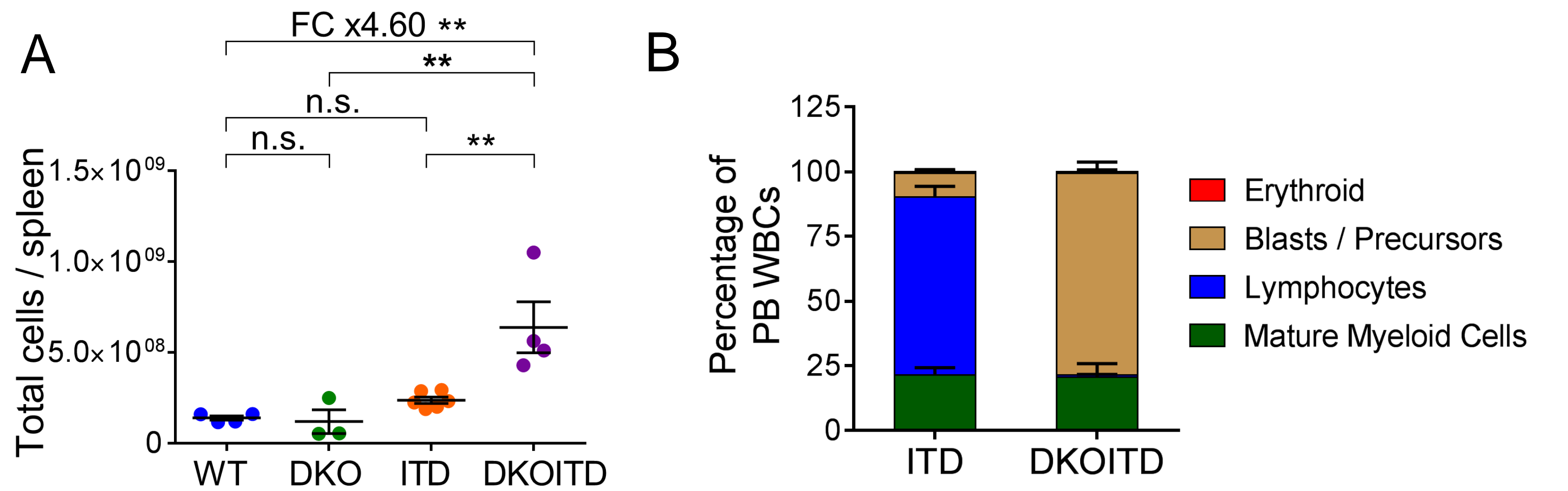
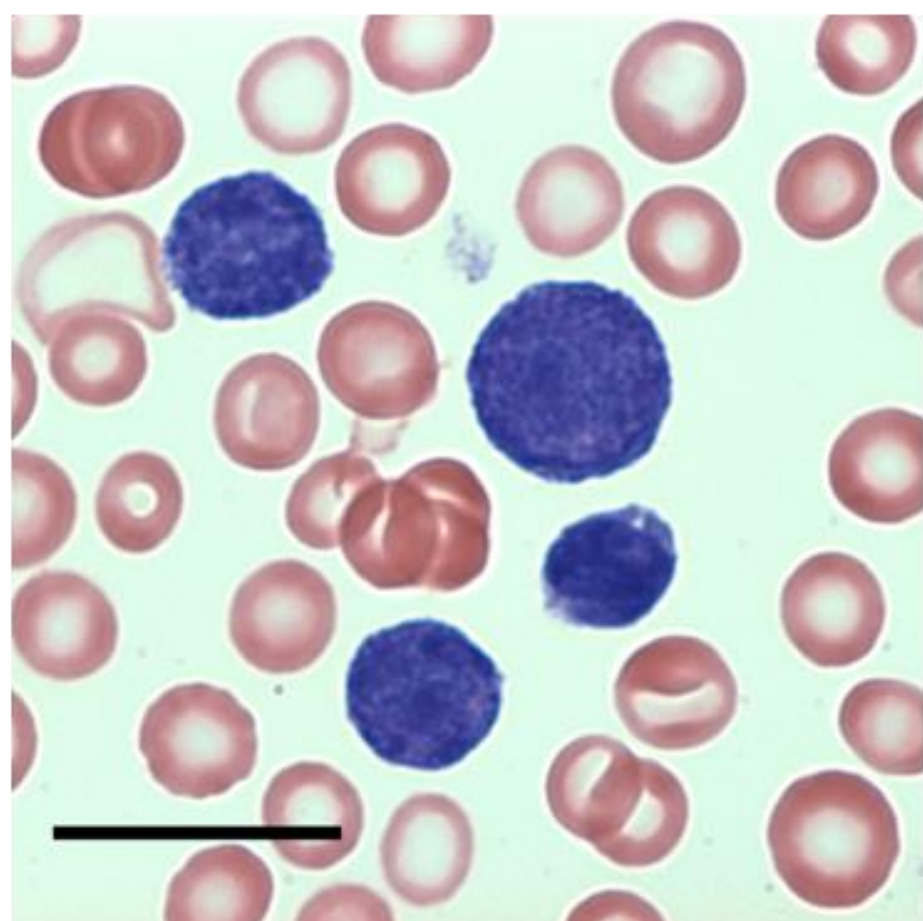


Figure S4, Related to Figure 4. Activating Flt3 Mutation Collaborates with Inactivating Ezh2 and Runx1 Mutations Targeted to Early Lymphoid Progenitors to Cause Acute Leukemia

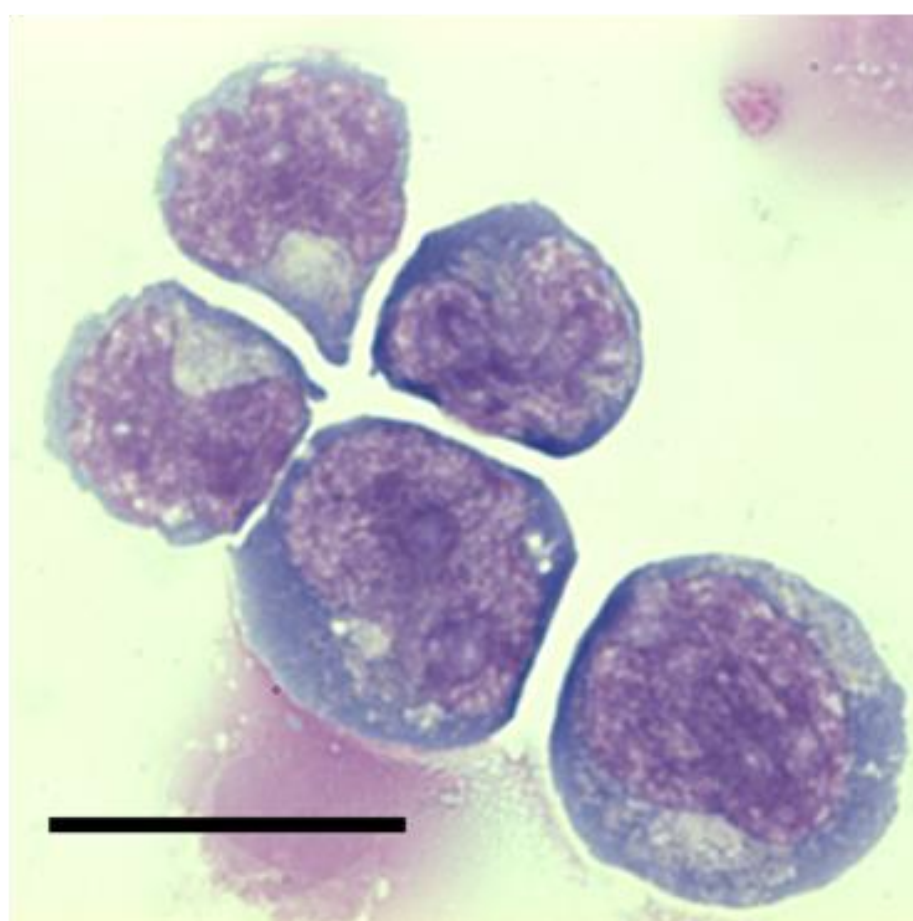
(A) Total spleen cellularity in 6-8 week old WT (n=4), DKO (n=3), ITD (n=6) mice and leukemic DKOITD (n=4) mice. (B) Morphology of peripheral blood leukocytes in leukemic DKOITD (n=3) and littermate ITD control (n=3) mice. One hundred cells were scored according to morphology for each sample. Bars show mean \pm SEM. (C) Overview of analysis of data from exome sequencing of DKOITD leukemias. Genomic DNA was extracted from bone marrow cells of 8 DKOITD leukemic mice, 2 WT mice from the same colony, and 8 WT mice from an unrelated C57BL/6 colony. (D) Total cellularity and FACS analysis of absolute numbers of Kit⁺Mac1^{low} (myeloid precursor cells) per femur and tibia from 6-8 week old WT (n=9), DKO (n=5), ITD (n=4) mice and leukemic DKOITD (n=4) mice. (E) Representative FACS plots showing lack of co-expression of Mac1 with surface CD3 (left panels) and positive co-expression of CD5 with surface CD3 (right panels) in both WT and leukemic DKOITD bone marrow. Figures represent the mean percentage of total bone marrow cells falling into each gate across all experiments. (F) Expression relative to WT of leukemia oncogenes in leukemic DKOITD Mac1⁺ BM cells (WT n=3, DKOITD n=4). p values are by ANOVA, *p<0.05, **p<0.01 and ***p<0.001. n.s.; not significant (p>0.05). Horizontal lines show mean \pm SEM (A, D).

A

Peripheral blood



Bone marrow



B

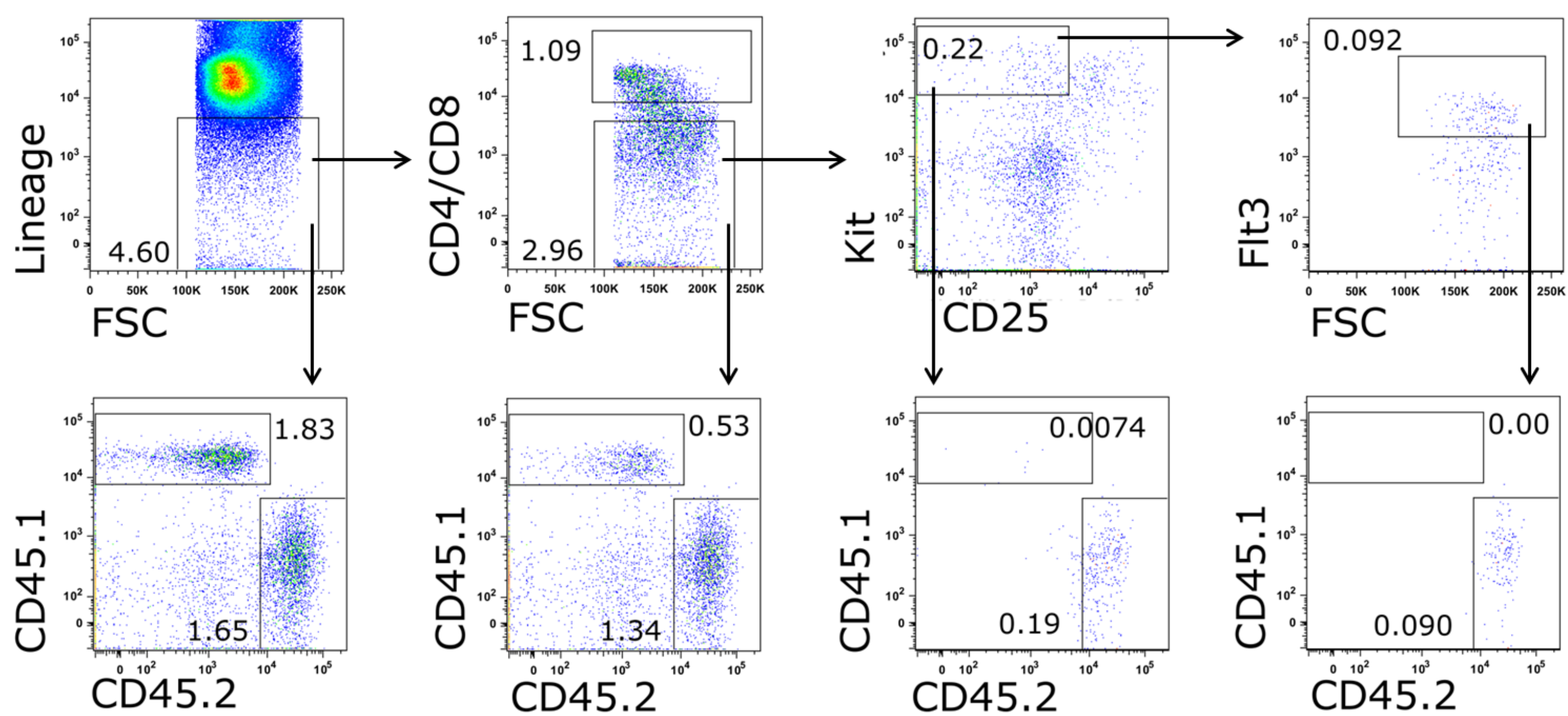


Figure S5, Related to Figure 5. Leukemia Induced by Activating Flt3 Mutation Combined with Inactivating Runx1 and Ezh2 Mutations can be Propagated by ETPs

(A) Representative peripheral blood smear and bone marrow cytospin images from a leukemic DKOITD ETP transplant recipient. Scale bars represent 20 μ m. (B) Representative FACS plots showing relative contribution of CD45.1 and CD45.2 cells to thymocyte populations in moribund DKOITD ETP-transplant recipient mice. Figures represent the mean percentage of total thymocytes falling into each gate across all replicates.

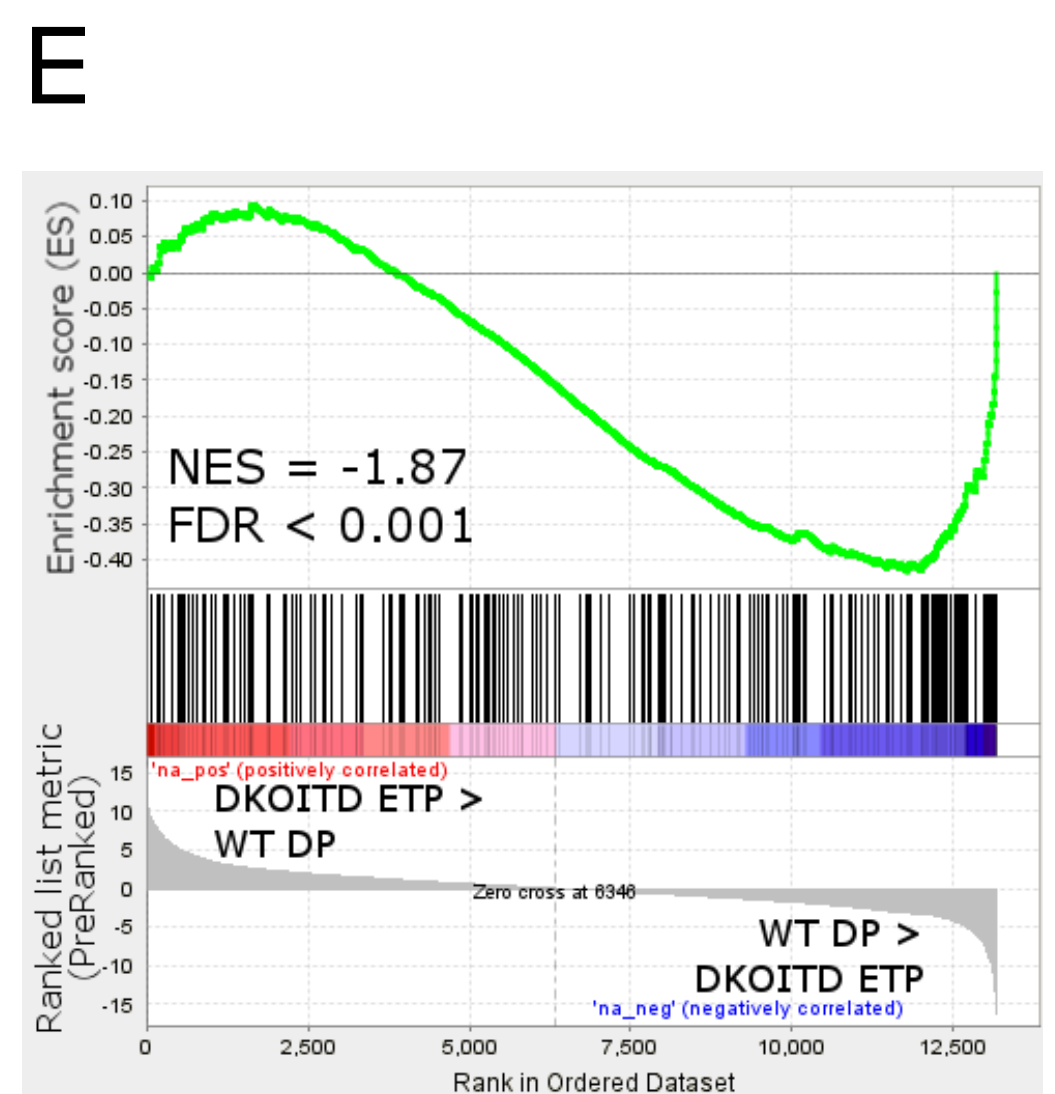
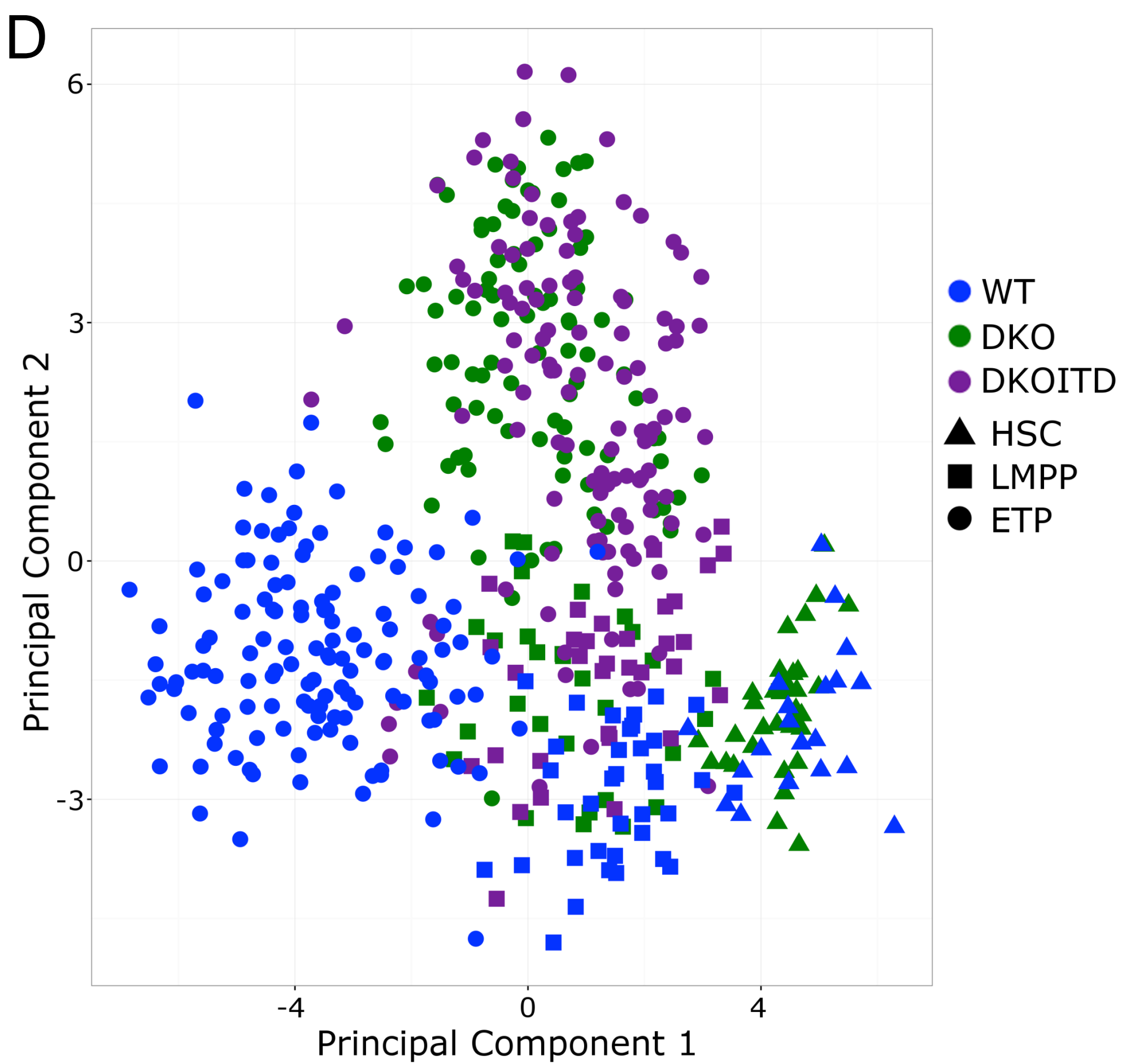
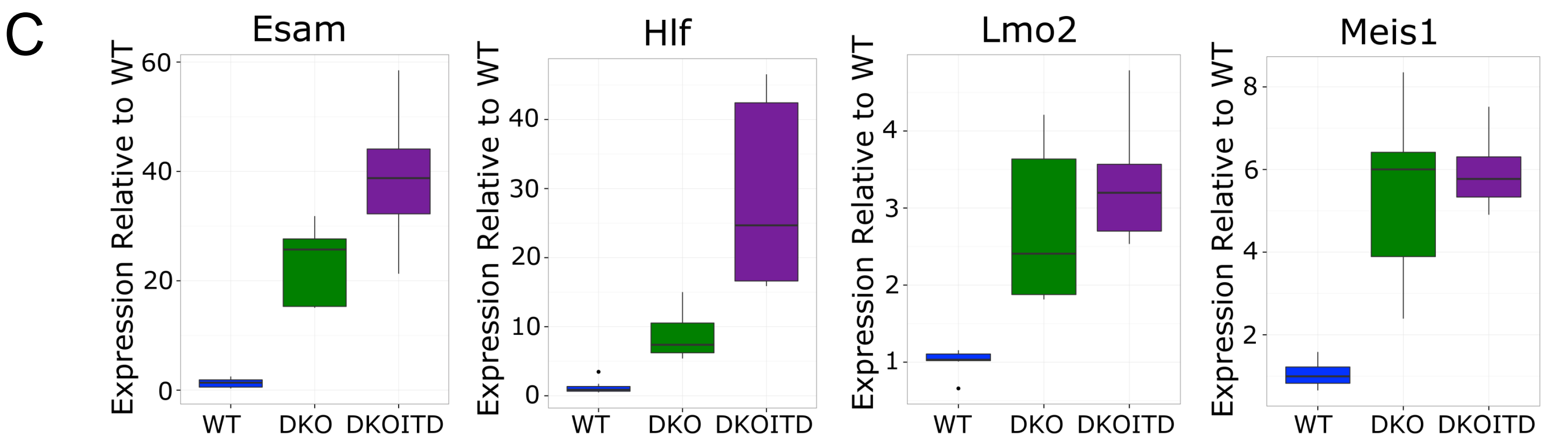
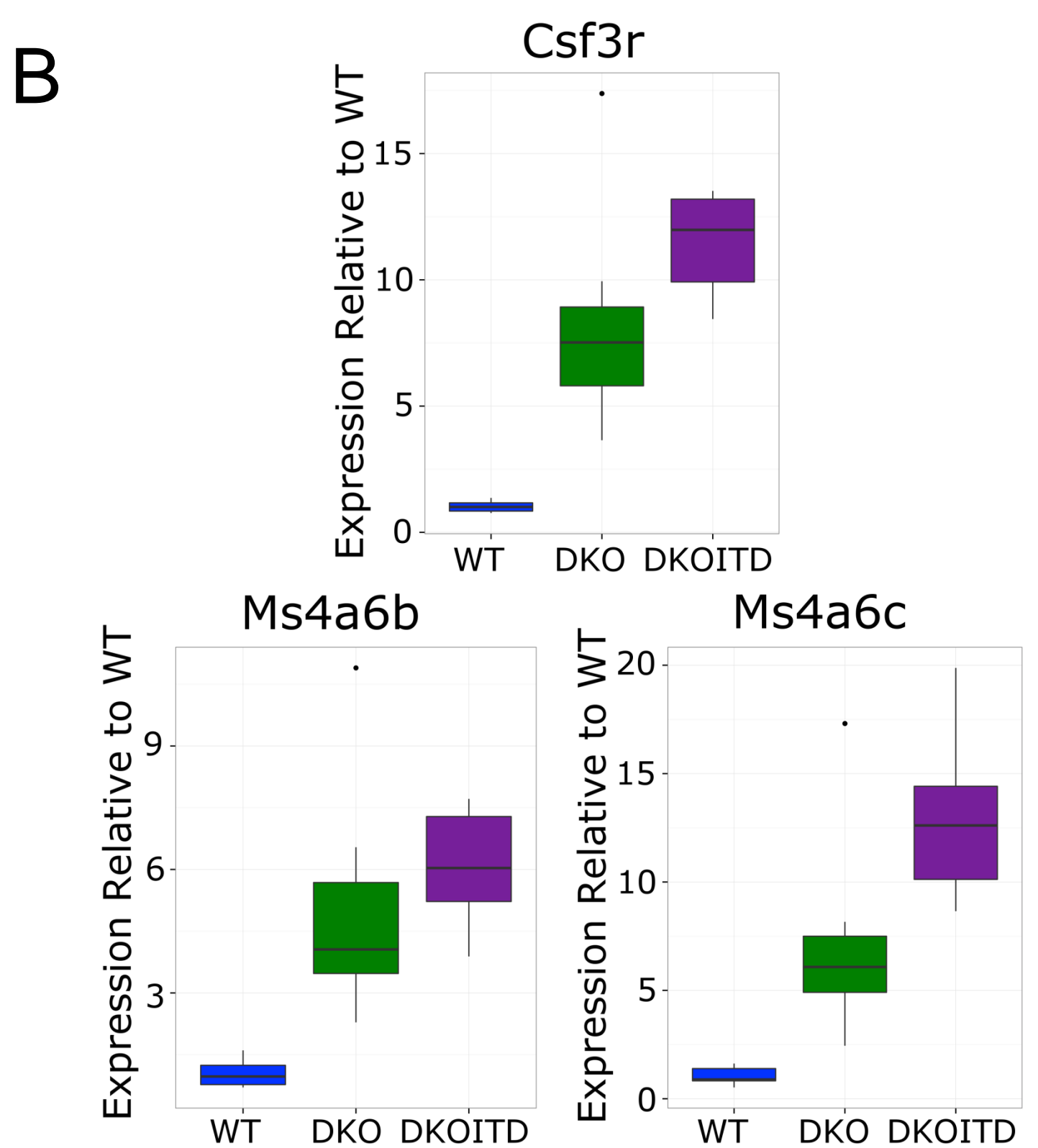
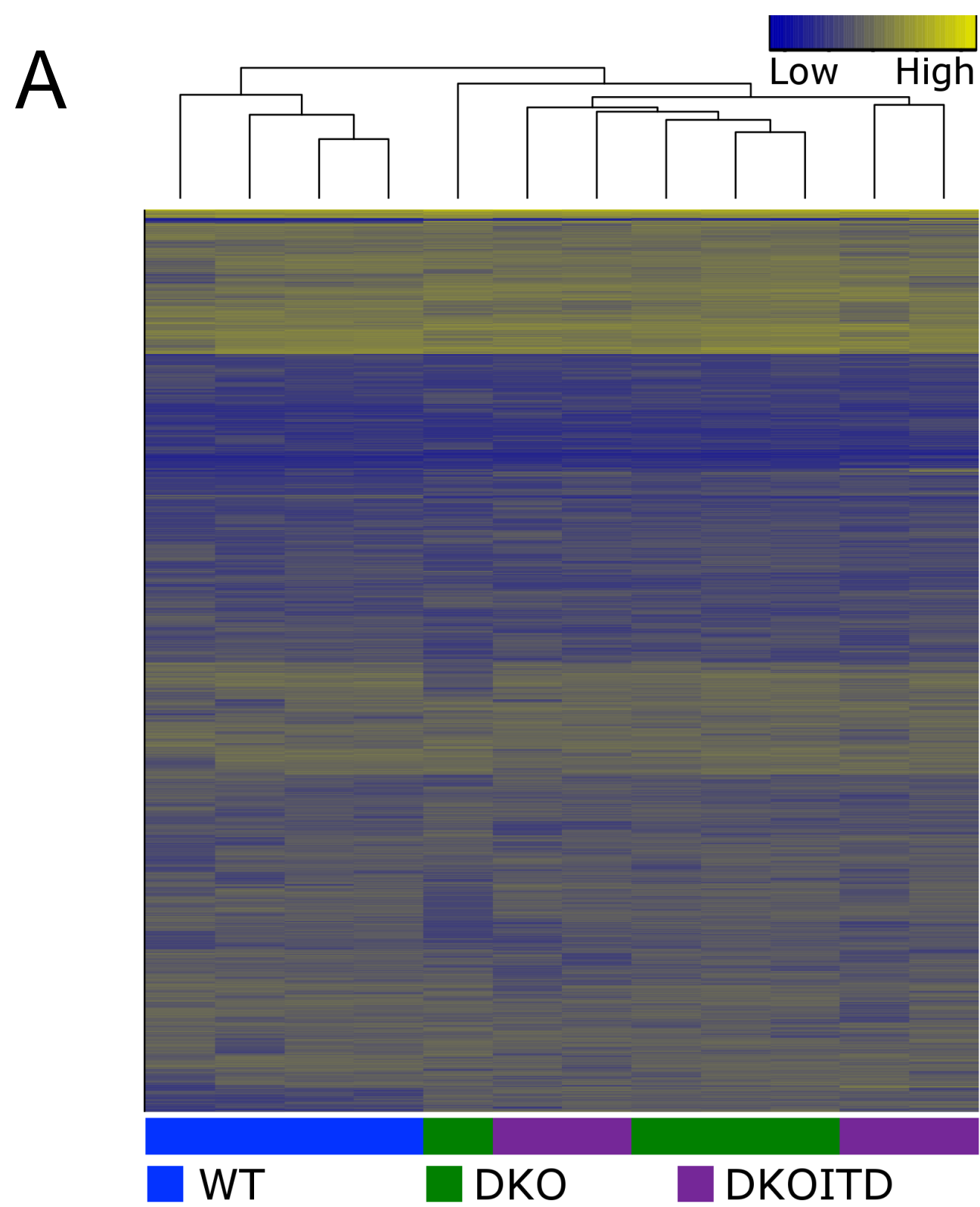


Figure S6, Related to Figure 6. Activating Flt3 Mutation Augments Upregulation of Signaling Pathway-Associated Transcription in Ezh2 and Runx1-Inactivated ETPs

(A) Hierarchical clustering and heatmap showing expression levels, scaled per gene, of the 3000 most variable genes between WT, DKO and DKOITD ETPs (WT n=4, DKO n=4, DKOITD n=4). Each replicate represents 100 purified ETPs from individual mice at 6-8 weeks of age. (B-C) Expression relative to WT of myeloid (B) and HSC-associated genes (C) in DKO and DKOITD ETPs as determined by qPCR (WT n=8, DKO n=7, DKOITD n=6). Box plots show median, lower and upper quartiles. Replicates shown as dots when outside 1.5 times the inter-quartile range. (D) Principal component analysis of single-cell qPCR data from WT HSCs (n=20), LMPPs (n=36) and ETPs (n=129), DKO HSCs (n=33), LMPPs (n=31) and ETPs (n=91), and DKOITD LMPPs (n=33) and ETPs (n=122). Cells were collected from 12 WT, 9 DKO and 8 DKOITD mice. (E) GSEA comparing WT DP thymocytes and DKOITD ETPs for genes downregulated in human ETP-ALL relative to non-ETP T-ALL.

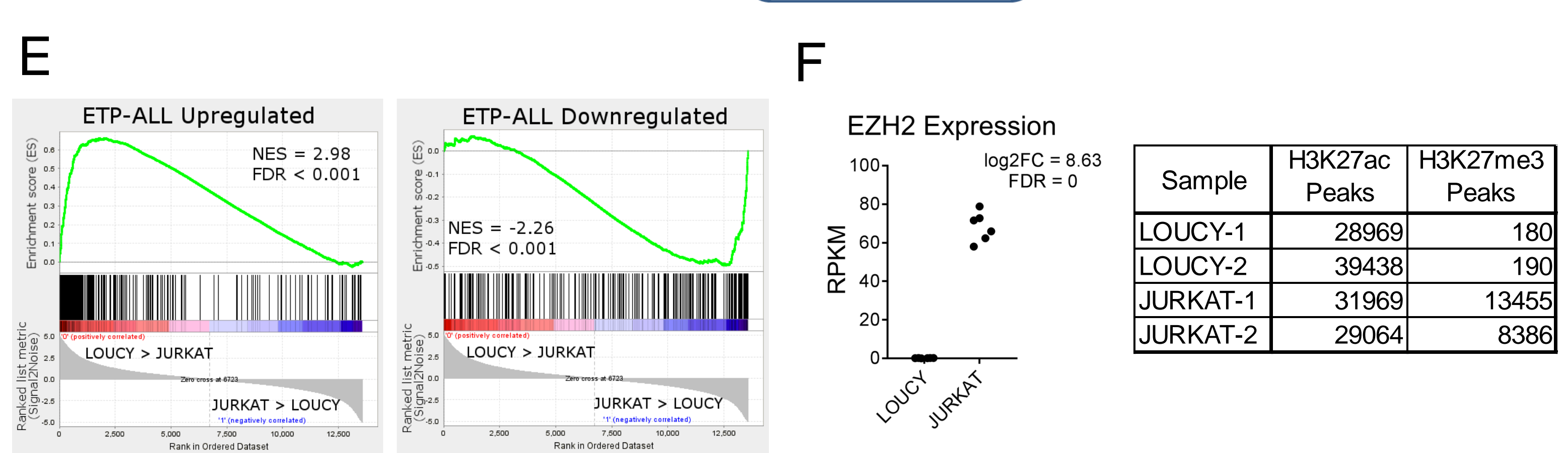
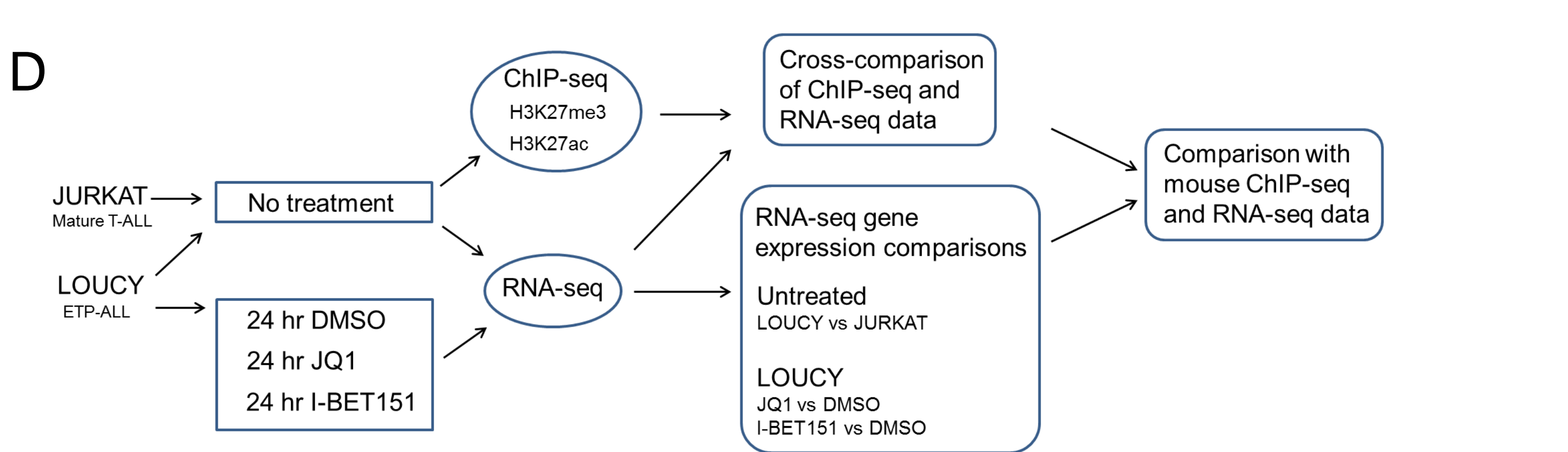
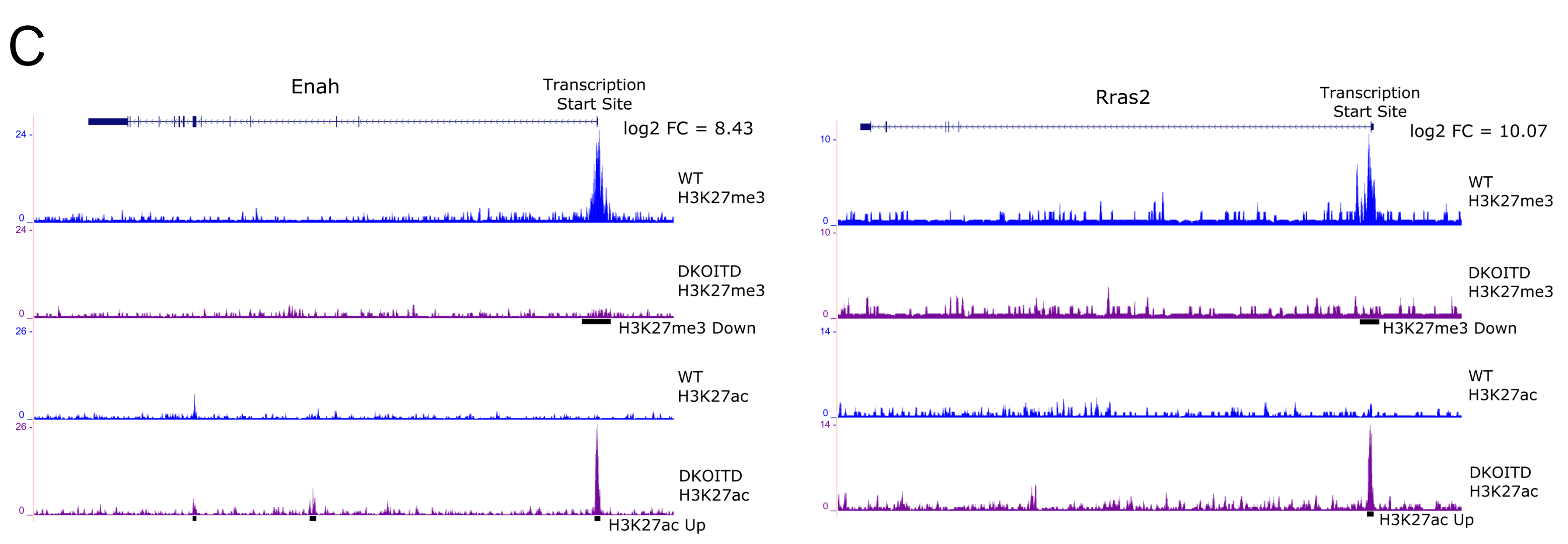
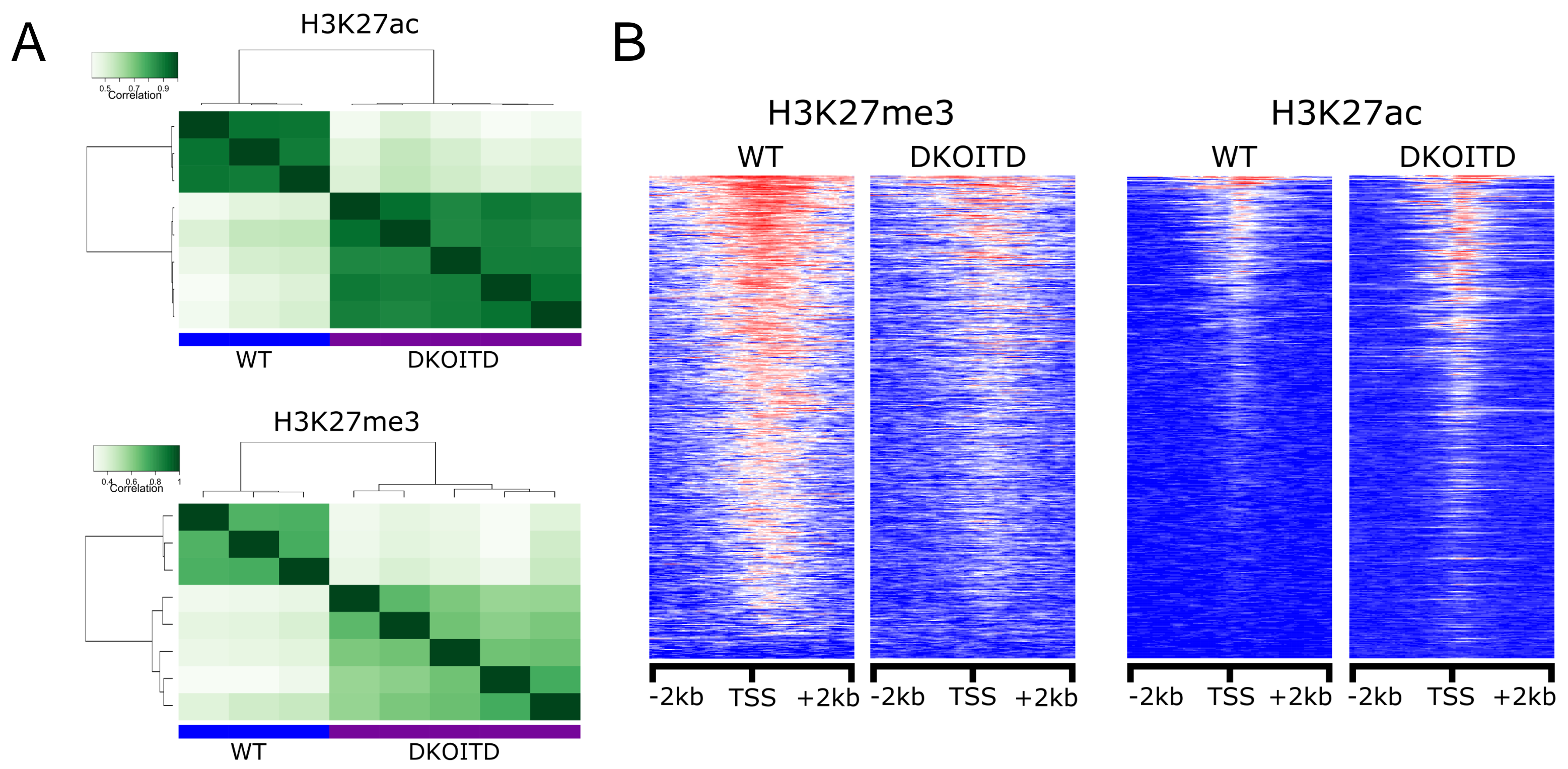


Figure S7, Related to Figure 7. BET Inhibition Reverses Gene Expression Changes Associated with Loss of PRC2 Function

(A) Cluster dendrograms and correlation between replicates of WT and DKOITD bone marrow ChIP-seq samples, comparing normalised read density at each H3K27ac (top) and H3K27me3 (bottom) peak location. (B) Heatmaps showing normalised read density of H3K27me3 and H3K27ac at the transcription start site for all genes showing significantly decreased H3K27me3 in DKOITD relative to WT bone marrow cells (n=520 genes). Tracks are centred on the transcription start site and extend 2 kb upstream (left) and 2 kb downstream (right). Genes are ordered separately for H3K27me3 and H3K27ac by average intensity in WT. (C) Genome browser tracks showing H3K27me3 and H3K27ac at the *Enah* and *Rras2* loci in WT and DKOITD bone marrow cells. Fold change refers to gene expression in DKOITD relative to WT Mac1⁺ BM cells. (D) Experimental design for ChIP-seq and RNA-seq experiments in LOUCY and JURKAT cells. ChIP-seq n=2 per cell line per histone mark, RNA-seq n=6 per cell line (untreated cells) and n=4 per condition (DMSO, JQ1 and I-BET151-treated LOUCY cells). (E) GSEA comparing LOUCY and JURKAT cells for genes upregulated (left) or downregulated (right) in human ETP-ALL relative to non-ETP T-ALL. (F) RPKM expression levels of EZH2 (left), and number of peaks detected genome-wide per sample for H3K27ac and H3K27me3 (right) in LOUCY and JURKAT cells.

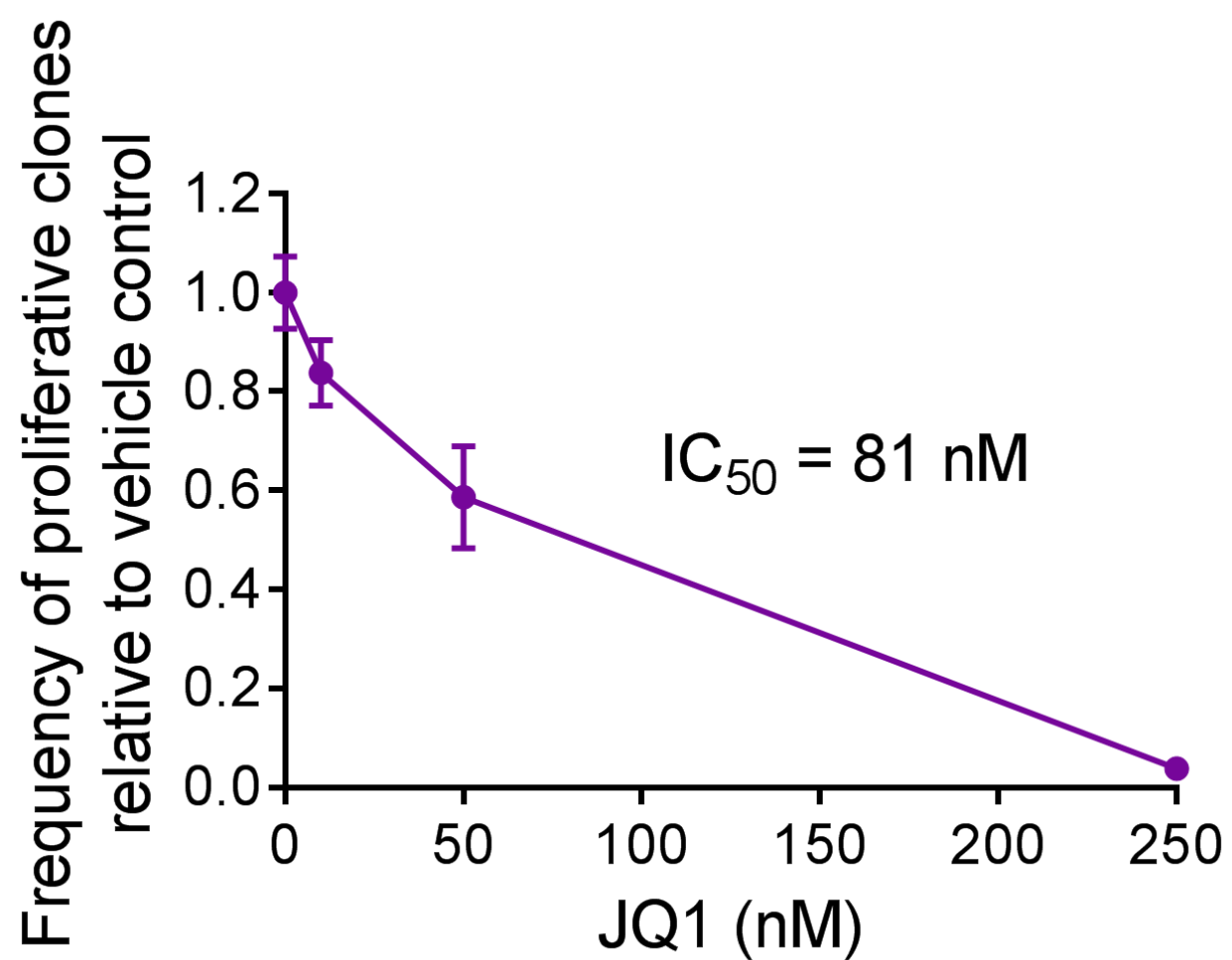
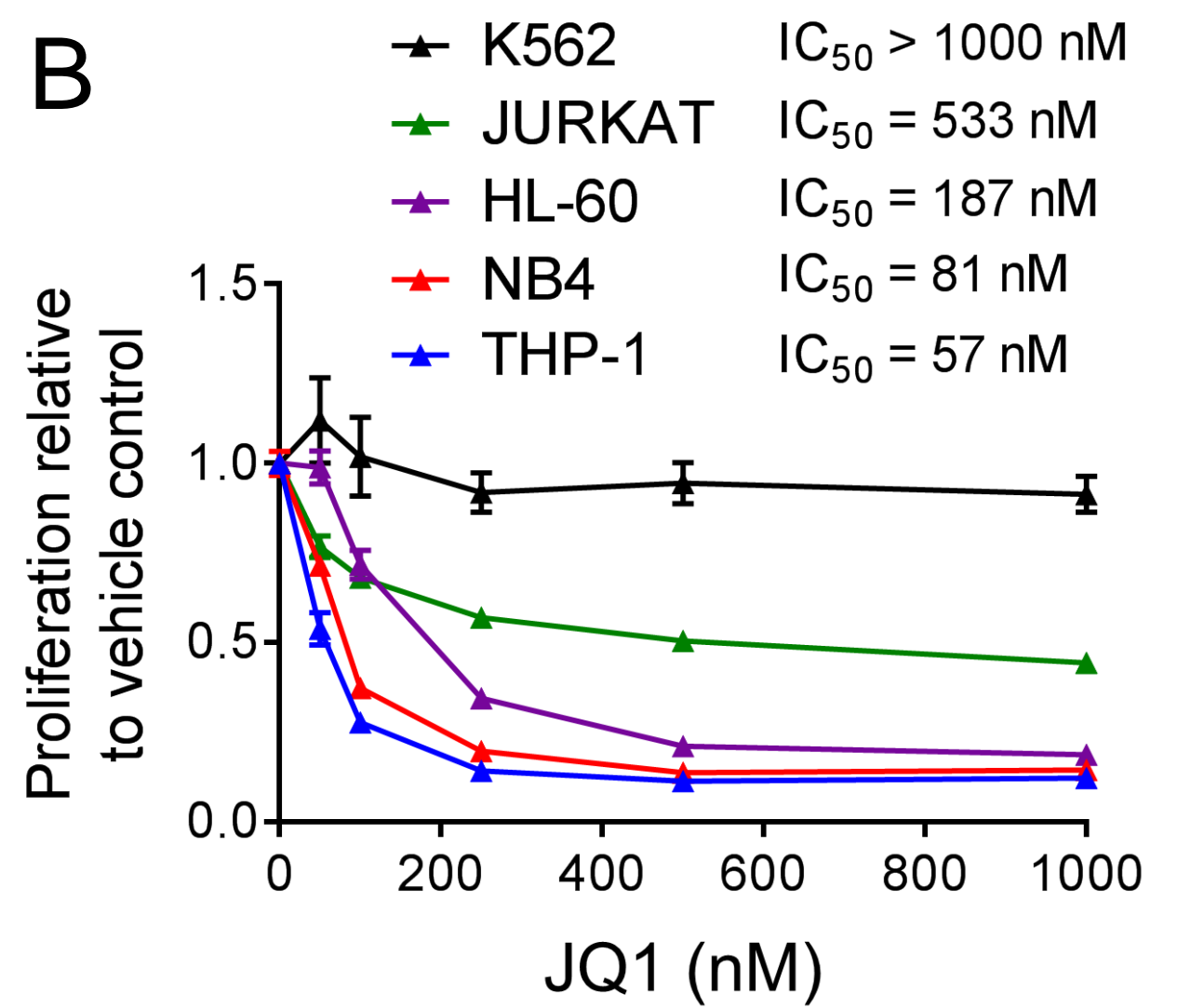
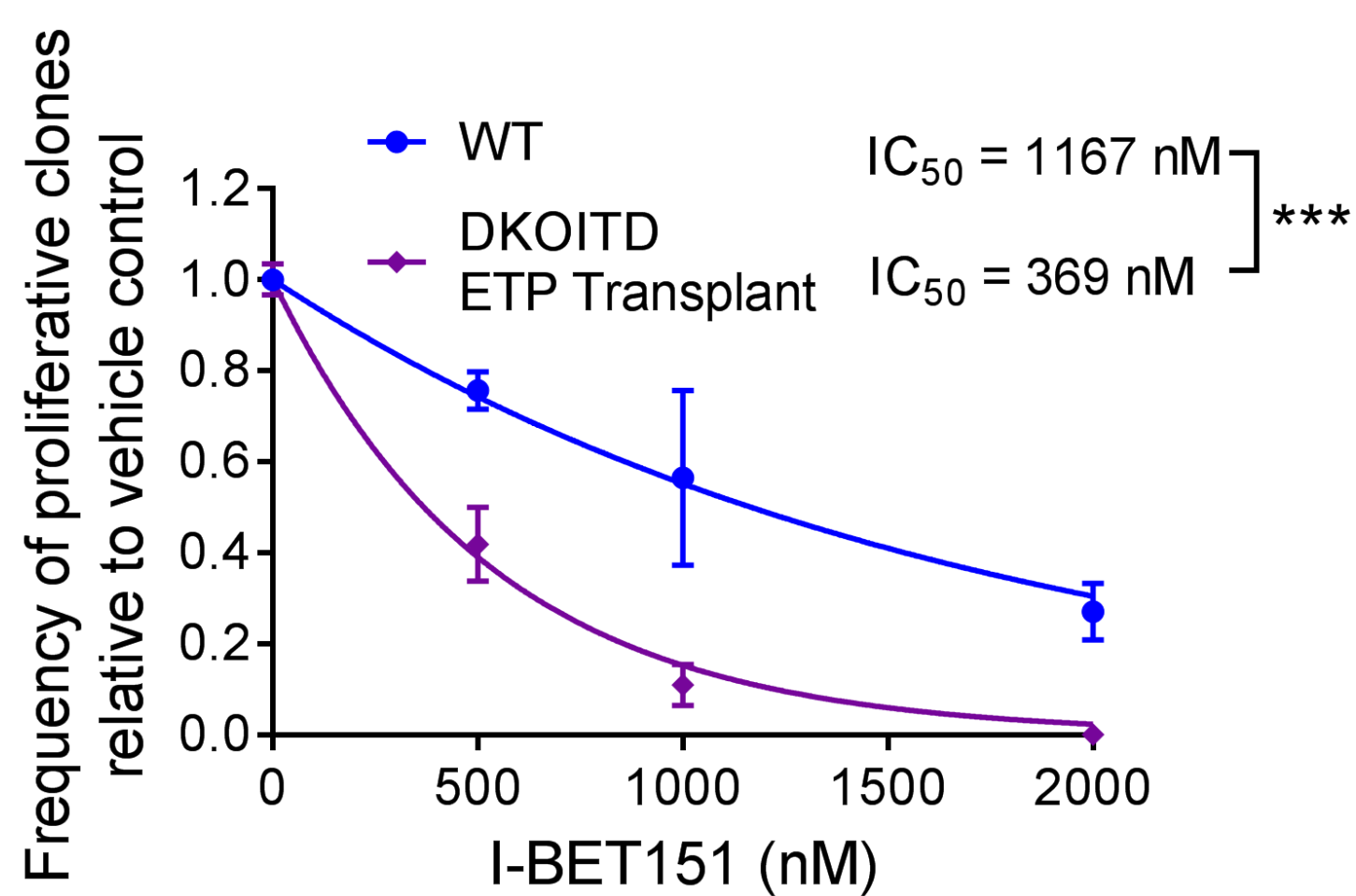
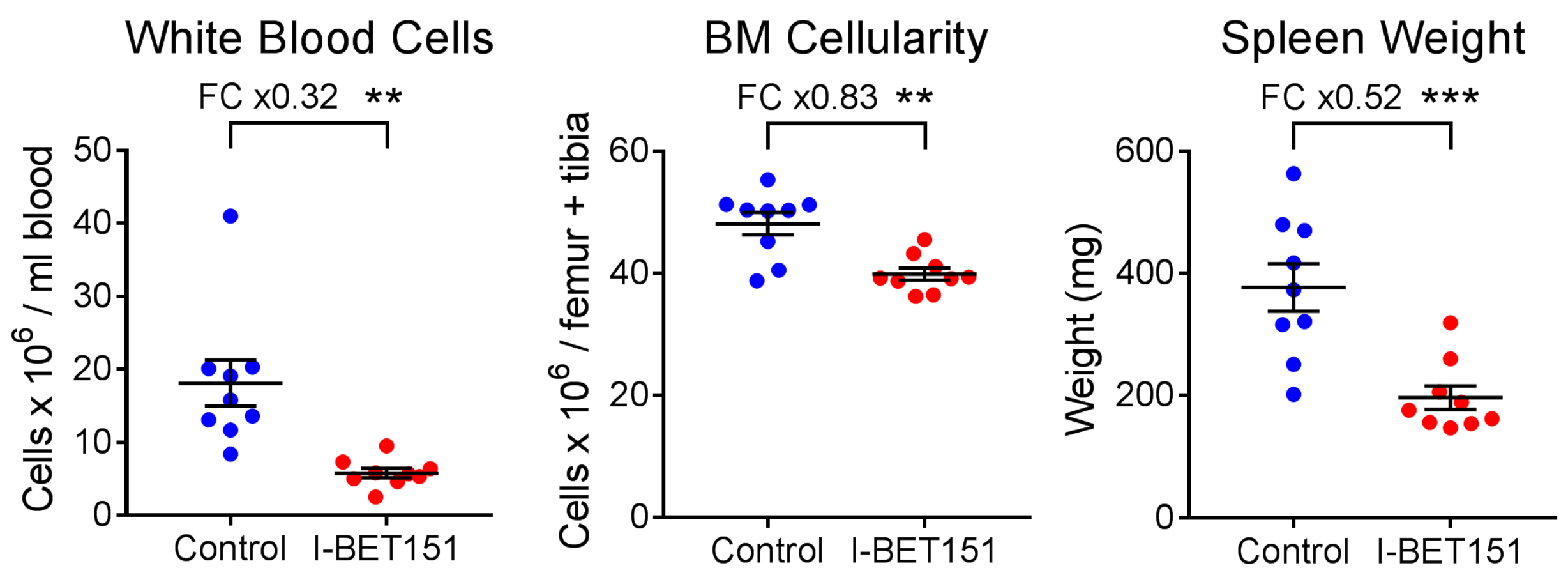
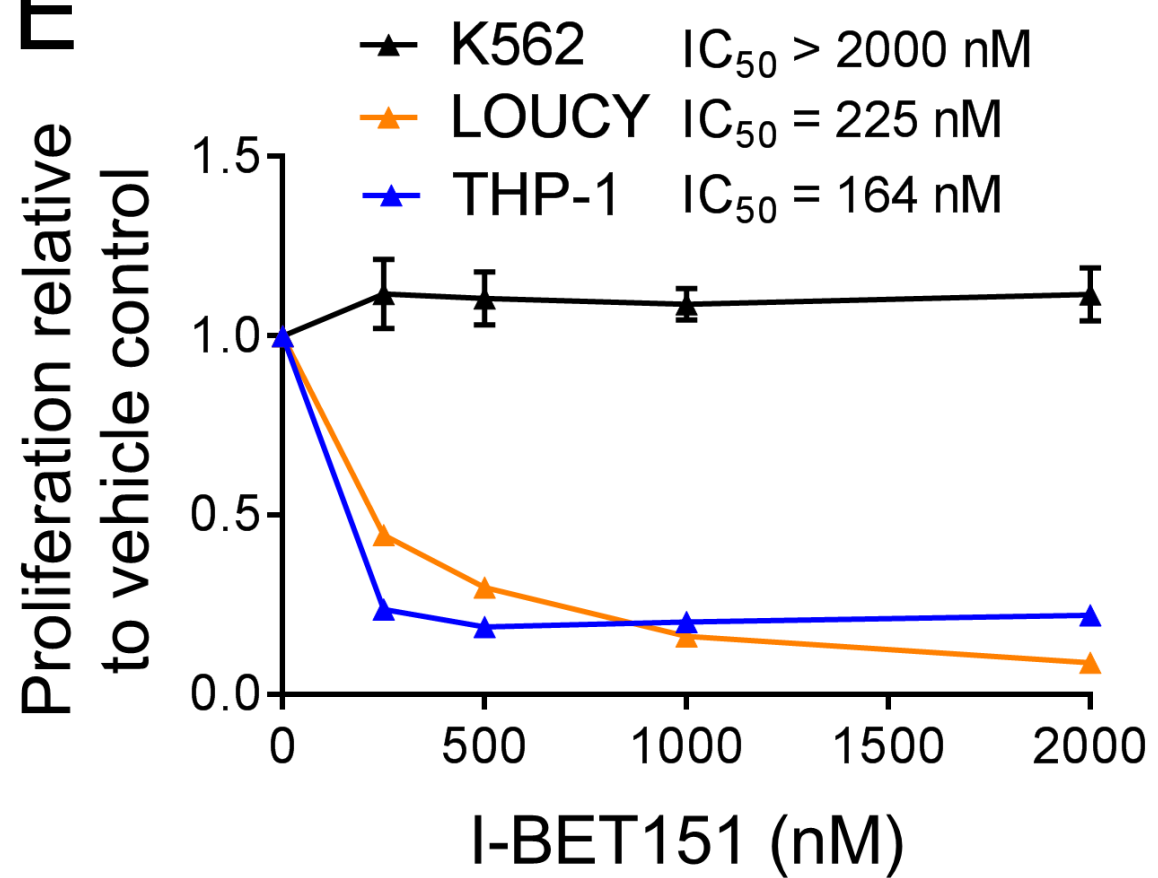
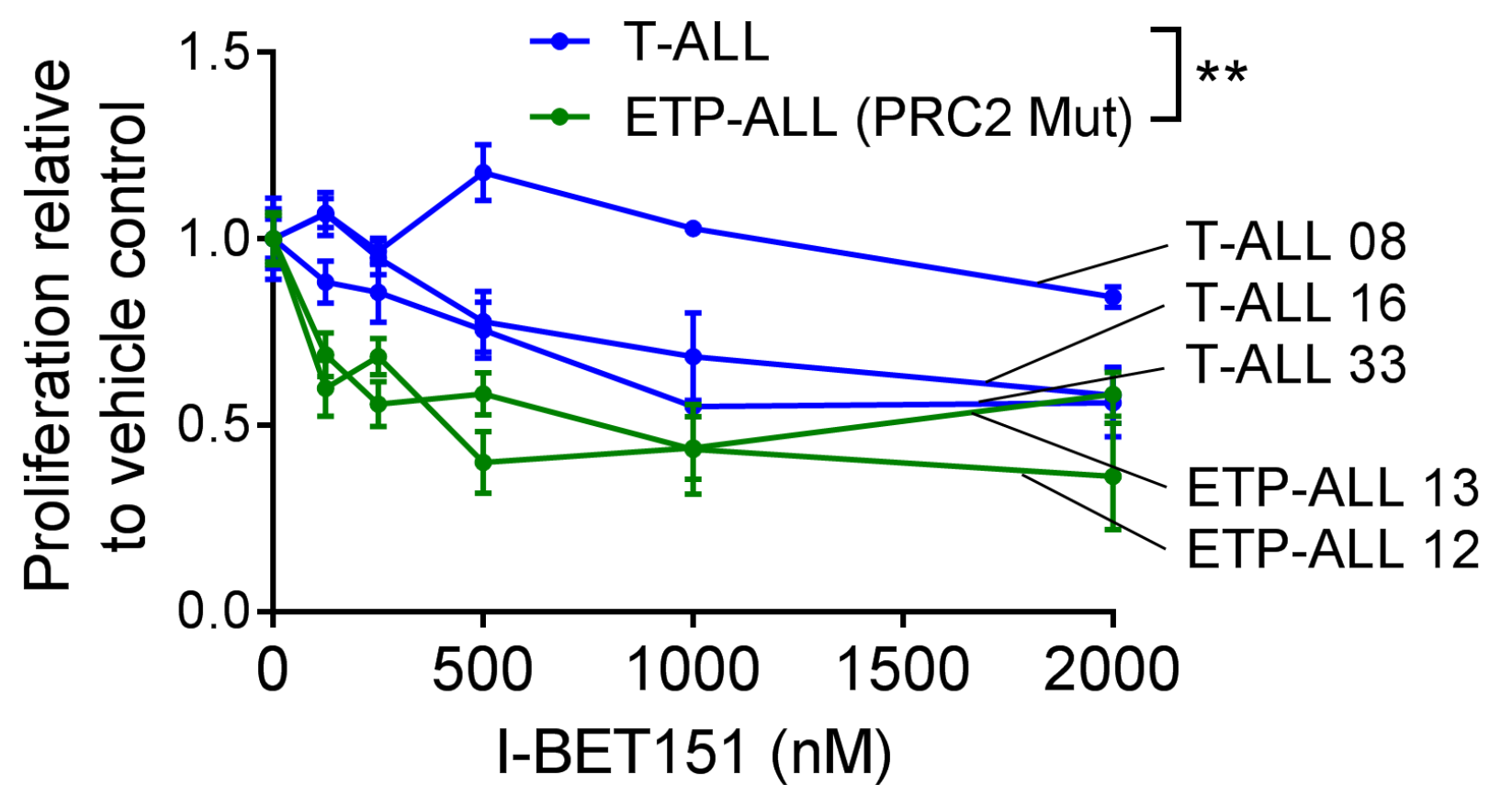
A**B****C****D****E****F**

Figure S8, Related to Figure 8. BET Inhibition Selectively Targets Proliferation of ETP Propagated Leukemia Cells

(A) Single-cell proliferation assay of DKOITD ETPs cultured with increasing concentrations of JQ1.

Frequency of clones showing high proliferation at each concentration is shown relative to DMSO control (n=3-5 for each concentration). (B) MTS proliferation assay of leukemia cell lines cultured with increasing concentrations of JQ1, shown relative to DMSO control (n=6 for each concentration). Data were collected across two independent experiments. (C) Single-cell proliferation assay of CD45.2 Lin⁻Kit⁺ BM progenitor cells FACS-sorted from recipient mice transplanted with WT BM or DKOITD ETP cells and cultured with increasing concentrations of I-BET151. Frequency of clones showing high proliferation at each concentration is shown relative to DMSO control (WT n=3-5 and DKOITD n=4-8 for each concentration). Data were collected from two WT BM and four DKOITD ETP recipient mice. (D) White blood cell counts, total BM cellularity and spleen weights of wild-type mice transplanted with DKOITD bone marrow and administered modified murine feed containing 0.018% (180ppm) I-BET151 or control feed. Control n=9, I-BET151 n=9. (E) MTS proliferation assay of K562, LOUCY and THP-1 leukemia cell lines cultured with increasing concentrations of I-BET151, shown relative to DMSO control. Data were collected across two independent experiments. (F) MTS proliferation assay of T-ALL and ETP-ALL patient-derived xenografts cultured with increasing concentrations of I-BET151, shown relative to DMSO control (n=3 for each concentration). See STAR Methods for mutations carried by ETP-ALL samples. p values are by F-test (C, E) or T-test (D), *p<0.05, **p<0.01 and ***p<0.001. n.s.; not significant (p>0.05). Horizontal lines show mean \pm SEM.

Table S8, Related to STAR Methods. List of Taqman probes used for gene expression analysis of ETPs.

| Target gene | Assay ID |
|-----------------------|---------------|
| Actb | Mm00607939_s1 |
| Anxa1 | Mm00440225_m1 |
| Arpp21 | Mm00473630_m1 |
| B2M | Mm00437762_m1 |
| Bcl11a | Mm00479358_m1 |
| Bmi1 | Mm03053308_g1 |
| Ccl9 | Mm00441260_m1 |
| Ccr7 | Mm01301785_m1 |
| Ccr9 | Mm02620030_s1 |
| Cd160 | Mm00444461_m1 |
| Cebpb | Mm00843434_s1 |
| Cish | Mm01230623_g1 |
| Cited2 | Mm01188099_g1 |
| Cpa3 | Mm00483940_m1 |
| Csf1r | Mm01266652_m1 |
| Csf2ra | Mm00438331_g1 |
| Csf3r | Mm00432735_m1 |
| Ctsc | Mm00515580_m1 |
| Ctsg | Mm00456011_m1 |
| Cxcr4 | Mm01996749_s1 |
| Dtx1 | Mm00492297_m1 |
| Dyrk1a | Mm00432934_m1 |
| Erg | Mm01214246_m1 |
| Esam | Mm00518378_m1 |
| Etv6 | Mm00468390_m1 |
| Ezh2 - WT and Deleted | Mm00468449_m1 |
| Ezh2 - WT only | Mm00468464_m1 |
| F2r | Mm00438851_m1 |
| Fcer1g | Mm02343757_m1 |
| Fcgr3 | Mm00438882_m1 |
| Fes | Mm01318102_m1 |
| Fli1 | Mm00484410_m1 |
| Flt3 | Mm01210882_m1 |
| Fos | Mm00487425_m1 |
| Gapdh | Mm99999915_g1 |
| Gata2 | Mm00492301_m1 |
| Gata3 | Mm00484683_m1 |
| Gfi1 | Mm00515855_m1 |
| Gfi1b | Mm00492318_m1 |
| Hes1 | Mm01342805_m1 |
| Hey1 | Mm00468865_m1 |
| Hlf | Mm00723157_m1 |
| Hoxa9 | Mm00439364_m1 |
| Hprt | Mm01545399_m1 |
| Id1 | Mm00775963_g1 |
| Id2 | Mm00711781_m1 |

| | |
|------------------------|-----------------------------------|
| Igf2r | Mm00439576_m1 |
| Ikzf1 | Mm01187882_m1 |
| Il2ra | Mm00434261_m1 |
| Il3ra | Mm00434273_m1 |
| IL4 | Mm00445259_m1 |
| Il7r | Mm00434295_m1 |
| Itgam | Mm00434455_m1 |
| Jag1 | Mm00496902_m1 |
| Jun | Mm00495062_s1 |
| Kit | Mm00445212_m1 |
| Lat | Mm00456761_m1 |
| Lck | Mm00802897_m1 |
| Lef1 | Mm00550265_m1 |
| Lmo2 | Mm01281680_m1 |
| Ly6a | Mm00726565_s1 |
| Ly6d | Mm00521959_m1 |
| Lyz1 | Mm00657323_m1 |
| Lyz2 | Mm01612741_m1 |
| Mcl1 | Mm00725832_s1 |
| Mef2c | Mm01340842_m1 |
| Meis1 | Mm00487664_m1 |
| Mpl | Mm00440310_m1 |
| Mpo | Mm01298424_m1 |
| Ms4a6b | Mm00728225_m1 |
| Ms4a6c | Mm00459296_m1 |
| Myb | Mm00501741_m1 |
| Myc | Mm00487804_m1 |
| Mycn | Mm00476449_m1 |
| Nfe2 | Mm00801891_m1 |
| Notch1 | Mm00435249_m1 |
| Nrarp | Mm00482529_s1 |
| Pbx1 | Mm04207617_m1 |
| Pecam1 | Mm01242584_m1 |
| Pim1 | Mm00435712_m1 |
| Pim2 | Mm00454579_m1 |
| Prkcd | Mm00440891_m1 |
| Ptcra | Mm00478363_m1 |
| Rag1 | Custom assay |
| | Forward: TGTGGAGCAAGGTAGCTTAGC |
| | Reverse: TCATCGGGTGCAGAACTGAAG |
| | Reporter: CATGGCTGCCTCCTTG |
| Rag2 | Mm00501300_m1 |
| Runx1 - WT and Deleted | Mm01213405_m1 |
| Runx1 - WT only | Mm01213404_m1 |
| Runx3 | Mm00490666_m1 |
| Selp | Mm01295931_m1 |
| Socs1 | Mm00782550_s1 |
| Socs2 | Mm00850544_g1 |

| | |
|-------------|---------------------------------------|
| Spi1 | Mm00488142_m1 |
| Sterile IgH | Custom assay |
| | Forward: GGACTTTGGGATGGGTTTGGTT |
| | Reverse: CCCTGGTCCTAGACATCAGAGTAAT |
| | Reporter: CCCAGATGAAGGGCTAC |
| Tcf12 | Mm00441699_m1 |
| Tcf3 | Mm01175588_m1 |
| Tcf7 | Mm00493445_m1 |
| Zfp467 | Mm00465678_g1 |



[Click here to access/download](#)

Supplemental Movies and Spreadsheets
Table S1.xlsx





[Click here to access/download](#)

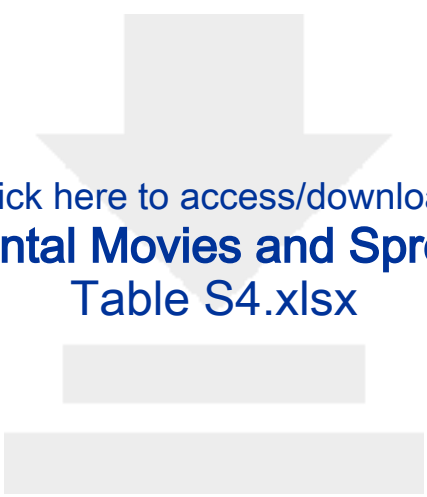
Supplemental Movies and Spreadsheets
Table S2.xlsx



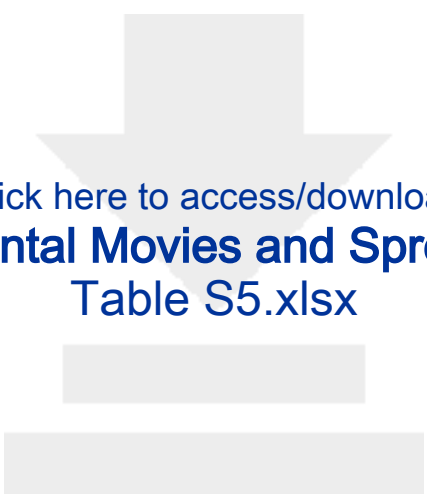


[Click here to access/download](#)

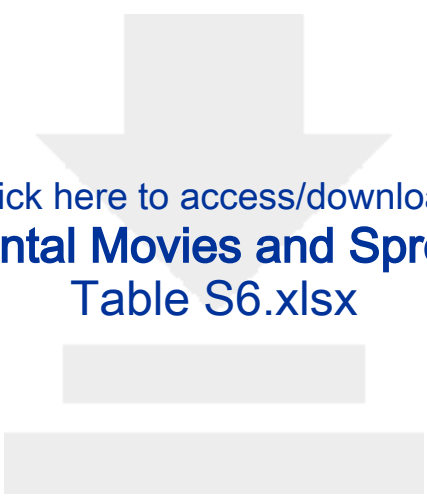
Supplemental Movies and Spreadsheets
Table S3.xlsx



[Click here to access/download](#)
Supplemental Movies and Spreadsheets
Table S4.xlsx



[Click here to access/download](#)
Supplemental Movies and Spreadsheets
Table S5.xlsx



[Click here to access/download](#)
Supplemental Movies and Spreadsheets
Table S6.xlsx



[Click here to access/download](#)

Supplemental Movies and Spreadsheets
Table S7.xlsx